

GPO PRICE \$ _____

CESTI PRICE(S) \$ _____

Hard copy (HC) 165

Microfiche (MF) 75

FORM 602 JUL 65

THERMAL CONTACT CONDUCTANCE IN A VACUUM ENVIRONMENT

13 DECEMBER 1964
DOUGLAS REPORT SM-47700

MISSILE & SPACE SYSTEMS DIVISION
DOUGLAS AIRCRAFT COMPANY, INC.
SANTA MONICA CALIFORNIA

FACILITY FORM 602

N66 33408

(ACCESSION NUMBER)

111

(PAGES)

CR-75148

(NASA CR OR TMX OR AD NUMBER)

(THRU)

1

(CODE)

33

(CATEGORY)

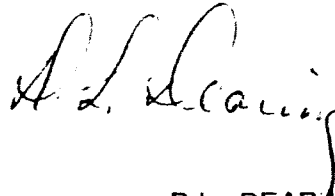


447-32023

THERMAL CONTACT CONDUCTANCE IN A VACUUM ENVIRONMENT

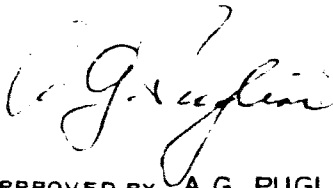
13 DECEMBER 1964
DOUGLAS REPORT SM-47700

PREPARED BY: M.F. BLOOM
AERO/THERMODYNAMICS DEPARTMENT
RESEARCH AND DEVELOPMENT



APPROVED BY: D.L. DEARING,
CHIEF, AERO/THERMODYNAMICS SECTION
SATURN ENGINEERING

PREPARED UNDER THE JOINT SPONSORSHIP
OF THE DOUGLAS AIRCRAFT COMPANY
INDEPENDENT RESEARCH AND DEVELOPMENT
PROGRAM ACCOUNT NO. 81695-200/54053
AND THE SATURN S-IVB CONTRACT NO. NAS7-101



APPROVED BY: A.G. PUGLISI
MANAGER, SATURN SYSTEMS DEVELOPMENT



APPROVED BY: E.P. WILLIAMS
CHIEF ENGINEER
ADVANCE AERO/THERMODYNAMICS DEPARTMENT
RESEARCH AND DEVELOPMENT

ABSTRACT

116633485

An apparatus was designed and constructed which produced values of thermal contact conductance in a vacuum environment at low temperatures. The materials tested were aluminum 7075-T6 and stainless steel 17-4 PH. The temperature range studied was -250°F to $+90^{\circ}\text{F}$ for aluminum and -200°F to $+150^{\circ}\text{F}$ for stainless steel. The vacuum environment was between 10^{-5} and 10^{-6} torr. Thermal contact conductance was obtained as a function of contact pressure, surface roughness and surface flatness deviation. The contact pressure ranged from 0 to 1000 psi.

Data in the literature and the present contact conductance data were plotted against contact pressure for various roughnesses on log-log graphs. The power dependence of contact conductance as a function of contact pressure was determined. Low temperature data dependencies were compared to high temperature data dependencies.

High temperature literature data and the present low temperature data were compared to Clausing and Chao's theoretical predictions of thermal contact conductance. Discrepancies between data and theoretical predictions are discussed.

DESCRIPTORS

Thermal
Contact
Conductance
Interface
Resistance
Macroscopic
Microscopic
Area
Experimental
Theoretical
Cryogenic
Vacuum

Pressure
Temperature
Roughness
Waviness
Flatness
Metals
Aluminum
Stainless Steel
Dissimilar
Joint
Bolted
Empirical
Dependence

PRECEDING PAGE BLANK NOT FILMED.

ACKNOWLEDGEMENTS

Sincere appreciation is extended to the Saturn Aero/Thermodynamics Section for their support of the experimental phase of this report.

The author wishes to thank all engineers and technicians of the Douglas Space Systems Center, Environmental Simulation Laboratory for their unstinted determination to obtain precise data and their constant efforts to improve the thermal contact conductance apparatus. The author also wishes to thank the many skilled craftsmen of the Douglas Model Shop and Electrical Laboratory for their precision work in fabricating the test column, specimens and thermocouples.

During the course of this investigation, the author appreciates that, on numerous occasions, he obtained valuable suggestions from Mr. E. D. Marion, Chief of Thermodynamics Section, Advance Space Technology, Douglas Aircraft Company, and from Dr. J. M. F. Vickers of the Jet Propulsion Laboratory of Pasadena, California.

The author thanks Mr. Louis Krichesky for his aid in computer programming.

PRECEDING PAGE BLANK NOT FILMED.

TABLE OF CONTENTS

Section		Page
1.	INTRODUCTION	1
2.	TEST EQUIPMENT	3
	2.1 Basic Thermal Contact Conductance Test Column	3
	2.2 Support Apparatus	9
	2.3 Vacuum Chamber	12
	2.4 Instrumentation	12
	2.5 Flatness Deviation	16
3.	DATA PROCUREMENT	17
	3.1 Test Program	17
	3.2 Test Procedures	19
	3.3 Difficulties Encountered in Controlling the Test Parameters	21
4.	DATA ANALYSIS	22
	4.1 Data Reduction	22
	4.2 Error Analysis	23
5.	RESULTS	26
	5.1 Aluminum 7075-T6	26
	5.2 Stainless Steel 17-4 PH	39
	5.3 Mating of Dissimilar Metals	49
	5.4 Effect of Surface Roughness on Contact Conductance	54
6.	COMPARISON OF REPORTED HIGH TEMPERATURE DATA	56
	6.1 Aluminum	57
	6.2 Stainless Steel	59
	6.3 Comments on the Dependence of Contact Conductance versus Contact Pressure	62
7.	COMPARISON OF LOW AND HIGH TEMPERATURE DATA	62
	7.1 Aluminum 7075-T6	66
	7.2 Stainless Steel 17-4 PH	66
8.	APPLICATION OF THERMAL CONTACT CONDUCTANCE DATA TO A TYPICAL BOLTED JOINT	69
	8.1 High Temperature Bolted Joint	69
	8.2 Low Temperature Bolted Joint	71

TABLE OF CONTENTS (Continued)

Section		Page
9.	THE ELECTRICAL ANALOGY OF THERMAL CONSTRICTION RESISTANCE	72
9.1	A Survey of Two Thermal Contact Conductance Theories	72
9.2	Thermal Constriction Problem	75
9.3	Electrical Constriction Problem	76
9.4	The Relation Between Electrical Resistance and Capacitance According to Holm	78
9.5	An Application of the Electrical Analogy	79
9.6	Extensions of Holm's Theory to Elliptical Contact Areas	80
10.	CONSTRICTION RESISTANCE THEORY OF CLAUSING AND CHAO	82
10.1	Roess' Solution of a Concentric Cylinder Applied to Thermal Contact Resistance	82
10.2	Relationship Between Thermal Resistance and Thermal Conductance	84
10.3	Clausing's Model of One Macroscopic Contact Area	84
10.4	Definition of Total Thermal Conductance	85
10.5	Microscopic Thermal Conductance	85
10.6	Ratio of Macroscopic to Microscopic Constriction Resistance	87
11.	COMPARISON OF CLAUSING'S MACROSCOPIC CONSTRICTION RESISTANCE THEORY TO DATA	89
11.1	Clausing's Macroscopic Theory Compared to Clausing's Data	89
11.2	Clausing's Macroscopic Theory Compared to DACO's Low Temperature Data	92
11.3	Summary of Comparisons of Clausing's Macroscopic Theory to Data	95
12.	CONCLUSIONS - THERMAL CONTACT CONDUCTANCE IN A VACUUM ENVIRONMENT	96
12.1	Low Temperature Aluminum 7075-T6 Data	96
12.2	Low Temperature Stainless Steel 17-4 PH Data	97

TABLE OF CONTENTS (Continued)

Section		Page
	12.3 Mating of Dissimilar Metals at Low Temperatures	97
	12.4 Dependence of h upon Contact Pressure	98
	12.5 Application of Contact Conductance Results to a Typical Bolted Joint	99
	12.6 Comparison of Theory to Data	100
13.	RECOMMENDATIONS FOR FUTURE VACUUM CONDUCTANCE WORK	101
	13.1 Experimental Work	101
	13.2 Analytical Work	102
14.	REFERENCES	104
15.	NOMENCLATURE	106

LIST OF ILLUSTRATIONS

<u>Figure</u>	<u>Title</u>	<u>Page</u>
2-1	Diagram of Thermal Contact Conductance Test Column	4
2-2	Thermal Contact Conductance Test Column	5
2-3	Test Blocks with Thermocouples	8
2-4	Diagram of Total Thermal Contact Conductance Test Apparatus	10
2-5	Total Thermal Contact Conductance Test Apparatus	11
2-6	Vacuum Chamber and Lid Supporting the Thermal Contact Conductance Apparatus	13
2-7	Schematic Diagram of the Test Setup for the Thermal Contact Conductance Apparatus	14
2-8	Diagram of the Surface Flatness Deviation Areas of Four Test Blocks	18
5-1	The Dependence of Contact Conductance on Contact Pressure Aluminum Roughness = 3 to 4.5 Micro-Inches	27
5-2	The Dependence of Contact Conductance on Contact Pressure Aluminum Roughness = 16 Micro-Inches	29
5-3	The Dependence of Contact Conductance on Contact Pressure Aluminum-Oil, Grease and Metal-Metal Compared; Roughness = 16 Micro-Inches	31
5-4	The Dependence of Contact Conductance on Contact Pressure Aluminum Roughness = 45 Micro-Inches	33
5-5	The Dependence of Contact Conductance on Contact Pressure Aluminum Roughness = 55 to 60 Micro-Inches	34
5-6	The Dependence of Contact Conductance on Contact Pressure Aluminum Roughness = 125 to 135 Micro-Inches	36
5-7	The Dependence of Contact Conductance on Contact Pressure Aluminum Roughness = 130 Micro-Inches; Steam, Water, and LN ₂ Coolants	37
5-8	The Dependence of Contact Conductance on Contact Pressure Stainless Steel Roughness = 6 to 8 Micro-Inches	40
5-9	The Dependence of Contact Conductance on Contact Pressure Stainless Steel - Grease and Metal-Metal Compared; Roughness = 6 to 8 Micro-Inches	41
5-10	The Dependence of Contact Conductance on Contact Pressure Stainless Steel Roughness = 17 Micro-Inches	43
5-11	The Dependence of Contact Conductance on Contact Pressure Stainless Steel Roughness = 35 Micro-Inches	45

LIST OF ILLUSTRATIONS (Continued)

<u>Figure</u>	<u>Title</u>	<u>Page</u>
5-12	The Dependence of Contact Conductance on Contact Pressure Stainless Steel Roughness = 63 Micro-Inches	47
5-13	The Dependence of Contact Conductance on Contact Pressure Stainless Steel Roughness = 100 to 125 Micro-Inches	48
5-14	The Dependence of Contact Conductance on Contact Pressure Stainless Steel (Top) Aluminum (Bottom) Roughness = 16 Micro-Inches	50
5-15	The Dependence of Contact Conductance on Contact Pressure Aluminum (Top) Stainless Steel (Bottom) Roughness = 16 Micro-Inches	53
5-16	The Dependence of Contact Conductance on Surface Roughness	55
6-1	The Dependence of Contact Conductance on Contact Pressure-- Comparison of Results at Higher Temperatures for Aluminum (I)	58
6-2	The Dependence of Contact Conductance on Contact Pressure-- Comparison of Results at Higher Temperatures for Aluminum (II)	60
6-3	Thermal Conductances of Aluminum--Log-Log Plot Showing Power Dependence on Contact Pressure	61
6-4	The Dependence of Contact Conductance on Contact Pressure-- Comparison of Results at Higher Temperatures for Stainless Steel	63
6-5	Thermal Conductance of Stainless Steel--Log-Log Plot Showing Power Dependence on Contact Pressure	64
7-1	Log-Log Plot of Thermal Conductance at Low Temperatures-- Aluminum 7075-T6	67
7-2	Log-Log Plot of Thermal Conductance at Low Temperatures-- Stainless Steel 17-4 PH	68
8-1	Cross-Section of a Bolted Joint	70
8-2	Thermal Conductance Across a Bolted Joint	70
9-1	Constriction of Heat Flow from Cylinder into Macroscopic Contact Area	74
9-2	Rotational Semi-ellipsoid Surrounding Circular Spot of Radius a	81
11-1	Clausing's Macroscopic Constriction Theory Compared to Clausing's Data for Aluminum 2024-T4	90
11-2	Clausing's Macroscopic Constriction Theory Compared to Clausing's Data for Stainless Steel 303	91

LIST OF ILLUSTRATIONS (Continued)

<u>Figure</u>	<u>Title</u>	<u>Page</u>
11-3	Clausing's Macroscopic Constriction Theory Compared to DACO Low Temperature Data for Aluminum 7075-T6	93
11-4	Clausing's Macroscopic Constriction Theory Compared to DACO Low Temperature Data for Stainless Steel 17-4 PH	94

LIST OF TABLES

2-1	Measurements of the Surface Flatness Deviations of Four Test Blocks	18
6-1	Conversion Table for Hardness of Specimens Used by Investigators of Contact Conductance	65

1. INTRODUCTION

This report presents thermal contact conductance data and theory for conditions simulating deep space.

Heat flowing across (perpendicular to) two metallic surfaces in contact results in a temperature difference across the interface. The heat flux across an interface divided by that temperature difference is the thermal contact conductance.

To design systems to operate in space, knowledge of accurate values of thermal conductance is necessary. For example, temperatures of many electronic components must not exceed 160°F. Components are kept cool by bolting their boxes to liquid-cooled plates. In another example, heat must be prevented from entering the liquid hydrogen and oxygen fuel tanks. As heat enters the tanks through metallic joints, boiloff of fuel will occur. Thus at both high and low temperatures, knowledge of the ability of metallic joints to transfer heat must be known. A measure of that ability is the joint's thermal conductance.

For joints at temperatures below 1000°F, radiation heat transfer is negligible. Heat is conducted across joints in a vacuum primarily by metal-to-metal contact.

There are seven major and three minor parameters upon which thermal contact conductance depends (Reference 1). Conductance depends strongly upon:

1. Ambient (atmospheric) pressure.
2. Contact pressure.
3. Thermal conductivities of mating materials (temperature dependent).
4. Hardnesses of mating materials (temperature dependent).
5. Elastic moduli of mating materials (temperature dependent).
6. Roughnesses of mating surfaces.
7. Flatness deviations of mating surfaces.

Conductance depends less predictably upon:

1. Orientation of mating surface lays.
2. Direction of heat flow between dissimilar metals.
3. Length of time in contact (not studied in this report).

The first five sections of this report will present new, low temperature (-150°F to -250°F) values of contact conductance. Materials tested were aluminum 7075-T6 and stainless steel 17-4 PH. Vacuum conditions were from 10^{-5} to 10^{-6} torr. Contact pressures varied from zero to 1000 psi. Surface roughnesses ranged from .4 to 135 micro-inches. The author believes these data are the first reported for structural materials at low temperatures.

In Sections 6 and 7, the dependence of thermal conductance upon contact pressure is considered. Both high and low temperature data are plotted as a function of pressure. High temperature data were obtained from the literature. Low temperature data were selected from among the results presented in Section 5. Mathematical relationships between contact conductance and contact pressure are produced from the graphs.

In Section 8, the average contact conductance is calculated for a bolted joint using the results from Sections 6 and 7. The bolt and nut hold two aluminum flat plates together, across which heat is passing. The relations between contact pressure and radius from bolt axis were obtained from the literature. Average contact conductances are calculated for high and low temperature bolted joints in a vacuum.

The final three sections of this report deal with the theories of thermal contact conductance. In Section 9, Holm's electrical analogy to thermal constriction resistance is clarified. Section 10 is a review of Clausing and Chao's theory of thermal constriction resistance, which was based on Holm's work. In Chapter 11, contact conductance data are compared to Clausing and Chao's predictions. The materials used are aluminum and stainless steel. Comparisons are made for high temperature and low temperature contacts.

2. TEST EQUIPMENT

2.1 Basic Thermal Contact Conductance Test Column

The thermal contact conductance apparatus consisted essentially of a heating head, two cylindrical test specimen blocks, and a cooling head. A diagram of the thermal contact conductance test column is shown in Figure 2-1, and a photograph is shown in Figure 2-2.

2.1.1 Heating Head

The heating head consisted of a 2-inch diameter cylinder of 7075-T6 aluminum. Around this cylinder was wrapped a double layer of 100 turns of #16, B and S, Tophet A, glass-covered resistance wire. The resistance of the wire was measured at approximately 16 ohms.

2.1.2 Test Blocks

Located below the heating head were the two cylindrical test blocks, each of which was 2.0-inches in diameter and 1.0-inch thick.

There was a total of 10 sets of specimens; five of 7075-T6 aluminum, and five of 17-4 PH stainless steel.

Both the contact surface and the reverse surface of each test block were finished on a standard Thompson stone grinder. The grinding process resulted in a surface profile consisting of microscopic striations superimposed on a wavy macroscopic profile.

The surface roughnesses of the contact surfaces ranged from approximately 3 micro-inches to 135 micro-inches, rms, measured perpendicular to the surface lay (grain). Roughness measurements were made using a Micro-metrical Profilometer. The roughness value selected was an average of several passes made in the same direction with respect to the surface lay, only spaced over the entire contact surface. Similar measurements were made in the direction parallel to the surface lay. Roughness values over the entire surface, in any particular direction, were usually about the same, if occasional scratches were neglected.

M-19312A

**DIAGRAM OF
THERMAL
CONTACT
CONDUCTANCE
TEST COLUMN**

(X = THERMOCOUPLE)

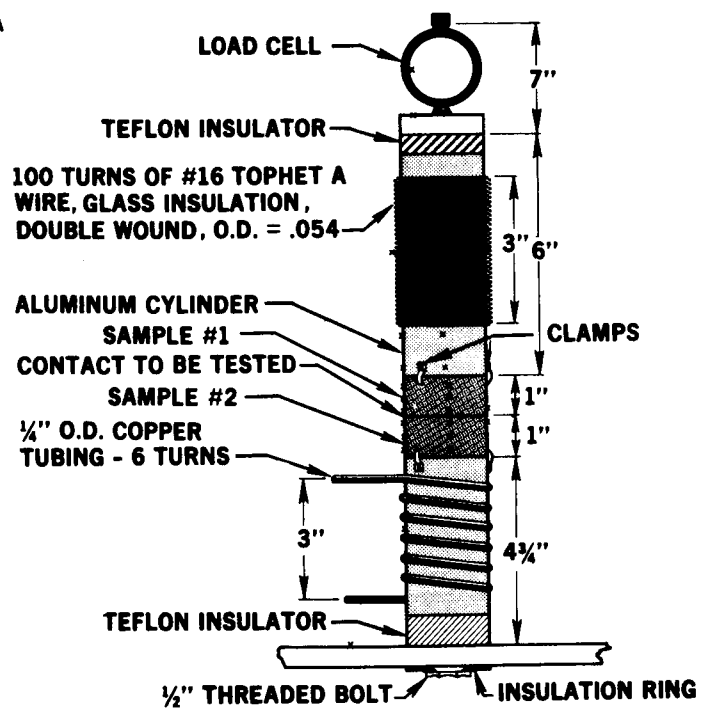
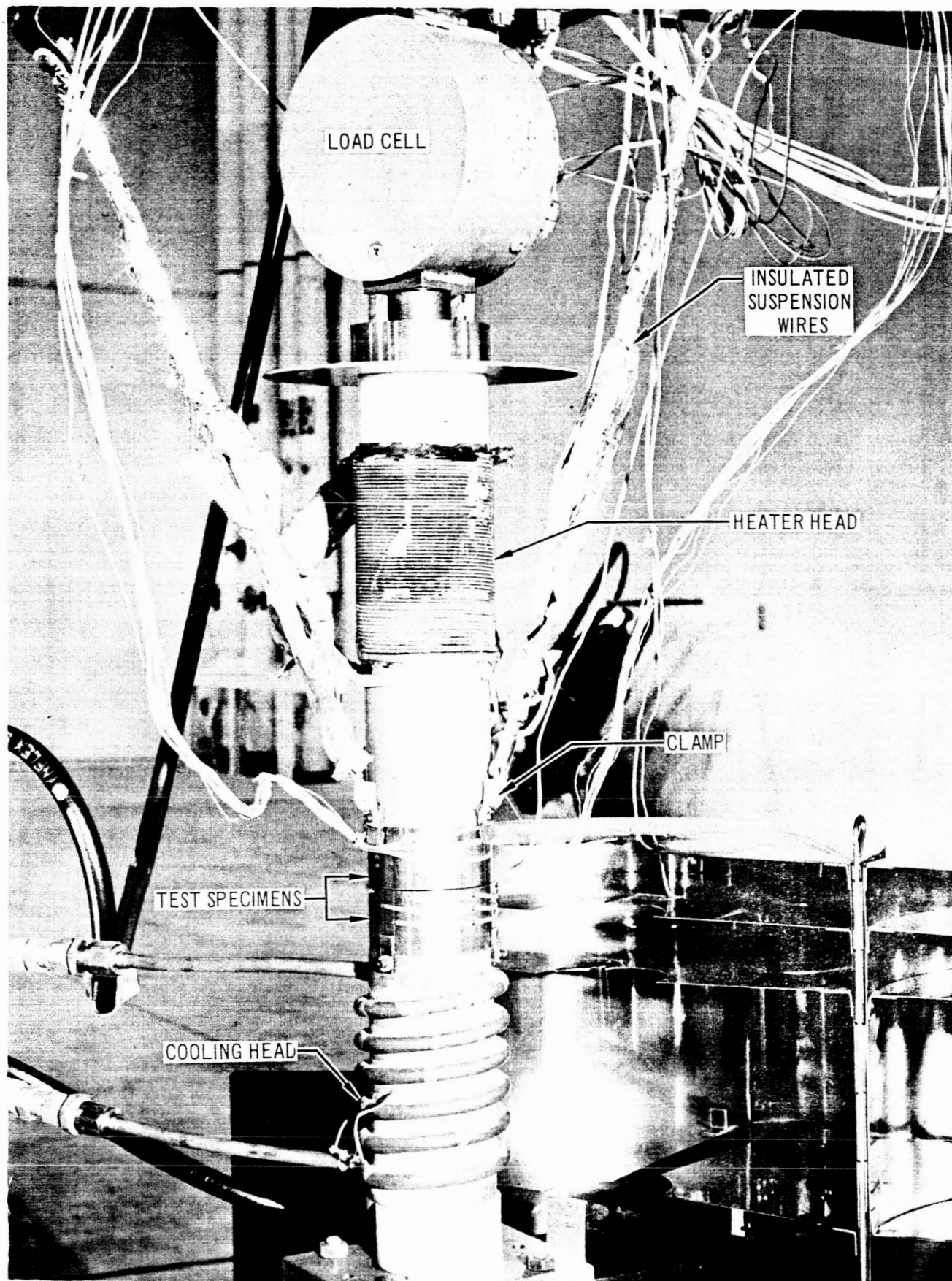


FIGURE 2-1



THERMAL CONTACT CONDUCTANCE TEST COLUMN

FIGURE 2-2

All possible efforts were made to maintain the surface flatness deviation from exceeding 200 micro-inches, as measured by a height gauge on a flat marble table. Test blocks were often ground two or three times in the attempts to achieve this flatness. As the results indicate, however, this desired flatness could not always be achieved.

The method which was used to measure the surface flatness was to zero the gauge with the ball indicator at the center of the test surface. Deviations from surface flatness could be estimated to the nearest 0.00005 inch or 50 micro-inches. With the test block held stationary, the ball gauge was moved across the surface in two mutually perpendicular directions, and then around a circular path near the edge of the contact surface. The maximum deviation from the zero reading was recorded. This procedure was applied to both surfaces of the test block.

In addition to the test specimens being ground flat, the upper and lower surfaces of both the heating head and the cooling head were ground to about a 200 micro-inch flatness deviation.

To verify that our test specimens were, in fact, 7075-T6 aluminum and 17-4 PH stainless steel, a Douglas Company spectrographic analysis and a hardness test were performed on both materials. The composition for 7075-T6 aluminum was found to have 5.70 percent zinc and a small percentage of other metals; its hardness was 91 on the Rockwell B scale. The composition of 17-4 PH stainless steel was found to have 16.55 percent chromium and 4.42 percent nickel; its hardness was 35.1 on the Rockwell C scale (Reference 2). These data verified that the materials used were 7075-T6 aluminum and 17-4 stainless steel.

Each test block contained seven chromel constantan thermocouples. Four of these were located on the cylindrical surface and three were located on the axis of each test block. The distances of the thermocouples from the test surface were approximately 1/2-inch, 1/8-inch, and 1/16-inch. The side-mounted surface thermocouples were composed of #26 gauge wire and the center thermocouples, inserted at a later date, were composed of #36 gauge wire. The side-mounted surface thermocouples were staked

into 1/16-inch deep and 0.037-inch diameter holes; the center thermocouples were inserted into 1.0-inch deep, 0.025-inch diameter holes containing wet, silver-impregnated, epoxy cement of high thermal conductivity. The center thermocouples, which were installed at a later date, agreed in output to 0.1°F with the side-mounted surface thermocouples for tests conducted in an isothermal environment.

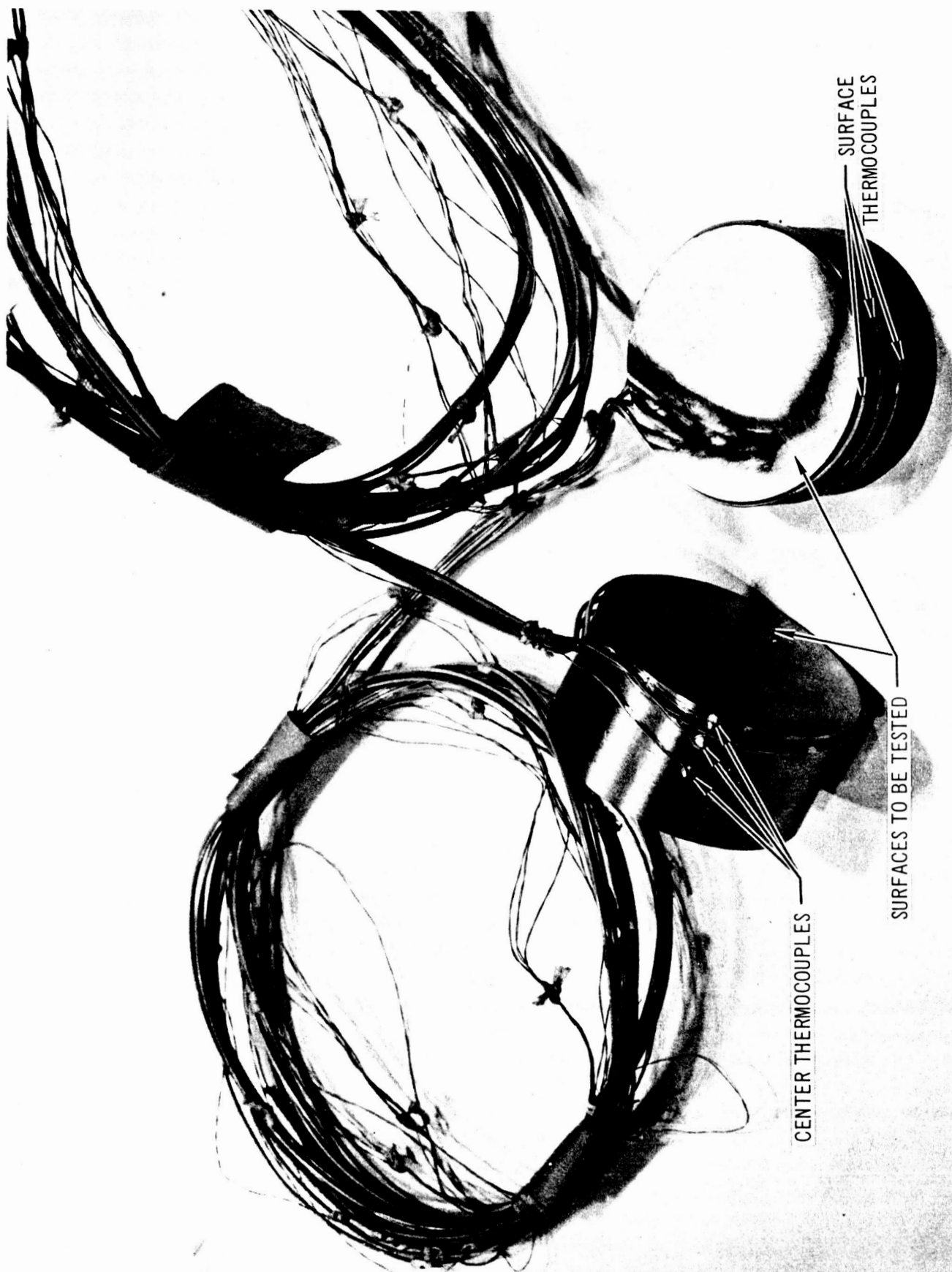
The side-mounted and the center thermocouples were insulated with nylon. The side-mounted surface thermocouples were wrapped around the circumference of the test specimen for approximately 1-inch before going to the terminal board. Figure 2-3 shows the specimens and the thermocouples attached to them.

The accuracy of the side-mounted thermocouples were measured previously in the Douglas Temperature Standards Laboratory (Reference 3) over a wide range of temperatures for tests conducted in an isothermal environment (+300°F to -320°F) to approximately 0.1°F according to NBS tables.

Three clamps spaced 120° apart held the upper test specimen to the heating head, and three clamps 120° apart kept the lower test specimen from sliding on the cooling head. The clamps were made from a low conductivity material, micarta, and contacted the specimens over small areas near the heating and cooling head interfaces. The clamps were screwed into the heating and cooling heads, as shown in Figure 2-2.

2.1.3 Cooling Head

The cooling head consisted of six turns of 1/4-inch copper tubing silver soldered to a 2-inch diameter, 4-inch high copper cylinder. Either liquid nitrogen or water could be used as a coolant. When liquid nitrogen was used, a pressurized reservoir tank was inserted in the liquid nitrogen line to eliminate gas bubbles from entering the cooling head coils. Gas bubbles previously had greatly changed the heat transfer ability of the cooling coils and affected the temperatures in the test specimens noticeably during steady state periods.



TEST BLOCKS WITH THERMOCOUPLES

FIGURE 2-3

2.1.4 Load Cell

A 5000 pound calibrated load cell was positioned above the heating head and below a steel beam used to exert pressures on the test column. Detailed information on the loading mechanism will follow in Sections 2.2 and 2.4.

2.2 Support Apparatus

(A diagram and a photograph of the combined test column and support apparatus are shown in Figures 2-4 and 2-5, respectively.)*

2.2.1 Steel Beams

The thermal contact conductance test column was positioned between two steel beams, the upper one of which acted as a lever arm and exerted a controlled load on the test apparatus column. The load was caused by a force exerted on a steel plate, attached to the end of the upper beam, by an 8-inch diameter electromagnet which was separated approximately 0.320-inch from the plate. The electromagnet was water cooled and was operated continuously without vibration or fluctuation up to specimen contact pressures of 1000 psi.

2.2.2 Steel Ball

In order to achieve axial loads on the test column, a steel ball was positioned between the lever arm and the load cell. The steel ball made contact with the steel beam and sat in the hemispherical cavity of the bolt head attached to the load cell immediately below it. The axis of the load cell bolt was aligned with the axis of the test column.

2.2.3 Suspension Wires

To insure that no residual air molecules were trapped in the interface between the specimens during the process of evacuation, three suspension wires supported the upper half of the test column to the lever arm. This device permitted a small (0.020-inch) gap to be maintained between the test blocks during the no-load condition.

*The upper specimen was inadvertently reversed for the photographs shown in Figures 2-2 and 2-5.

DIAGRAM OF TOTAL THERMAL CONTACT CONDUCTANCE TEST APPARATUS

M-19306A

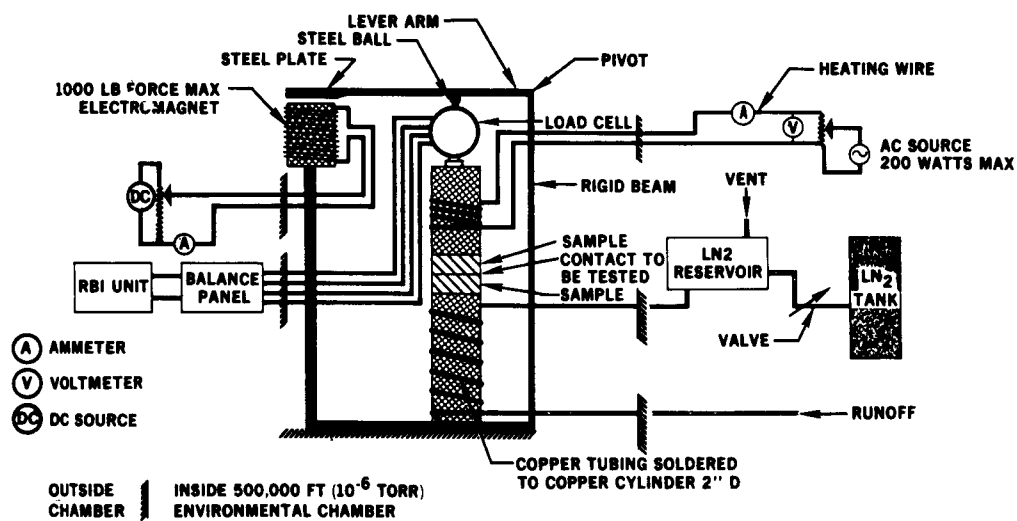
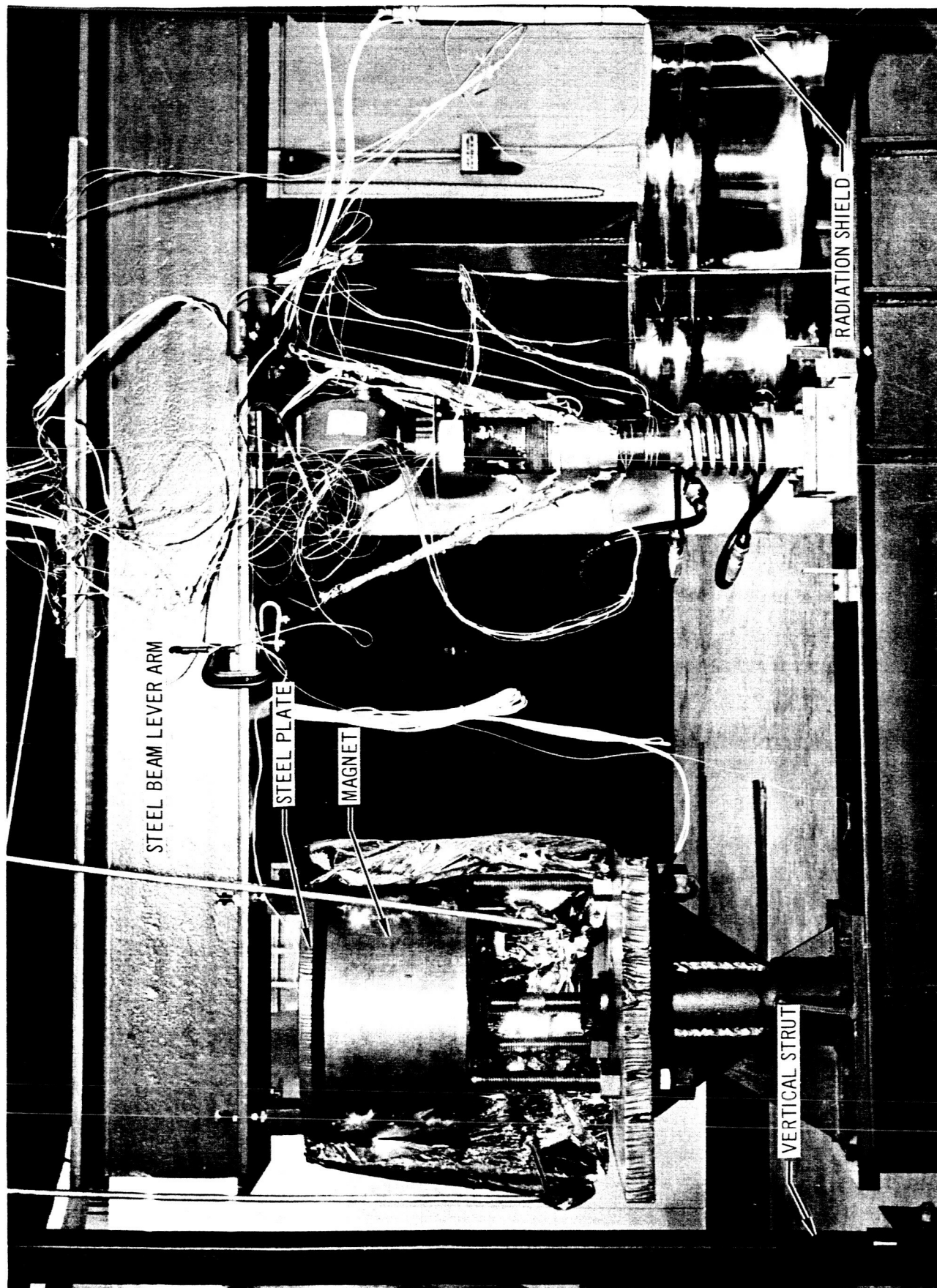


FIGURE 2-4



TOTAL THERMAL CONTACT CONDUCTANCE
TEST APPARATUS

FIGURE 2-5

2.2.4 Lid Support

The steel beam lever arm and the whole associated support structure including electromagnet were attached to the lid of the vacuum chamber by means of three vertical struts. In order to change specimens, it was only necessary to disconnect electrical lines and remove the lid from the chamber. The photograph in Figure 2-6 shows the vacuum chamber in the background and the apparatus suspended from the chamber in the foreground. The lid is resting on its support stand.

2.3 Vacuum Chamber

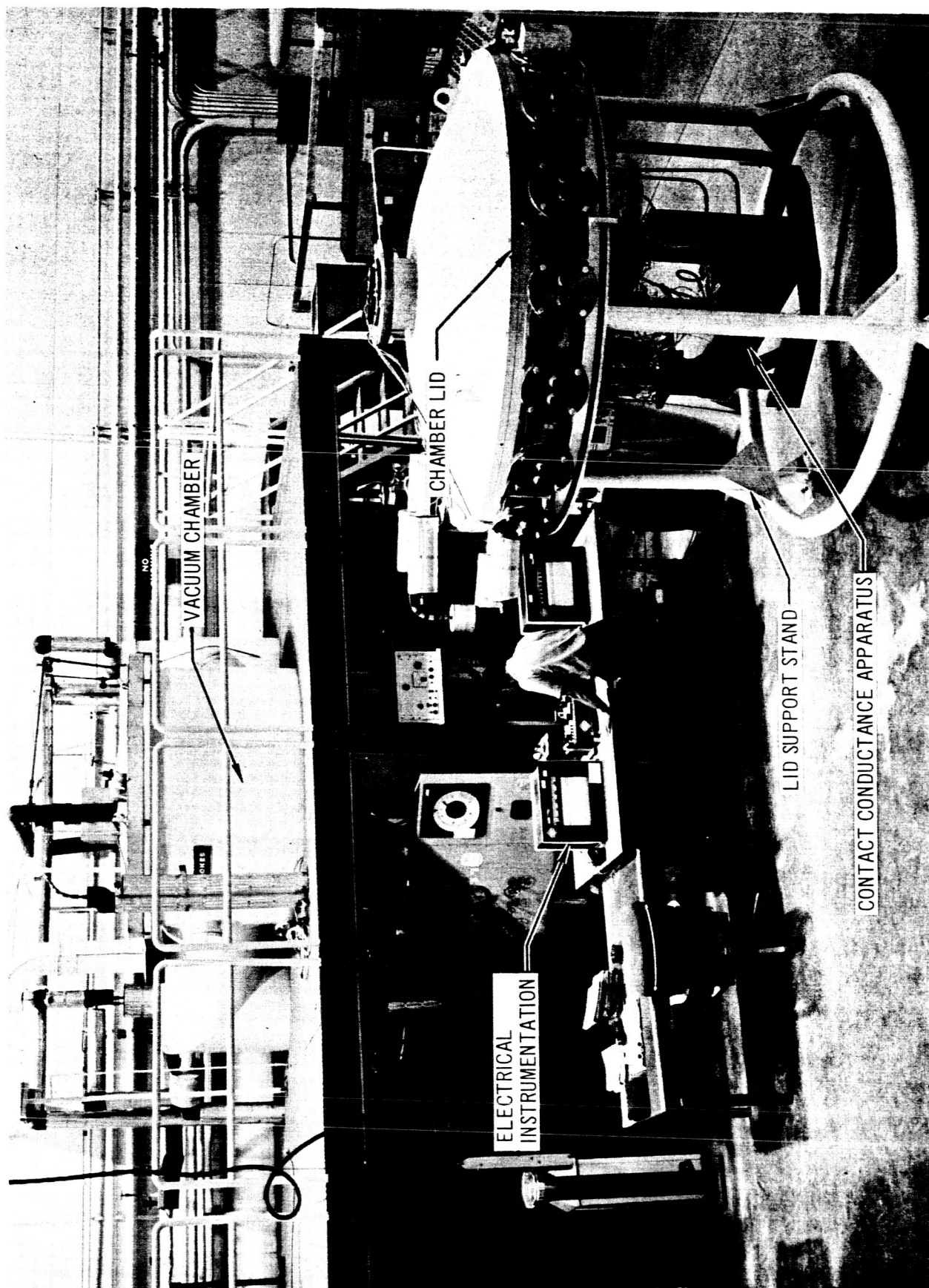
Tests on the thermal contact conductance apparatus were performed in the new five-feet by five-feet cylindrical chamber at the Douglas Space Systems Center in Huntington Beach, California. Clean and empty, the chamber is capable of producing a pressure of 2×10^{-9} torr providing its inner walls are at a temperature of -315°F . Nearly all of the data presented in this paper were obtained at ambient pressure conditions in the 10^{-6} torr range.

Testing at 10^{-7} torr or below required cold inner chamber walls which resulted in thermal contraction of the steel beam support structure. This contraction altered the critical air gap distances between magnet and plate, and between the test specimens, thereby preventing a contact pressure of 1000 psi from being obtained at the interface.

The ambient (atmospheric) pressure in the chamber was measured by a Cooke ionization gauge below 10^{-4} torr; an alphasatron gauge was used above 10^{-4} torr.

2.4 Instrumentation

(A schematic diagram of the total instrumentation, power sources and liquid flow lines is shown in Figure 2-7.)



VACUUM CHAMBER AND LID SUPPORTING
THE THERMAL CONTACT CONDUCTANCE APPARATUS

FIGURE 2-6

SCHEMATIC DIAGRAM OF THE TEST SETUP FOR THE THERMAL CONTACT CONDUCTANCE APPARATUS

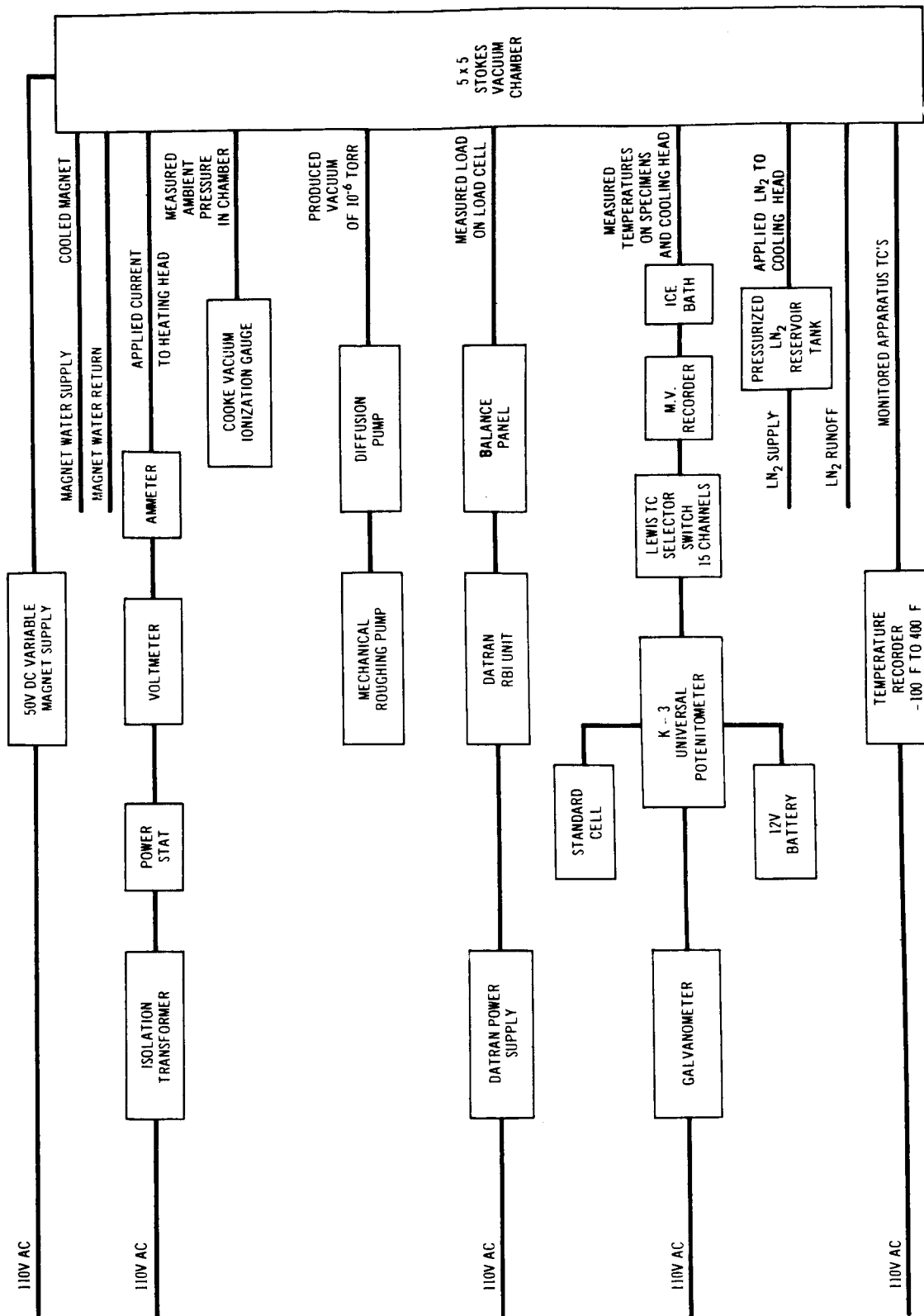


FIGURE 2-7

2.4.1 Heating Head

Alternating current power was supplied to the heating head by a variac power supply. Current to the heating head was monitored by a Weston Model 639 Industrial Analyzer and voltage was monitored by a Model 615 VTVM, Hycon, digital voltmeter. Both current and voltage measurements could be read to three significant figures.

2.4.2 Electromagnet

Power to the electromagnet was supplied by a filtered DC power supply, Electro-Model NFB, the voltage of which could be increased to a maximum of 50 volts and current to a maximum of 7 amperes. At maximum current, the electromagnet was capable of exerting a pull on a steel plate located 0.320-inch above it of 1000 pounds.

2.4.3 Load Cell

The force on the load cell was measured by a DATRAN Resistance Bridge Indicator (RBI) powered by a DATRAN Electronics Bridge Voltage Power Supply. The load cell was previously calibrated for loads up to 4000 pounds. The load was found to vary linearly with the RBI reading. During this test program, loads on the load cell seldom exceeded 3100 pounds (1000 psi at the contact interface). The load cell consisted of a four leg bridge circuit, each leg of which was a resistance wire strain gauge. A balance panel was connected in the circuit between the load cell and the Resistance Bridge Indicator to periodically calibrate the load cell. The RBI unit was continuously monitored by a technician and was not allowed to vary by more than 2 RBI units which correspond to less than 3 psi.

2.4.4 Thermocouples

The critical dependence of thermal contact conductance values on the temperature difference at the interface, ΔT , necessitated the utmost precision in determining the temperatures at the various distances from the contact interface.

Seven thermocouples were mounted on each test block. The 14 thermocouples of the test blocks were routed through the vacuum chamber port, through a chromel-constantan connector, to an ice bath. From the ice bath, copper leads were routed in parallel to a 0-10 MV Minneapolis Honeywell Brown Recorder and a Lewis switch.

The purpose of the 0-10 MV recorder was to note when steady state conditions had been reached in the test specimens. At that time, the outputs of each test specimen thermocouple could be separately measured by tapping off the emf output from the Lewis switch and measuring the emf (microvolt accuracy) by a Leeds and Northrup K-3 Universal Potentiometer.

The K-3 Potentiometer was standardized each day by means of a Weston Standard Cell and a Leeds and Northrup Galvanometer.

The output of the thermocouple on the cooling head was also measured by the same procedure since the 0-10 MV recorder could measure temperatures far below -321°F .

Using this temperature measuring system, it is estimated that the temperatures in the test block could be found to $\pm 0.25^{\circ}\text{F}$.

The remaining 12 thermocouples, located at various positions on the apparatus except the test blocks, also chromel-constantan, were routed directly to a 12 channel chromel-constantan Minneapolis Honeywell recorder. The range of temperatures which could be measured on this recorder was from -100°F to $+450^{\circ}\text{F}$. Sensitivity was estimated at $\pm 1^{\circ}\text{F}$, sufficient for the purposes of monitoring the various locations on the thermal contact conductance apparatus.

2.5 Flatness Deviation

After the tests were completed, the flatness deviation was measured in detail for two sets of specimens, one set of aluminum 7075-T6 and one set of stainless steel 17-4 PH. The roughnesses of both sets were approximately 17 micro-inches perpendicular to the surface lay. The contact conductance data obtained from these specimens are compared to theoretical predictions in Section 11.

To obtain the surface flatness deviation, each of the contact surfaces of the four test blocks was divided into 16 smaller areas as shown in Figure 2-8. The instrument used to measure the flatness deviation was Merz Electronic Gauge, Model S-48 from which could be read height changes to the nearest 5 micro-inches.

The specimen was mounted on a flat marble table and the steel ball of the height gauge was zeroed in the center of the specimen. The heights of the 16 areas were measured in consecutive order at a location approximately in the center of each of the areas. The results are shown in Table 2-1.

The Merz gauge indicated a maximum deviation of about 300 micro-inches for each of the aluminum test surfaces and about 200 micro-inches for each of the stainless steel test surfaces. These deviations are greater than those listed in Tables 5-2 and 5-10 for the same test blocks before testing. The deviations before testing were, however, measured on a height gauge accurate only to 50 micro-inches.

3. DATA PROCUREMENT

3.1 Test Program

3.1.1 Original Test Program

The original test program was planned for the mating of five sets of aluminum specimens and five sets of stainless steel specimens. The roughnesses of each set were to be approximately 7, 16, 32 and 125 micro-inches (rms). Only specimens of similar roughnesses were to be mated. Mating was to be done first with contact surface lays perpendicular, then parallel. Liquid nitrogen was to be the coolant. Because tests were conducted on a 24 hour-per-day basis, the original test program was completed ahead of schedule. This allowed the opportunity for obtaining thermal contact conductance values under conditions of different mating combinations and the changing of certain other parameters previously held constant.

**DIAGRAM OF
THE SURFACE
FLATNESS
DEVIATION AREAS
OF FOUR TEST
BLOCKS**

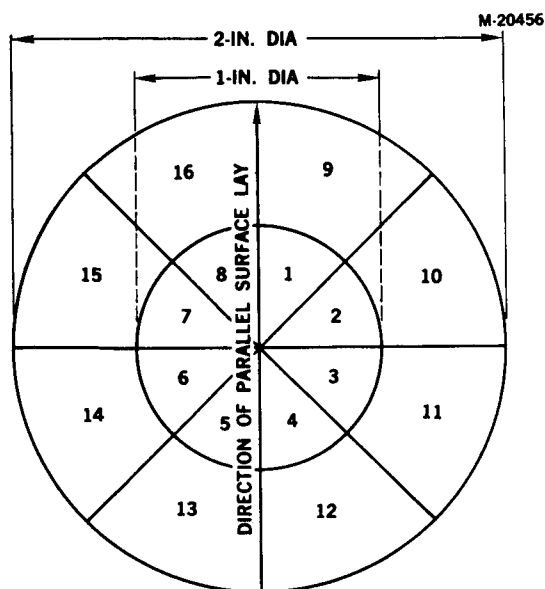


FIGURE 2-8

MEASUREMENTS OF THE SURFACE FLATNESS DEVIATIONS OF FOUR
TEST BLOCKS *

TABLE 2-1
All Units in Micro-Inches

Area Number	Aluminum 7075-T6 Top Test Block (Compare To Figure 5-2)	Aluminum 7075-T6 Bottom Test Block (Compare To Figure 5-2)	Stainless Steel 17-4 PH Top Test Block (Figure 5-10)	Stainless Steel 17-4 PH Bottom Test Block (Compare to Figure 5-10)
1	+20	-30	-40	-15
2	-10	-55	-50	-40
3	-40	-40	-50	-30
4	-90	+15	-20	-50
5	-60	+60	+50	+10
6	-10	+100	+40	+25
7	+20	+85	+30	+35
8	+20	+30	+10	+20
9	+60	-100	-160	-50
10	-40	-160	-140	-150
11	-120	-150	-80	-150
12	-220	+40	-20	-100
13	-180	+180	+45	-150
14	-40	+160	+70	+70
15	+20	+140	-10	+100
16	+90	0	-90	+30

* Temperature approximately 77°F. Roughness approximately 17 micro-inches.
Measurements taken after testing. Zero reading is at the center of the specimen in
all cases. Plus sign means elevation; minus sign means depression.

3.1.2 Extended Test Program

Tests not originally planned, but which were also completed, were the effect on thermal contact conductance of:

1. Inserting a thin layer of Dow Corning 1280 silicone grease at the contact interface.
2. Inserting a thin layer of Dow Corning 510 silicone oil at the contact interface.
3. Using water as a coolant with several sets of specimens, the purpose of which was to note the effect of increasing the interfacial temperature by several hundred degrees, all other variables remaining nearly constant.
4. Mating a stainless steel block with an aluminum block and then reversing the specimens to observe a reported dissimilar metal effect (Reference 4) that the contact conductance may depend on the direction of heat flow.

3.2 Test Procedures

3.2.1 Preparation of Specimens

The test specimen contact surfaces were carefully wiped with a soft cloth soaked in isopropyl alcohol. The surface of the upper test specimen, which contacted the heating head, and the surface of the lower test specimen, which contacted the cooling head, had a thin layer of Dow Corning 1280 silicone grease spread over them. The purpose of the grease was threefold--to increase the conductance of those interfaces not under investigation, to make them less pressure dependent, and to create optimum conditions for a one-dimensional uniform heat flow path.

3.2.2 Procedures for Obtaining Data

The start of the procedure used in obtaining data was to place the vacuum chamber lid, with the thermal contact conductance apparatus supported beneath it, on the chamber by means of the overhead movable crane. A period of usually four hours was required to evacuate the chamber to an ambient pressure of 3 to 6×10^{-6} torr. Upon reaching this ambient pressure, current was applied to the magnet which resulted in a predetermined contact pressure being exerted on the test specimens; heat was applied to the heating head; and liquid nitrogen was permitted to flow through the cooling head. After a period of

not less than two and usually more than three hours, stable specimen temperatures were reached. The temperature of each thermocouple of the test specimen was recorded, one by one, by means of the Leeds and Northrup potentiometer. Observations of current and voltage to the heater head were made. Readings of contact pressure were made in RBI units which could be converted later to psi. The load on the specimens was then reduced to zero and the zero reading on the RBI unit was recorded. This zeroing of the load created a gap between the two specimens once again. The foregoing procedure was repeated for a new contact pressure until sufficient data were obtained to enable a plot of contact conductance versus pressure to be obtained over a wide range of contact pressures.

The test schedule was made out according to a predetermined number of contact pressure points to be reached, such that they would be spaced evenly apart to produce a graph of h versus p_c from 100 or less to 1000 psi.

3.2.3 Stability Criterion

The criterion for determining at which time stability of test specimen thermocouple temperatures were attained was that all of the temperatures on the 0-10 MV recorder should remain constant for a period of not less than thirty minutes. For the aluminum specimens, a period of from two to three hours was usually required to achieve stability; for stainless steel specimens, a period of at least three hours was required. Below contact pressures of 100 psi, the times required for reaching stability were frequently as long as six hours.

3.2.4 Procedure for Entrapping Air in the Interface

One of the minor objectives of this test program was to determine the effect of entrapping air molecules at 1 atmosphere pressure at the interface between the specimens. In Section 5 several data points are discussed where the specimen gap was closed at 1 atmosphere, the chamber evacuated to 10^{-6} torr, and then data taken. The gap between the speci-

mens was then opened for two minutes and closed again. No other parameters were changed; the original heat flux was maintained and the original contact pressure reached again. Stability was once more achieved and data for conditions of 10^{-6} torr ambient pressure at the interface was taken.

3.3 Difficulties Encountered in Controlling the Test Parameters

3.3.1 Magnet Setting

The gap between the magnet and the plate was set such that a contact pressure of 1000 psi would be attained at the contact interface after the apparatus was placed in the chamber. During the liquid nitrogen cooling process, the whole test column thermally contracted such that the magnet tended to contact the plate or "bottom out" preventing high contact pressures from being reached during testing. This problem was partially solved by setting the magnet-to-plate air gap slightly larger than that required for reaching 1000 psi outside the chamber. Even with this magnet gap setting, it was found that for some sets of specimens the magnet bottomed out before 900 psi could be reached. By increasing the electrical input to the heating head, it was found that the temperatures of the whole test column could be increased sufficiently to expand the test column and prevent bottoming out. This method had the drawback, however, of changing the mean interfacial temperature. Since available evidence in the literature (Reference 4) indicated that h depended weakly on mean temperature, a degree of latitude was permitted in using the heat flux as a controlling mechanism to increase contact pressure. This is the reason for the frequent variation in T_{mean} (arithmetic mean interface temperature) values in the results.

3.3.2 The Dependence of the Load Cell Output on Load Cell Temperature

After each set of data points consisting of 14 thermocouple readings were taken, the load was decreased to zero and the RBI reading for the no load condition was recorded. This procedure was followed because the wire resistances in the load cell were found to depend strongly on temperature. The true load was determined, therefore, by subtracting the RBI load reading from the RBI zero reading at the same temperature. Since the RBI readings were linear with load, this method of evaluating load could be used.

The temperature dependence of the load cell, which required a zeroing of the load after each data set was obtained, precluded efforts to obtain h as a function of p_c in monotonic, discrete increasing and/or decreasing steps and thus eliminated the possibility of obtaining a hysteresis curve.

4. DATA ANALYSIS

4.1 Data Reduction

The outputs of the 14 test specimen thermocouples referenced to an ice-water mixture were recorded for each contact pressure. The outputs in millivolts were converted to degrees Fahrenheit to the nearest tenth of a degree using interpolated values of the best line drawn through the graph of temperature versus emf according to the NBS tables.

The distance of each side-mounted thermocouple from the contact interface and the distance of the center-mounted thermocouple holes from the contact interface were measured to three significant figures.

4.1.1 Least Squares Program

The best straight line was mathematically plotted through the seven temperature-versus-interface-distance data points by means of a Douglas "Fables" least squares program employing a G-15 computer.

The extrapolated temperature at the contact interface of the test block, the slope of the temperature versus distance line, and the average deviation of the points from the best straight line were the program's output. The difference between the interfacial temperatures of two mated test blocks, defined as ΔT , was calculated as well as the arithmetic average of the interfacial temperatures, T_{mean} .

4.1.2 Heat Input

The heat input to the test specimens was obtained from the electrical power to the heating head, assuming a negligible loss (or gain) of heat

of the heating head and test specimens with the environment. This assumption is justified in Sections 4.2.4 and 4.2.5. The electrical power to the heating head was determined by the simple product of the current and the voltage to the heating level. The inductive reactance was calculated less than 1 percent of the heating wire resistance resulting in a phase angle of zero degrees. The resultant power in watts was converted to thermal units of BTU/hr and divided by the apparent contact area normal to the direction of heat flow, 3.14 (in)² in all cases, to yield the heat flux Q which was expressed in units of BTU/hr-ft².

4.1.3 Calculations of h

The values of the thermal contact conductance were obtained from its definition,

$$h = \frac{Q}{\Delta T} \quad (4-1)$$

where h was expressed in units of BTU/hr-ft²-°F.

The contact pressure was determined from the Resistance Bridge Indicator measurements immediately following each set of test block temperature measurements.

4.2 Error Analysis

4.2.1 Thermocouple Uncertainties

The errors in the extrapolated values of the temperatures at the interface are difficult to estimate. The accuracy of each individual thermocouple in the test blocks is estimated to be $\pm 0.25^{\circ}\text{F}$, but this accuracy was far better than the average deviation of the temperatures from the best least squares straight line.

4.2.2 Interface Temperature Uncertainties

A deviation of less than 2.0°F of the seven points from the straight line was considered good and occurred often with flat samples of aluminum. An average deviation on the order of 2°F may be judged high.

Considering, however, the differences in temperature between the side-mounted and center thermocouples located at the same distance from the interface in the same test block (which for wavy stainless steel specimens for p_c less than 200 psi were on the order of $3-10^{\circ}\text{F}$), the average deviation was judged to be satisfactory. One explanation for the disparity between center and surface thermocouples may be attributed to heat channeling into those macroscopic metal-metal contact areas due to the waviness of the surfaces. These contact areas sometimes occurred on the edge, sometimes in the center of the contact interface.

It is also possible that our loading mechanism exerted a non-uniform vertical force on the test column causing one sector of the edge of the contact interface to experience a greater pressure than another sector. To decrease the possibility of non-uniform loading, the test column and loading procedure were tested outside the chamber each day, with the specimens to be tested in their proper positions.

Test column loading up to 700 psi outside the chamber was checked from several angles of view by technicians prior to insertion in the chamber. The technicians further checked that the gap was uniform over the entire contact surface by means of ball gauges accurate to 0.001-inch. Nevertheless, unequal thermal contractions of the specimens and non-conforming, wavy contact surfaces may have caused the disparity in temperatures between the side-mounted and center thermocouples located at the same distance from the interface.

The work of Clausen (Reference 5) on the dominant effect of waviness over roughness on the thermal conductance was very apparent at low contact pressures, less than 200 psi. At these contact pressure, the greatest differences between side-mounted and center thermocouple temperatures occurred and the largest time was required to reach stability of temperatures.

4.2.3 Uncertainties in h

An estimate of maximum uncertainty in average interfacial temperature differences above a contact pressure of 300 psi would be 2°F for aluminum and 3°F for stainless steel, based on deviation of the data points from the best least squares straight line.

An estimate of the uncertainty in heat input to the heating head would be of the order of 2 percent at most. These errors resulted from reading the third significant figure on the AC ammeter and voltmeter.

Following standard error analysis procedures,

$$\left| \frac{dh}{h} \right| = \left| \frac{dQ}{Q} \right| + \left| \frac{d(\Delta T)}{\Delta T} \right| \quad (4-2)$$

The estimated uncertainty in h for p_c greater than 300 psi is approximately 15 percent for both aluminum and stainless steel. The value of ΔT increased and the uncertainty in ΔT increased as p_c decreased. For h less than 300 psi, the uncertainty is estimated to be 20 percent for both aluminum and stainless steel.

4.2.4 Environmental Heat Gains

The estimated gain of heat from the warm 70°F walls of the chamber through three layers of aluminum-wrapped super-insulation and thence to the heating head at a temperature of -300°F was calculated to be approximately 1 percent. This calculation was based on a value of k for the three layers of super-insulation of an order of magnitude greater than that usually used in engineering calculation (2×10^{-5} BTU/ft-hr-°F) and temperature of -300°F for the whole test column (actually the test column varied from -100°F to -315°F). The effect of the polished stainless steel radiation shield around this column was also neglected in the calculation.

4.2.5 Environmental Heat Losses

At high temperatures, the heat loss from the specimens and the heating head to the environment at 70°F was calculated to be less than 0.1 percent. The value of k for the three layers of super-insulation used was 2×10^{-4} BTU/ft-hr-°F and the temperature of the test column was chosen as +250°F, the maximum temperature of the heating head with stainless steel specimens. The effect of the stainless steel heat shield, mounted on insulated teflon supports, was again neglected.

4.2.6 Support Cable Heat Losses

Heat losses from the test specimens through the support cables and then to the relatively warm upper beam of the test apparatus were estimated to be negligible because the clamps which held the specimens were composed of low conductivity micarta and contacted the specimens over a very small area. Further, the support cable was composed of a section of teflon, further preventing heat transfer from clamp to beam.

5. RESULTS

The results will be discussed in the order of the presentation of the graphs. Below each figure, the corresponding experimental data are listed in the same sequence in which the data were obtained.

5.1 Aluminum 7075-T6

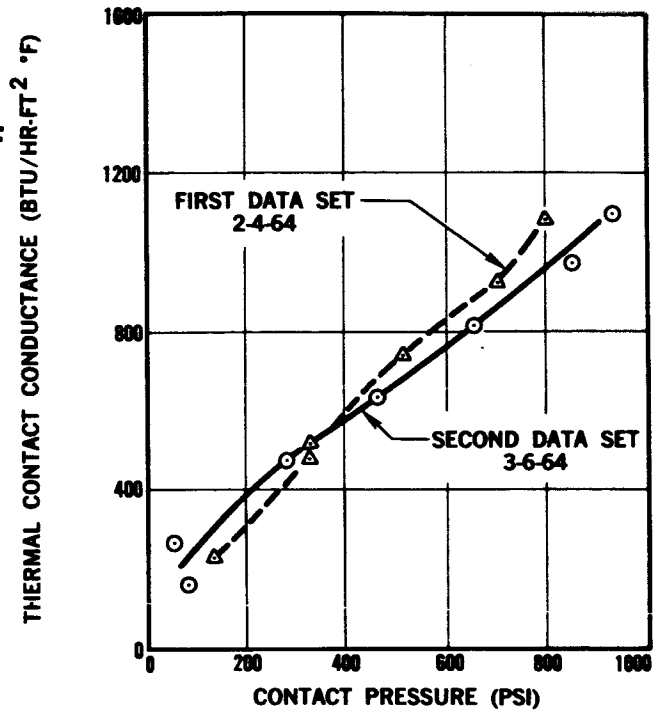
5.1.1 Specimens of 3-5 Micro-Inch Roughness

Figure 5-1 shows the results of two separate tests on the same specimen, only taken one month apart. The tests were repeated because the values of h obtained on 2-4-64 were considerably less than those obtained for the next roughest surface (Figure 5-2), contrary to theory (Reference 6). Surprisingly, the results of the second data set of 3-6-64 almost duplicated the first. It should be noted that no special orientation of mating surface lays could be defined because lapping the contact interfaces in a "figure 8" pattern to achieve a 3 micro-inch finish erased the directional grinding lay.

M-18476

THE DEPENDENCE OF CONTACT CONDUCTANCE ON CONTACT PRESSURE

ALUMINUM
ROUGHNESS =
3 TO 4.5 MICRO-INCHES



MATERIAL	SPECIMEN	ROUGHNESS - RMS (Micro-Inches)		FLATNESS DEVIATION (Micro-inches)	CHAMBER (Ambient) PRESSURE
		PERPENDICULAR	PARALLEL		
Aluminum 7075-T6	Upper	3	3	100	5×10^{-6} torr
	Lower	5	4	200	

NOTES: Liquid nitrogen used as coolant. Surfaces were lapped. No identifiable surface lay.

Order of Data Points	Contact Pressure p_c (psi)	Contact Conductance h (BTU/hr-ft ² · °F)	ΔT (°F)	T_{mean} (°F)	Orientation of Specimens and Data Set
1	280	465	22.7	-241	No orientation. Data run 3-6-64.
2	458	647	16.3	-256	
3	646	815	12.9	-262	
4	834	954	10.9	-268	
5	920	987	10.5	-270	
6	83	173	33.3	-236	
7	54	245	23.4	-225	
8	309	461	25.1	-232	No orientation. Data run 2-4-64.
9	312	488	23.7	-227	
10	512	741	16.9	-242	
11	713	953	14.6	-244	
12	802	1080	13.9	-244	
13	115	225	33.2	-224	

FIGURE 5-1

The flatness deviations for these specimens were 100 and 200 micro-inches, less than that of the next roughest surface. There is no explanation for the relatively low values of h for these specimens other than flatness deviations resulting in large areas of no metal-metal contact which were present but not observed by the method used for measuring surface flatness.

Data in Figure 5-1 show that the maximum estimate of uncertainty in conductance values of 15 percent to 20 percent was probably on the high side. Data taken a month apart on the same set of specimens differed by less than 10 percent over a wide range of contact pressures.

5.1.2 Specimens of 17-15 Micro-Inch Roughness

Figure 5-2 illustrates several interesting features of the thermal contact conductance problem. There was a marked difference in h depending on whether these specimens were mated with their surface lays perpendicular or parallel. Perpendicular mating resulted in higher values of h in this case, but as later graphs show, this was not always the case.

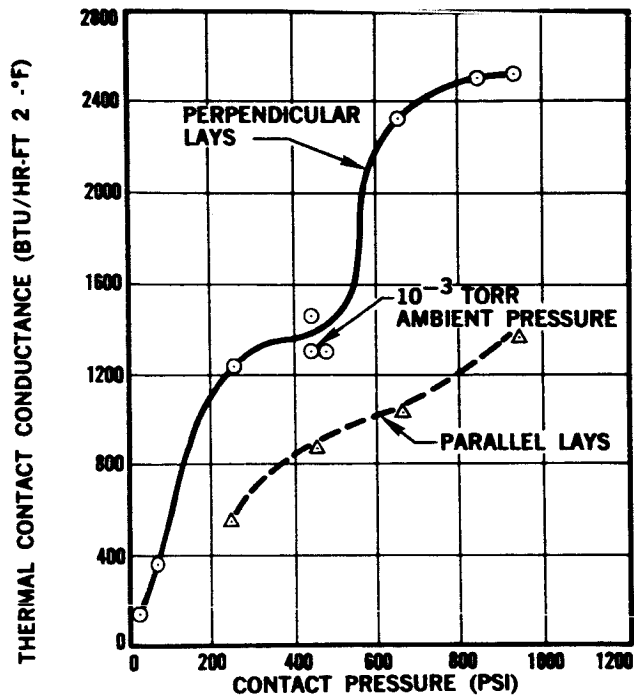
The values of h for parallel lays were close to those in Figure 5-1 for lapped surfaces of a roughness of about 4 micro-inches, while those for perpendicular lays were almost twice as great at high contact pressures. Unusually good conformity at the interface may have occurred for the perpendicular case. Rotating the specimens by 90 degrees may have changed the surface conformity of the specimen's flatness deviations. This may have resulted in a far greater influence on h than the change of orientation of surface lays alone.

One data point on the perpendicular curve was obtained by closing the gap between the specimens at an ambient pressure of 10^{-3} torr. The results are almost identical for the case of 10^{-6} torr ambient pressure, the atmospheric pressure at which these data were usually obtained.

M-18477

THE DEPENDENCE OF CONTACT CONDUCTANCE ON CONTACT PRESSURE

ALUMINUM
ROUGHNESS \approx
16 MICRO-INCHES



MATERIAL	SPECIMEN	ROUGHNESS - RMS (Micro-Inches)		FLATNESS DEVIATION (Micro-inches)	CHAMBER (Ambient) PRESSURE
		PERPENDICULAR	PARALLEL		
Aluminum 7075-T6	Upper	17	13	200	4 x 10 ⁻⁶ torr
	Lower	15	5	200	

NOTES: Liquid nitrogen used as coolant.

Order of Data Points	Contact Pressure P _c (psi)	Contact Conductance h (BTU/hr-ft ² -°F)	ΔT (°F)	T _{mean} (°F)	Orientation of Specimens and Data Set
1	484	1305	12.7	-245	Perpendicular
2	474	1310	12.7	-243	
3	73	382	42.9	-127	
4	267	1260	13.2	-221	
5	662	2330	7.2	-247	
6	856	2475	6.6	-251	
7	929	2515	6.6	-253	
8	449	1430	11.4	-238	Parallel
9	32	163	35.7	-213	
10	446	893	18.5	-237	
11	640	1025	16.2	-248	
12	933	1380	11.9	-255	
13	256	544	30.5	-220	

FIGURE 5-2

5.1.3 Specimens of 17-15 Micro-Inch Roughness--Oil, Grease and Metal-Metal Compared

In Figure 5-3, the influence on contact conductance is shown for:

1. A change of interfacial temperature using water as a coolant instead of liquid nitrogen.
2. The use of Dow Corning 1280 silicone grease at the interface.
3. The use of Dow Corning 510 silicone oil at the interface.

Note that the vertical scale is logarithmic while the horizontal scale remains linear. The specimens used in Figure 5-2 were used in Figure 5-3.

There was approximately a 3.5 fold increase of h with p_c as T_{mean} increased from -240°F to $+80^{\circ}\text{F}$ at 1000 psi. This result should be of special interest to designers of joints which will be at cryogenic temperatures. A plausible explanation of this phenomenon may be based on the changes in the thermal conductivity and the hardness properties of the mating materials as a function of temperature. (For thermal conductivity changes see Reference 7.)

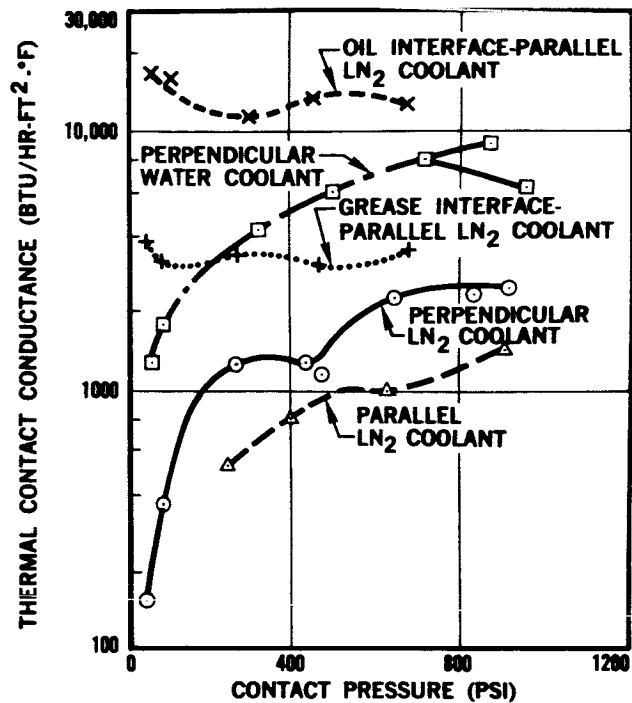
A second interesting result from Figure 3 is that at cryogenic temperatures, the effect of an interstitial grease is to greatly increase h , especially at low p_c . Using grease at the interface, it appears that over the contact pressure range from 40 psi to 700 psi, h is relatively independent of p_c . Values of h for parallel mating using grease at the interface can be compared to parallel mating for metal-metal contacts. Using grease resulted in increasing h by a factor of 3 or more for p_c less than 700 psi.

The results obtained using a thin layer of silicone oil at the interface are also shown in Figure 5-3. Generally, the values of h using oil increased to three times the values of h using grease as an interstitial material. It should be noted that the same sets of specimens were used, after being thoroughly cleaned with isopropyl alcohol, and were mated parallel as in the case of grease. Again it would appear that h is relatively independent of p_c over the range of p_c observed from 60 psi to 700 psi.

M-18475

THE DEPENDENCE OF
CONTACT
CONDUCTANCE ON
CONTACT
PRESSURE; ROUGHNESS =
16 MICRO-IN.

ALUMINUM
OIL, GREASE AND
METAL-METAL COMPARED



MATERIAL	SPECIMEN	ROUGHNESS - RMS (Micro-Inches)		FLATNESS DEVIATION (Micro-Inches)	CHAMBER (Ambient) PRESSURE
		PERPENDICULAR	PARALLEL		
Aluminum 7075-T6	Upper	17	13	200	2×10^{-6} torr
	Lower	15	5	200	

NOTES: These graphs compare contact conductances of low temperature metal-to-metal (see graph 5-2) to that of oil, grease, and high temperature metal-to-metal.

LEGEND: X - Dow Corning 510 oil at interface.
+ - Dow Corning PS-1280 grease at interface.
□ - Water used as coolant. Perpendicular mating lays.
○ - LN₂ used as coolant. Details on previous graph.
△ - LN₂ used as coolant. Details on previous graph.

Order of Data Points	Contact Pressure p_c (psi)	Contact Conductance h (BTU/hr-ft ² -°F)	ΔT (°F)	T_{mean} (°F)	Orientation of Specimens and Remarks
1	477	13,400	1.2	-243	Parallel - LN ₂ Oil at the Interface
2	664	12,900	1.3	-247	
3	306	11,600	1.6	-230	
4	60	16,900	0.5	-239	
5	89	15,800	0.5	-244	
6	315	4,080	4.1	+90	
7	509	6,000	2.8	+94	Perpendicular - Water Coolant
8	700	7,700	2.1	+90	
9	882	9,370	0.7	+75	
10	960	6,210	0.9	+73	
11	95	1,860	4.1	+77	
12	51	1,370	5.7	+79	
13	477	3,110	5.4	-242	Parallel - LN ₂ Grease at Interface
14	691	3,520	8.5	-213	
15	271	3,460	4.8	-221	
16	38	3,730	2.0	-203	
17	83	3,090	2.4	-218	

FIGURE 5-3

In summing up Figure 5-3, values of h at low temperatures (-250°F) can be increased to equal those at high temperatures ($+80^{\circ}\text{F}$) providing a thin layer of interstitial grease is used. Even higher values of h can be obtained using liquid silicone oils, but no guarantee exists that the oil will not seep out of the joint. In the cases of both the silicone oil and the silicone grease studied, there appears to be no dependency of h upon p_c in the pressure ranges from approximately 50 to 700 psi.

5.1.4 Specimens of 45-45 Micro-Inch Roughness

Figure 5-4 shows data for aluminum specimens of roughnesses of 45 micro-inches and flatness deviations of 150-500 micro-inches. The perpendicular surface lays resulted in higher conductance than the parallel except below 200 psi. The difference in values of h were never more than 100 BTU/hr-ft²-°F along the whole length of the curves. The percentage difference is from 20 percent to 10 percent as the contact pressure increases. In view of the inherent uncertainty in the data, this difference is judged not to be significant.

The values of h for parallel lays decreased from those of Figure 5-2 (16 micro-inch roughness). The flatness deviations for Figure 5-4 were approximately the same as Figure 5-2. The decrease in h compared to Figure 5-2 was, therefore, in the predicted direction according to Fenech (Reference 6), i.e., due to an increase in roughness.

5.1.5 Specimens of 60-60 Micro-Inch Roughness

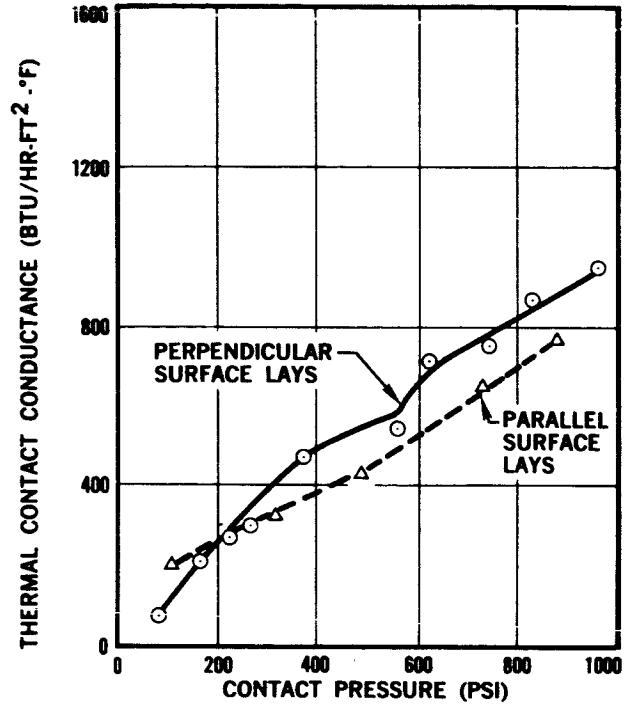
Figure 5-5 shows data which appear to contradict predictions based on theory and previous observable trends in the literature (References 5 and 6) and in Figures 5-2 and 5-4.

Even though roughness and flatness deviation measurements were greater for the test surfaces in Figure 5-5, values of h were higher than in Figure 5-4. Fried (Reference 8) has also observed this effect for magnesium specimens and attributed it to a possible "mismatch" of flatness deviations at the interface.

M-18480

THE DEPENDENCE OF CONTACT CONDUCTANCE ON CONTACT PRESSURE

ALUMINUM
ROUGHNESS =
45 MICRO-INCHES



MATERIAL	SPECIMEN	ROUGHNESS - RMS (Micro-Inches)		FLATNESS DEVIATION (Micro-Inches)	CHAMBER (Ambient) PRESSURE
		PERPENDICULAR	PARALLEL		
Aluminum 7075-T6	Upper	45	15	150	4×10^{-6} torr
	Lower	45	10	500	

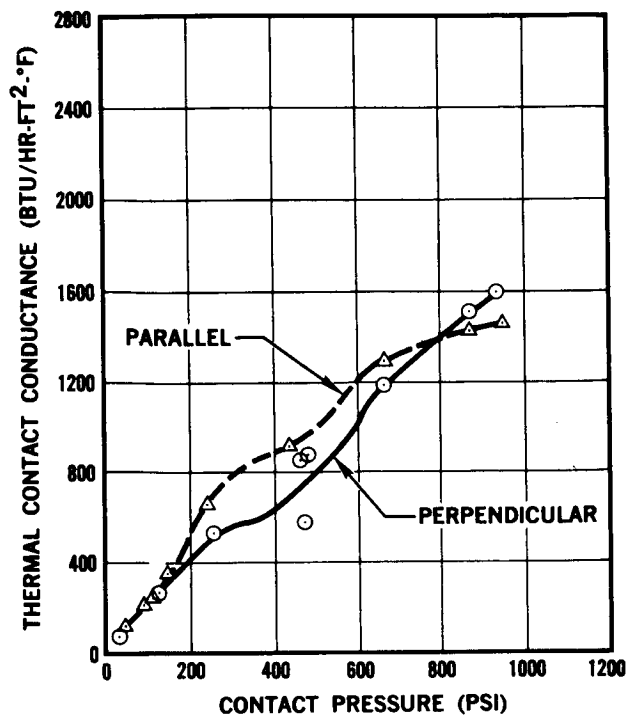
NOTES: Liquid nitrogen used as a coolant.

Order of Data Points	Contact Pressure P_c (psi)	Contact Conductance h (BTU/hr-ft²-°F)	ΔT (°F)	T_{mean} (°F)	Orientation of Specimens and Data Set
1	166	202	51.6	-145	Perpendicular
2	213	269	47.2	-232	
3	554	540	28.4	-230	
4	719	741	24.4	-229	
5	968	927	20.6	-231	
6	828	858	22.4	-229	
7	621	703	26.5	-222	
8	380	414	33.7	-231	
9	250	280	52.0	-204	
10	80	87	123.0	-130	
11	118	190	44.9	-223	Parallel
12	309	320	40.2	-222	
13	493	431	34.6	-227	
14	707	638	27.0	-230	
15	891	786	24.5	-238	

FIGURE 5-4

THE DEPENDENCE OF CONTACT CONDUCTANCE ON CONTACT PRESSURE

ALUMINUM
ROUGHNESS = 55 TO
60 MICRO-INCHES



MATERIAL	SPECIMEN	ROUGHNESS - RMS (Micro-Inches)		FLATNESS DEVIATION (Micro-Inches)	CHAMBER (Ambient) PRESSURE
		PERPENDICULAR	PARALLEL		
Aluminum 7075-T6	Upper	60	10	200	3×10^{-6} torr
	Lower	60	7	300	

NOTES: Liquid nitrogen used as coolant.

Order of Data Points	Contact Pressure P_c (psi)	Contact Conductance h (BTU/hr-ft²-°F)	ΔT (°F)	T_{mean} (°F)	Orientation of Specimens and Data Set
1	481	575	28.6	-249	Perpendicular
2	474	859	18.9	-236	
3	672	1180	13.8	-243	
4	866	1490	11.2	-245	
5	936	1600	10.5	-248	
6	465	852	19.8	-232	
7	264	518	31.8	-217	
8	25	69	105.6	-218	Parallel
9	126	260	29.3	-245	
10	251	678	24.3	-231	
11	439	910	17.9	-237	
12	668	1250	13.5	-245	
13	866	1410	11.7	-251	
14	945	1460	11.3	-253	
15	150	357	21.1	-256	
16	102	223	34.1	-238	
17	86	214	35.0	-237	
18	40	124	44.7	-234	

FIGURE 5-5

For these test specimens, values of h resulting from parallel mating are higher in the contact pressure range from 150 to 800 psi, above which the perpendicular mating values of h are greater. Below 150 psi no significant difference could be observed. The parallel and perpendicular curves would lay much closer together if the first data point in the perpendicular set in Figure 5-5 could be neglected. Unfortunately no valid reason exists for doing this.

5.1.6 Specimens of 125-135 Micro-Inch Roughness

The results of mated surfaces having the greatest roughnesses (125-135 micro-inches) are shown in Figure 5-6. Again, as in Figure 5-5, parallel lays resulted in higher conductance values but the difference, never much beyond 100 BTU/hr-ft²-°F, disappears at 700 psi.

It is of interest to note that for both parallel and perpendicular lays, h was significantly higher, 15 percent and 40 percent, respectively, for the cases in which air at 1 atmosphere was trapped in the gap compared to the cases in which the gap was exposed to ambient pressures of 10⁻⁶ torr before being closed.

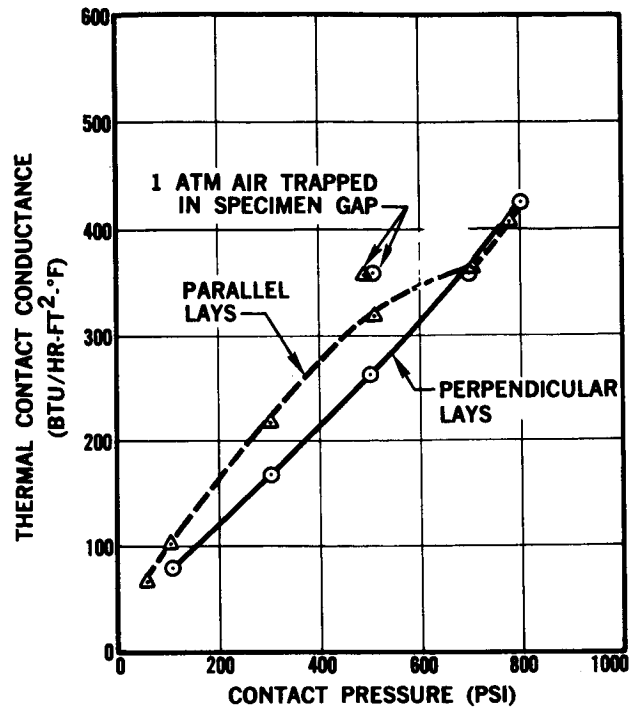
Finally, according to previous theoretical and experimental investigations, the contact conductance values of these specimens were considerably lower in magnitude, reaching only 400 BTU/hr-ft²-°F at 800 psi, than any of the previous specimens. This would be predicted on the basis of the large roughnesses and flatness deviations.

5.1.7 Specimens of 125-135 Micro-Inch Roughness--Effect of T_{mean} Change

Figure 5-7 shows the effect of changing the mean interfacial temperature, T_{mean} , of the previous set of specimens of Figure 5-6. Three data points were obtained for the case of a small amount of water used as coolant. From the temperature of the cooling head during these tests, the water was vaporized in absorbing the heat; therefore, the coolant is referred to as steam. One data point was obtained, however, using a large flow of water as a coolant.

THE DEPENDENCE OF CONTACT CONDUCTANCE ON CONTACT PRESSURE

ALUMINUM
ROUGHNESS = 125 TO
135 MICRO-INCHES



MATERIAL	SPECIMEN	ROUGHNESS - RMS (Micro-Inches)		FLATNESS DEVIATION (Micro-Inches)	CHAMBER (Ambient) PRESSURE
		PERPENDICULAR	PARALLEL		
Aluminum 7075-T6	Upper	125	25	500	3×10^{-6} torr
	Lower	135	10	200	

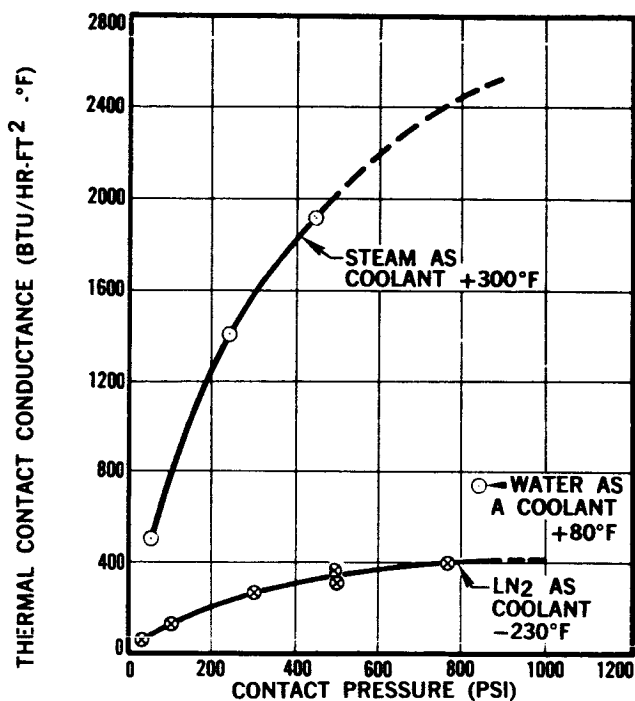
NOTES: Liquid nitrogen used as a coolant.

Order of Data Points	Contact Pressure P_c (psi)	Contact Conductance h (BTU/hr-ft ² -°F)	ΔT (°F)	T_{mean} (°F)	Orientation of Specimens
1	503	360	34.8	-245	Perpendicular
2	506	265	47.5	-234	
3	700	359	38.7	-242	
4	799	429	33.8	-246	
5	306	168	68.1	-222	
6	105	76	110.1	-191	Parallel
7	500	360	35.1	-248	
8	509	320	39.8	-246	
9	707	361	36.6	-248	
10	793	407	35.6	-247	
11	306	215	52.7	-234	
12	105	105	79.9	-214	
13	57	66	87.3	-213	

FIGURE 5-6

THE DEPENDENCE OF CONTACT CONDUCTANCE ON CONTACT PRESSURE

ALUMINUM
ROUGHNESS =
130 MICRO-INCHES;
STEAM, WATER AND
LN₂ COOLANTS



MATERIAL	SPECIMEN	ROUGHNESS - RMS (Micro-Inches)		FLATNESS DEVIATION (Micro-Inches)	CHAMBER (Ambient) PRESSURE
		PERPENDICULAR	PARALLEL		
Aluminum 7075-T6	Upper	125	25	500	3×10^{-6} torr
	Lower	135	10	200	

NOTES: Steam as a coolant for three points; Water as a coolant for one point; comparison made with same specimen configuration with liquid nitrogen as a coolant (figure 5-6).

Order of Data Points	Contact Pressure p_c (psi)	Contact Conductance h (BTU/hr-ft ² -°F)	ΔT (°F)	T_{mean} (°F)	Orientation of Specimens
1	51	520	9.9	+243	Parallel ↓
2	242	1390	4.7	+295	
3	446	1900	3.4	+299	
4	958	666	10.6	+ 79	

FIGURE 5-7

It is of interest to observe the effect (which increases with increasing p_c) of T_{mean} on h as T_{mean} increases from -230°F to $+80^{\circ}\text{F}$ and then to $+300^{\circ}\text{F}$ for a constant value of p_c . The value of h increases by a factor of approximately six over a wide pressure range.

5.1.8 Summary of Aluminum 7075-T6

Generally, the values of h decrease as surface roughness increases, although exceptions were noted in Figures 5-1 and 5-5.

Values of h at low temperatures (-250°F) for 16 micro-inch roughness specimens were found to equal values of h at high temperatures ($+80^{\circ}\text{F}$) providing a thin layer of interstitial vacuum grease was applied to the contact interface. Even higher values of h , by a factor of 3 times those using grease, were obtained using liquid silicone oil at the contact interface. In the cases of both grease and oil, there appears to be no dependency of h upon p_c in the pressure range from 50 to 700 psi.

In the cases in which air at 1 atmosphere pressure was trapped at the interface and then compared to the values of h obtained with the interface exposed to a 10^{-6} torr atmosphere, the values of h were noticeably greater, i.e., up to 40 percent.

The effect of increasing the mean interfacial temperature from -230° to $+300^{\circ}\text{F}$ for the 130 micro-inch specimens was to increase the values of h by a factor of approximately 6.

No definite conclusions could be reached concerning the effect of mating the contact surfaces with their lays perpendicular or parallel. Differences in h due to rotating the specimens from parallel to perpendicular orientations may have been caused by changes in the conformity of the large scale, surface flatness deviations (waviness).

The solution to the design of a passive thermal contact conductance control system of metal-metal contact, subject to a temperature cycle ranging from $+300^{\circ}\text{F}$ to -300°F , might be found in the large increase of h with T_{mean} as shown in Figures 5-3 and 5-7.

5.2 Stainless Steel 17-4 PH

5.2.1 Specimens of 6-8 Micro-Inch Roughness

Figure 5-8 shows the results of the smoothest stainless steel data for one data run. The vertical axis, h , is logarithmic while the horizontal is linear. An observed spread of data points was also noted by Barzelay (Reference 4) for 30-30 micro-inch specimens, his smoothest set of stainless steel specimens.

The magnitude of h indicates that the conformity of the mating surfaces must have been very good. The magnitude of h was much higher than that of aluminum specimens of similar roughness (Figures 5-1 and 5-2). The extremely low values of ΔT in Figure 5-8 together with the knowledge of the uncertainty in ΔT would tend to discredit the accuracy of these high values of h . A second test with these same specimens (results not shown) was therefore later made, and the plot of h versus p_c were spread over an even greater range than the first set, with values of h higher.

5.2.2 Specimens of 6-8 Micro-Inches Roughness--Grease and Metal-Metal Compared

In Figure 5-9, the results of both sets of data discussed in Section 5.2.1 are compared to h values having a Dow Corning 1280 grease at the interface. Note that both the vertical and horizontal axes remain linear, but the vertical axis is measured in units of $10,000 \text{ BTU/hr-ft}^2\text{-}^\circ\text{F}$.

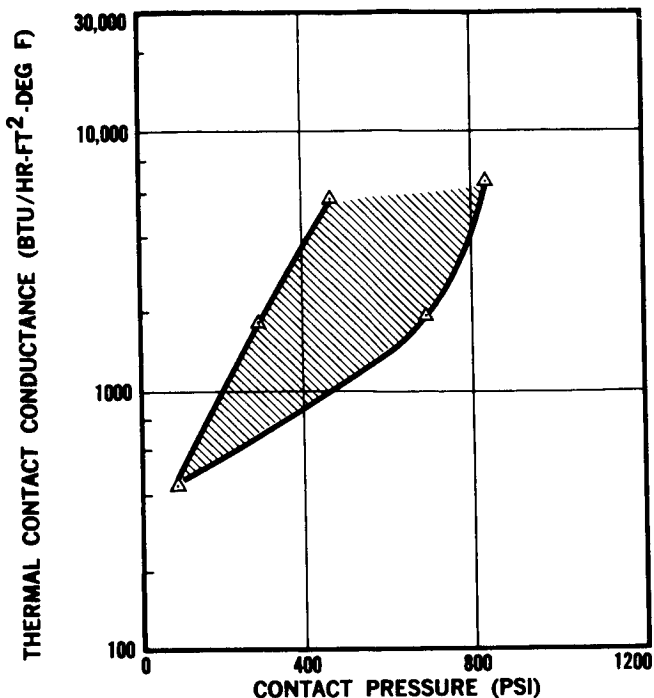
It is interesting to note that for metal-metal and for grease in the 500 psi contact pressure range a large spread occurred. Whether this occurrence reflected a real change in conductance due to a change in the conformity of the surfaces or to elastic-plastic property changes of the mating materials is as yet undecided.

Most of the data for grease were taken at higher interfacial temperatures ($+40^\circ\text{F}$) than metal-metal data (-120°F). The increase of h for

M-18472

THE DEPENDENCE OF CONTACT CONDUCTANCE ON CONTACT PRESSURE

STAINLESS STEEL
ROUGHNESS = 6 TO 8
MICRO-INCHES



MATERIAL	SPECIMEN	ROUGHNESS - RMS (Micro-Inches)		FLATNESS DEVIATION (Micro-Inches)	CHAMBER (Ambient) PRESSURE
		PERPENDICULAR	PARALLEL		
Stainless Steel 17-4 PH	Upper	6 - 8	6 - 8	200	9×10^{-6} torr
	Lower	6 - 8	6 - 8	200	

NOTES: Liquid nitrogen used as coolant. Surfaces were lapped. No identifiable surface lay.

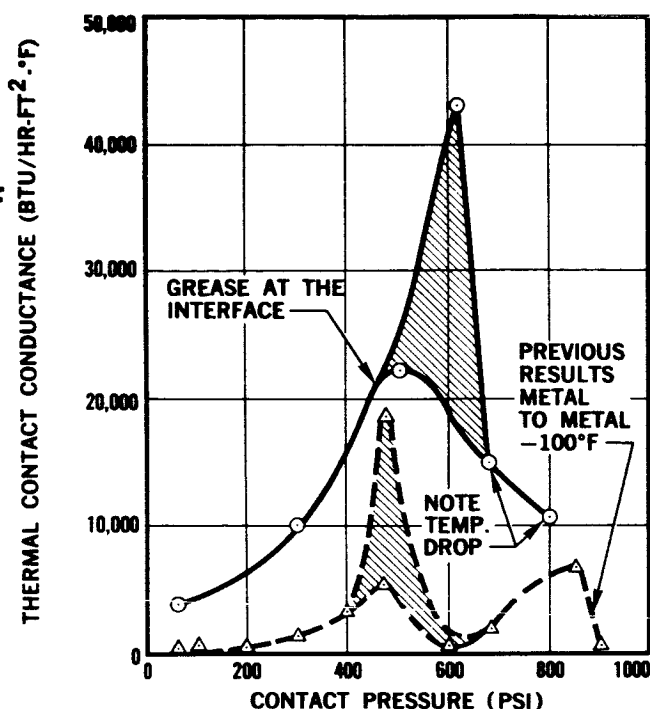
Order of Data Points	Contact Pressure p_c (psi)	Contact Conductance h (BTU/hr-ft ² -°F)	ΔT (°F)	T_{mean} (°F)	Orientation of Specimens
1	474	5700	2.0	-126	None ↓
2	691	1920	7.4	-116	
3	853	6760	2.4	-95	
4	290	1820	5.6	-132	
5	92	472	17.6	-119	

FIGURE 5-8

M-18474

THE DEPENDENCE OF CONTACT CONDUCTANCE ON CONTACT PRESSURE

STAINLESS STEEL,
GREASE AND
METAL-METAL COMPARED;
ROUGHNESS=
6 TO 8 MICRO-INCHES



MATERIAL	SPECIMEN	ROUGHNESS - RMS (Micro-Inches)		FLATNESS DEVIATION (Micro-Inches)	CHAMBER (Ambient) PRESSURE
		PERPENDICULAR	PARALLEL		
Stainless Steel 17-4 PH	Upper	6 - 8	6 - 8	200	2×10^{-6} torr
	Lower	6 - 8	6 - 8	200	

NOTES: Liquid nitrogen used as coolant. Points No. 2 and 6 were computed using center TC's only. Dow Corning No. 1280 grease was at the interface. After test was completed, it was noted that some grease spilled over surface thermocouples.

Results are compared to previous specimen configuration without grease. Two data sets of smooth stainless steel combined, one of which was graphed (Figure 5-8).

Order of Data Points	Contact Pressure P_c (psi)	Contact Conductance h (BTU/hr-ft ² -°F)	ΔT (°F)	T_{mean} (°F)	Orientation of Specimens
1	306	10,100	1.0	+35	None ↓
2	493	21,900	0.5	+42	
3	630	43,000	0.2	+44	
4	76	3,710	1.6	-1	
5	678	15,200	0.4	-73	
6	802	11,400	0.7	-41	

FIGURE 5-9

metal-metal contacts could be partly attributed to the increase in T_{mean} . The last two data points for the grease curve show a decrease in h . Note that the values of T_{mean} for these two points were less than for the first four points.

As mentioned in Figure 5-9, some grease spilled over the interface and may have contacted the surface thermocouples, further detracting from the validity of the data in Figure 5-9.

5.2.3 Specimens of 17-17 Micro-Inches

Figure 5-10 shows the results of the next roughest set of specimens, 17 micro-inches, and compares the results of perpendicular and parallel mated surfaces at low temperatures with perpendicular mating at high temperatures ($+135^{\circ}\text{F}$ average T_{mean}). Perpendicular mating resulted in higher values of h than parallel mating.

Note that there was a considerable decrease in h compared to the smoothest specimens in Figure 5-8. The nominal flatness of these specimens was 100-200 micro-inches, respectively, less than that of the smooth, lapped surfaces of Figure 5-8. Roughness, therefore, appears to play an increasingly important role for stainless steel specimens.

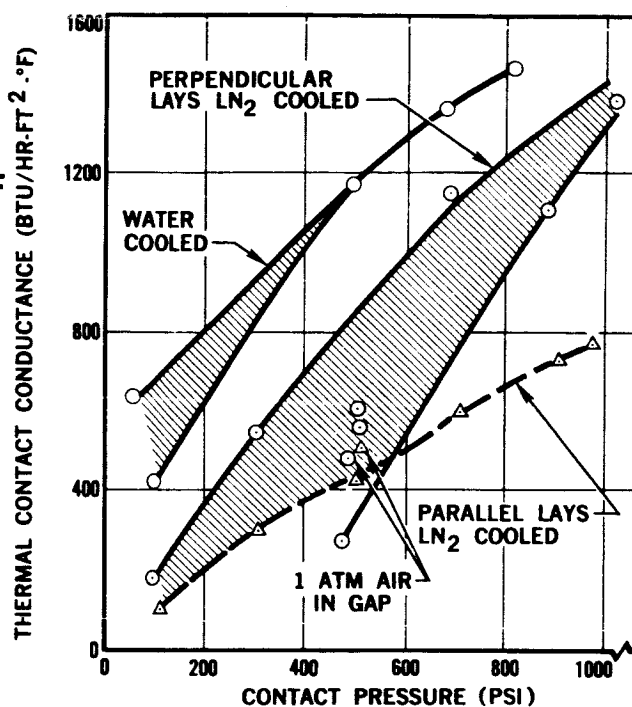
It is interesting to observe that the curve for parallel lays, using LN_2 coolant, was very nearly a straight line. The one data point in which 1 atmosphere pressure air was entrapped at the interface was 20 percent higher than the data point in which the gap was opened to an ambient pressure of 10^{-6} torr, with the same contact pressure and heat flux used.

The data for perpendicular lays, using LN_2 as coolant was spread over such a wide range as to preclude any one line connecting the data points. A region, therefore, is indicated. The first two data points again exhibit the marked decrease in conductance between 1 atmosphere air trapped in the interface and the case in which the surfaces were exposed to an ambient pressure of 10^{-6} torr for several minutes.

M-18466

THE DEPENDENCE OF CONTACT CONDUCTANCE ON CONTACT PRESSURE

STAINLESS STEEL
ROUGHNESS =
17 MICRO-INCHES



MATERIAL	SPECIMEN	ROUGHNESS - RMS (Micro-Inches)		FLATNESS DEVIATION (Micro-Inches)	CHAMBER (Ambient) PRESSURE
		PERPENDICULAR	PARALLEL		
Stainless Steel 17-4 PH	Upper	17	5	100	3×10^{-4} torr
	Lower	17	7	200	

NOTES: Liquid nitrogen used as coolant and water used as a coolant.

Order of Data Points	Contact Pressure pc (psi)	Contact Conductance h (BTU/hr-ft²-°F)	ΔT (°F)	T_{mean} (°F)	Orientation of Specimens
1	490	485	26.0	-124	LN ₂ Perpendicular
2	490	274	47.7	-111	
3	694	1090	12.7	-68	
4	894	1000	14.3	-86	
5	1034	1370	11.1	-86	
6	298	523	21.9	-68	LN ₂ Parallel
7	102	170	42.9	-80	
8	503	541	22.8	-91	
9	503	590	21.0	-93	
10	500	504	25.2	-119	
11	500	413	30.6	-110	Water - Perpendicular
12	699	580	25.0	-96	
13	898	725	21.4	-97	
14	971	775	19.4	-103	
15	302	299	38.8	-114	
16	107	105	70.3	-111	
17	500	1150	9.0	+151	
18	695	1300	5.7	+129	
19	800	1400	3.1	+103	
20	95	402	18.9	+142	
21	51	619	12.3	+150	

FIGURE 5-10

The last two data points for the perpendicular set, Figure 5-10, show a definite increase in conductance over the first two, even though they were exposed to ambient pressures of 10^{-6} torr and the contact pressures were the same, 500 psi. A possible explanation is that with repeated loading and unloading of the specimens, certain flatness deviations might have been altered such that better surface conformity could have resulted, a case not unlike hysteresis.

It is interesting to note the increase of h with T_{mean} for the water-cooled curve above that of the perpendicular mated LN_2 -cooled region. The increase was of the order of $600 \text{ BTU/hr-ft}^2\text{-}^\circ\text{F}$ at 500 psi, or a factor of 2 greater at higher T_{mean} . The change in T_{mean} was about 240°F . Compare this increase for stainless steel specimens with aluminum specimens of Figure 5-3. In that case the increase in h was by a factor of 3.5, the only change being an increase of T_{mean} by 320°F .

5.2.4 Specimens of 35-35 Micro-Inches Roughness

The values of h for surface roughnesses of 35 micro-inches are shown in Figure 5-11. Perpendicular mating again results in higher values of h than parallel mating. The shape of the curve, especially the inflection point near 800 psi, is of interest and may be related to elastic and plastic properties of metals under loads. That a peak occurred at 700 psi for two separate sets of data, with mutually perpendicular orientations, suggests a real phenomenon and not merely uncertainties in the data processing.

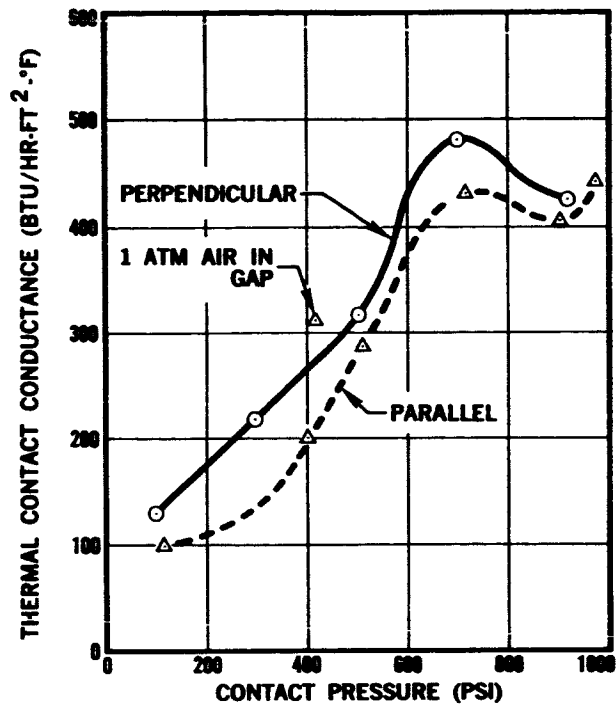
Once more the effect of entrapping air at 1 atmosphere in the interface was observed. The contact conductance, for the parallel curve at 500 psi contact pressure, decreased by 50 percent when the gap was exposed to 10^{-6} torr ambient pressure and the data point repeated.

Generally the values of h in Figure 5-11 were lower than in Figure 5-10 for all values of contact pressure.

M-18470

THE DEPENDENCE OF CONTACT CONDUCTANCE ON CONTACT PRESSURE

STAINLESS STEEL
ROUGHNESS =
35 MICRO-INCHES



MATERIAL	SPECIMEN	ROUGHNESS - RMS (Micro-Inches)		FLATNESS DEVIATION (Micro-Inches)	CHAMBER (Ambient) PRESSURE
		PERPENDICULAR	PARALLEL		
Stainless Steel 17-4 PH	Upper	35	15	200	4×10^{-6} torr
	Lower	35	16-20	50	

NOTES: Liquid nitrogen used as coolant

Order of Data Points	Contact Pressure P_c (psi)	Contact Conductance h (BTU/hr-ft ² -°F)	ΔT (°F)	T_{mean} (°F)	Orientation of Specimens
1	296	216	53.7	-60	Perpendicular
2	493	313	43.8	-100	
3	684	481	34.0	-80	
4	95	126	74.3	-70	
5	907	423	25.2	-140	
6	411	311	36.7	-102	Parallel
7	407	201	56.9	-90	
8	497	289	43.8	-93	
9	700	431	32.1	-94	
10	898	413	36.5	-90	
11	964	446	34.0	-91	
12	108	100	70.0	-11	

FIGURE 5-11

5.2.5 Specimens of 63-85 Micro-Inches Roughness

In Figure 5-12, the results of mating specimens of 65-85 micro-inch roughnesses are reported. The flatness deviations were also greater than previous specimens (see Figures 5-11 and 5-12). It should be noted that these roughness and flatness values were obtained from Micrometrical Profilecorder profiles of the surface roughness and waviness greatly magnified (10,000 X) in the vertical direction and not measured as the other specimens were using a Profilometer and a height gauge.

The data points for both perpendicular and parallel mated surfaces fall along smooth curves, with the perpendicular mated lays once again yielding the greater values of h than the parallel mated lays. The order of magnitude of the values of h are generally lower than those of Figure 5-11.

5.2.6 Specimens of 125-100 Micro-Inches Roughness

Figure 5-13 shows the results of mating the roughest set of stainless steel specimens. For the fourth consecutive time, perpendicular mated lays yielded higher values of h than parallel mated lays, except at pressures below 150 psi. At pressures above 800 psi, there was a tendency for the two curves to converge, a phenomenon observed also in Figures 5-5, 5-6 and 5-11. The magnitude of h continued to decrease compared to the less rough specimens, even though the flatness was better for these specimens than those in Figure 5-12.

5.2.7 Summary of Stainless Steel 17-4 PH

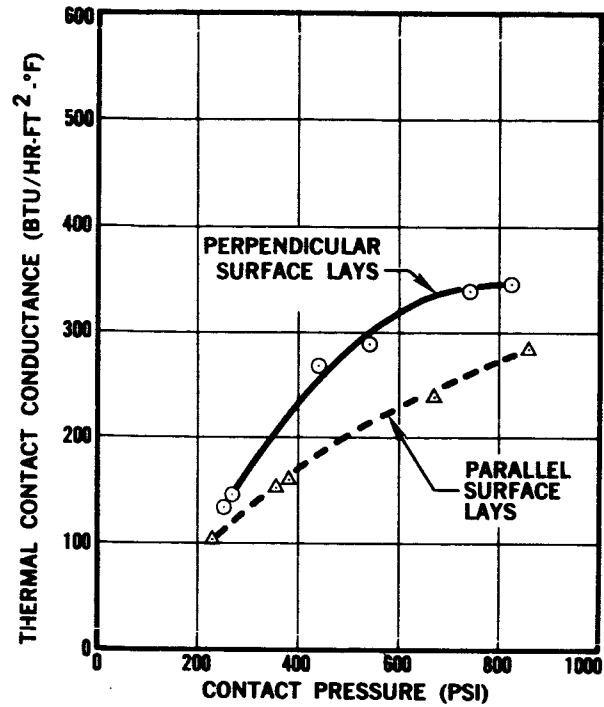
Except for the very smooth, lapped surface specimens of Figure 5-8, the values of h increase as a function of p_c in a smooth fashion (the hump in Figure 5-11 being an exception). Perpendicular mated surfaces resulted always in a higher value of h than parallel mated surfaces, a phenomenon to be discussed in Section 9.6.

As the roughness of the mated surfaces increased, regardless of the flatness of the surfaces, the values of h decreased.

M 18469

THE DEPENDENCE OF CONTACT CONDUCTANCE ON CONTACT PRESSURE

STAINLESS STEEL
ROUGHNESS \approx
63 MICRO-INCHES



MATERIAL	SPECIMEN	ROUGHNESS - RMS (Micro-Inches)		FLATNESS DEVIATION (Micro-Inches)	CHAMBER (Ambient) PRESSURE
		PERPENDICULAR	PARALLEL		
Stainless Steel 17-4 PH	Upper	63	25	300	4×10^{-6} torr
	Lower	85	85	500	

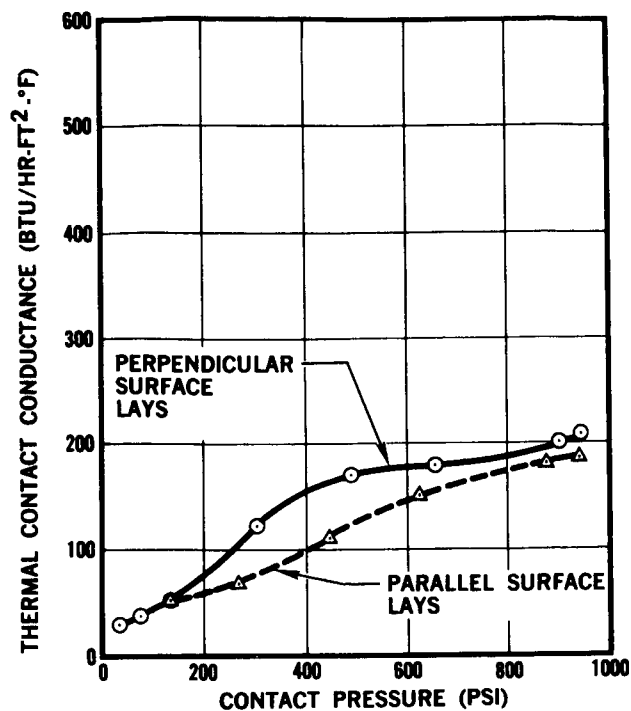
NOTES: Liquid nitrogen used as coolant. Roughness and waviness estimates from micrometrical profilometer charts (Reference 2).

Order of Data Points	Contact Pressure P_c (psi)	Contact Conductance h (BTU/hr-ft ² -°F)	ΔT (°F)	T_{mean} (°F)	Orientation of Specimens
1	242	129	113.8	-60	Perpendicular ↓
2	251	137	103.3	-40	
3	417	269	53.1	-75	
4	538	292	52.8	-10	
5	742	337	47.4	-51	
6	828	342	42.9	-56	
7	221	101	158.4	+10	Parallel ↓
8	369	164	95.7	-15	
9	376	152	69.6	-105	
10	664	238	43.0	-130	
11	856	284	36.5	-135	

FIGURE 5-12

THE DEPENDENCE OF CONTACT CONDUCTANCE ON CONTACT PRESSURE

STAINLESS STEEL
ROUGHNESS = 100
TO 125 MICRO-
INCHES



MATERIAL	SPECIMEN	ROUGHNESS - RMS (Micro-Inches)		FLATNESS DEVIATION (Micro-Inches)	CHAMBER (Ambient) PRESSURE
		PERPENDICULAR	PARALLEL		
Stainless Steel 17-4 PH	Upper	125	45	200	2×10^{-6} torr
	Lower	100	30	200	

NOTES: Liquid nitrogen used as a coolant.

Order of Data Points	Contact Pressure p_c (psi)	Contact Conductance h (BTU/hr-ft²-°F)	ΔT (°F)	T_{mean} (°F)	Orientation of Specimens
1	299	122	85.8	-64	Perpendicular
2	490	169	60.3	-110	
3	656	178	33.0	-186	
4	901	203	28.6	-192	
5	936	205	28.2	-195	
6	127	50	115.3	-109	Parallel
7	70	36	161.4	-48	
8	35	31	185.3	-4	
9	261	68	84.6	-149	
10	439	109	52.9	-172	
11	630	149	40.0	-184	
12	869	184	31.7	-198	
13	939	193	30.0	-190	
14	127	520	108.6	-127	

FIGURE 5-13

For very smooth, flat surfaces, the data spread was quite large, but it decreased with the contact pressure. Interstitial Dow Corning 1280 vacuum grease increased the value of h of the smoothest specimens by a variable factor, depending on the contact pressure and interfacial temperature.

With water used as a coolant, an increase in T_{mean} resulted. The increase in T_{mean} caused an increase in h along the complete range of contact pressures (Figure 5-10). The value of h was greater by more than a factor of 2 at $+140^{\circ}\text{F}$ than at -100°F at 500 psi.

The effect of entrapping air molecules at 1 atmosphere pressure produced an increase of h over that of exposure of the interface to 10^{-6} torr pressure by variable percentages up to 50 percent.

5.3 Mating of Dissimilar Metals

5.3.1 Stainless Steel (Top) to Aluminum (Bottom)

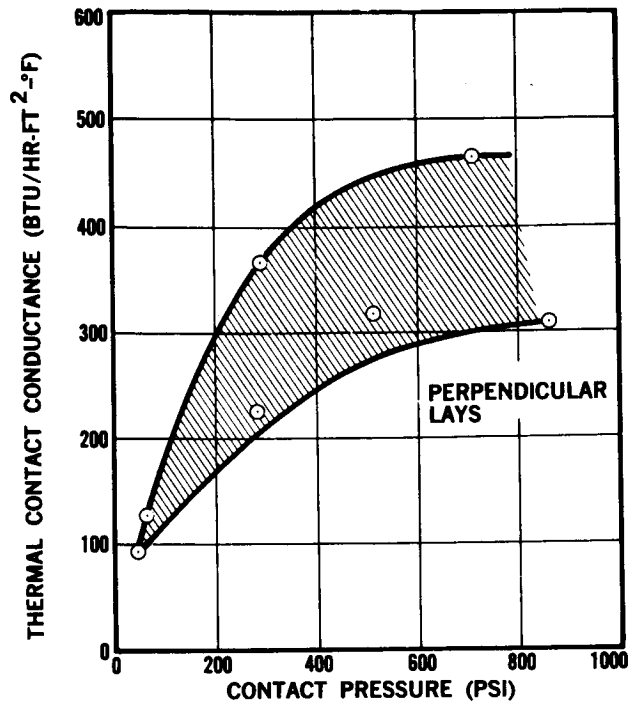
Figure 5-14 shows the results of mating a stainless steel test block of roughness 17 micro-inches, flatness deviation 100 micro-inches, with a test block of aluminum of roughness 15 micro-inches, flatness deviation of 200 micro-inches.

The values of h are considerably less than those for mating stainless steel to stainless steel (Figure 5-10) or aluminum to aluminum (Figure 5-2). The expected result would have been that these values of h would lay between those resulting from the mating of the softer and harder materials.

The shaded region in Figure 5-14 appears to remain below 500 BTU/hr-ft²-°F. The mean interfacial temperatures of the data in Figure 5-14 was about -200°F , not too different from the -240°F average temperature for the data in Figure 5-2 for aluminum specimens. The values of T_{mean} were higher (-100°F) for stainless steel specimens (Figure 5-10) which could have accounted for part of the increase of h in Figure 5-10 over that of h in Figure 5-14. Since there exists data showing a noticeable effect

THE DEPENDENCE OF CONTACT CONDUCTANCE ON CONTACT PRESSURE

STAINLESS STEEL (TOP)
TO ALUMINUM (BOTTOM)
ROUGHNESS =
16 MICRO-INCHES



MATERIAL	SPECIMEN	ROUGHNESS - RMS (Micro-Inches)		FLATNESS DEVIATION (Micro-Inches)	CHAMBER (Ambient) PRESSURE
		PERPENDICULAR	PARALLEL		
Stainless Steel 17-4 PH	Upper	17	5	100	1×10^{-6} torr
Aluminum 7075-T6	Lower	15	5	200	

NOTES Liquid nitrogen used as a coolant.

Order of Data Points	Contact Pressure p_c (psi)	Contact Conductance h (BTU/hr-ft ² -°F)	ΔT (°F)	T_{mean} (°F)	Orientation of Specimens
1	506	321	52.3	-218	Perpendicular ↓
2	703	464	35.9	-232	
3	863	310	78.3	-195	
4	299	374	67.8	-205	
5	280	229	73.0	-202	
6	60	128	58.5	-196	
7	41	94	81.2	-170	

FIGURE 5-14

on h as T_{mean} changes by 150°F , the explanation for the low values of h in Figure 5-14 could lie in the mean temperature change of the specimens.

A plausible explanation for the low values of h in Figure 5-14 might also be that poor surface conformity was obtained for these specimens, which were tested in the last days of the experimental program. While all surface cleaning measures were scrupulously observed, it must be remembered that these specimens had been previously tested at -240°F , compressed to 1000 psi many times, heated to $+250^{\circ}\text{F}$, greased and oiled and recleaned many times.

Examination at 500 psi of the temperature differences between side-mounted and center thermocouples on the stainless steel specimen show differences of 70°F for the thermocouples at the same level nearest the interface, an extremely high temperature difference. The corresponding thermocouples for the bottom aluminum specimen show a difference of 50°F . The side-to-center temperature differences diminish to the order of 8°F for stainless steel and 2°F for aluminum as the distance from the interface increases to $1/2$ -inch.

Poorest interface contact was obtained at the center of the specimens at which the largest value of ΔT was found. Surface thermocouple values of ΔT were much less, indicating that heat was conducted mainly along the outer edges of the specimens.

In the data analysis, all seven of the thermocouples of each test specimen were used to compute the extrapolated value of interfacial temperatures of each test block. The differences between center and side thermocouples should emphasize the need to place thermocouples on the sides as well as in the center of the specimens, especially for cases of mating dissimilar metals.

Another possible explanation for the low values of h in Figure 5-14, and also the poor mating at the interface, may lie in the different

thermal expansion coefficients of the different metals which were at widely differing temperatures. According to Clausing (Reference 5), macroscopic thermal contacts may move relative to each other due to thermal strains causing unpredictable changes in the contours of the mating surfaces, and therefore in the conductance.

5.3.2 Aluminum (Top) to Stainless Steel (Bottom)

Figure 5-15 shows the effect of reversing the specimens in Figure 5-14. At low contact pressures, the spread of the data points was even wider than in Figure 5-14. The range of h is slightly higher as a function of p_c , but not enough data were obtained to definitely conclude that h is higher for heat flowing in one direction or the other.

It should be noted that the T_{mean} of Figure 5-15 varied from -51°F to $+59^{\circ}\text{F}$ while that of Figure 5-14 was about -200°F . On this basis, it would seem that values of h in Figure 5-15 should be somewhat higher than those of Figure 5-14, providing mating orientation was the same. That h is higher in Figure 5-15 at low pressures would tend to affirm that line of reasoning. Beyond a contact pressure of 400 psi, there is, however, small difference in the shaded regions of h . If compensation is made for the differences in T_{mean} , data in Figure 5-14 would agree with data in Figure 5-15 at low contact pressures. But disagreement would be obtained at high contact pressures; that is Figure 5-14 data would be 2 to 3 times greater.

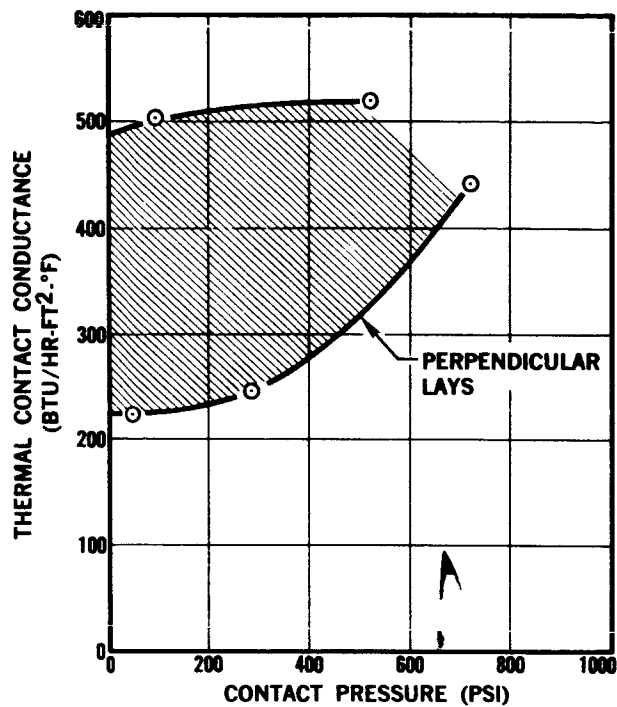
Hence, if a tentative hypothesis must be drawn on the basis of this widely spread data, it would be that, if interfacial temperatures were equal in both cases (Figure 5-14 and 5-15), values of h would be greater for the case of heat flowing from stainless steel to aluminum than from aluminum to stainless steel.

The temperature differences between side-mounted and center thermocouples at the same level were less than in Figure 5-15 than Figure 5-14. For the aluminum (top) the difference was 7°F and in the stainless steel

THE DEPENDENCE OF CONTACT CONDUCTANCE ON CONTACT PRESSURE

ALUMINUM (TOP) TO
STAINLESS STEEL
(BOTTOM)

ROUGHNESS = 16
MICRO-INCHES



MATERIAL	SPECIMEN	ROUGHNESS - RMS (Micro-Inches)		FLATNESS DEVIATION (Micro-Inches)	CHAMBER (Ambient) PRESSURE
		PERPENDICULAR	PARALLEL		
Aluminum 7075-T6	Upper	15	5	200	2×10^{-6} torr
Stainless Steel 17-4 PH	Lower	17	5	100	

NOTES: Liquid nitrogen used as a coolant.

Order of Data Points	Contact Pressure p_c (psi)	Contact Conductance h (BTU/hr-ft ² -°F)	ΔT (°F)	T_{mean} (°F)	Orientation of Specimens and Data Set
1	528	518	32.8	-25	Perpendicular ↓
2	726	441	55.1	+59	
3	286	246	68.2	+36	
4	99	504	16.1	-51	
5	48	221	34.4	-23	

FIGURE 5-15

(bottom) it was 32°F. At a half inch from the interface, the differences were 2°F for aluminum and 20°F for stainless steel. Finally, heat channeled mainly down the specimens axis.

5.3.3 Summary for Dissimilar Metals

The data in Figures 5-14 and 5-15 for dissimilar metals are insufficient to indicate any definite conclusions concerning a change in h with direction of heat flow. An order of magnitude of the values of h were obtained, however, but it must be remembered that these specimens were subject to previous tests which may have altered their surface irregularities and physical properties. An unexpected low value of h was obtained for the both cases of dissimilar metals compared to both similar metals of earlier tests.

5.4 Effect of Surface Roughnesses on Contact Conductance

5.4.1 Thermal Contact Conductance Versus Surface Roughness

In Figure 5-16, values of h are plotted as a function of the average rms surface roughness of the mating test blocks. The data, obtained from previous graphs, are shown for the case of one contact pressure only, 500 psi. The effect of hardness of the mating materials is apparent in the comparison between the stainless steel (hard material) and the aluminum (softer material) groups. The ambient pressure was in the low range of 10^{-6} torr. The orientation of the lays of the mating surfaces was perpendicular in all cases.

It is interesting to observe the higher values of h for aluminum compared to stainless steel, even though T_{mean} of aluminum was -235°F and T_{mean} of stainless steel was -100°F.

If the mating materials were at the same mean interfacial temperature, either -235°F or -100°F, the difference between the two curves would be expected to change based on evidence collected thus far regarding the dependence of h on T_{mean} .

M-19309

THE DEPENDENCE OF
CONTACT
CONDUCTANCE ON
SURFACE
ROUGHNESS

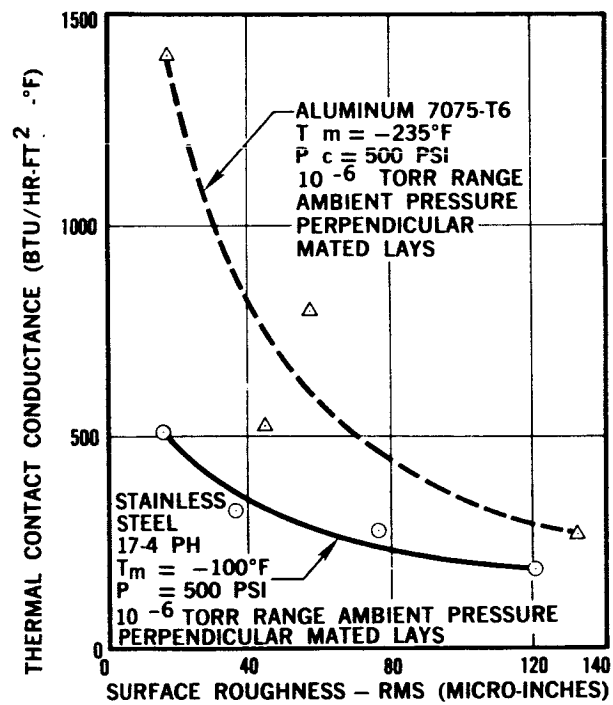


FIGURE 5-16

The slope of the conductance versus roughness curve increases negatively as the roughness decreases. The main reason for this was that the flatness deviation of the test surfaces usually decrease as the specimen was subjected to a smoother grinding operation. This means that the smoother the surface, the flatter the surface; the rougher the surface, the wavier the surface. Thus, a decrease in roughness would result in an increase in the area of the macroscopic contact surface. Furthermore, a smoother surface would result in more microscopic metal-metal contact points at those macroscopic areas already in contact.

The curve for aluminum shows a spread in data points previously discussed in Section 5. This spread is far greater than in the case of stainless steel. Nevertheless, the trend, despite the spread for aluminum, is quite clear. There is not much increase in h as roughness values, δ , decrease from 130 to 65 micro-inches. There is a greater increase in h as δ decreases from 65 to 30 micro-inches, and finally a sizable increase in h as δ decreases to 16 micro-inches.

No data for the cases of the 4 micro-inch roughness aluminum and 6-8 micro-inch roughness stainless steel were included in Figure 5-16. These data were obtained from lapped surfaces in contact, surfaces exhibiting no definite surface lay, while all the other data were for perpendicular surface lays.

Two other reasons exist for excluding the lapped surface data. First, the aluminum values of h for 4 micro-inch roughness were inexplicably low compared to the 16 micro-inch roughness values (see Figure 5-1). Secondly, the stainless steel values of h for 6-8 micro-inch surface roughness were extraordinarily high and widely scattered (see Figure 5-8).

6. COMPARISON OF REPORTED HIGH TEMPERATURE DATA

The high temperature data reported in the literature are compared in this section to high temperature data of this report. Section 6 shows

all of the data reported thus far in the literature at high temperatures for aluminum-aluminum, and stainless steel-stainless steel specimens mated in a vacuum environment in which all of the important parameters were tabulated. Furthermore, the data taken in air by Henry of MIT (Reference 10) at very high contact pressures is also listed. Finally, Table 6-1 at the end of the section converts all of the hardnesses of all the test materials to units of psi, for purposes of comparison.

6.1 Aluminum (I)

Figure 6-1 shows the results of mated aluminum test specimens in a vacuum environment. The data of Fried and Clausing lie reasonable close to the present data of the 125-135 micro-inch roughness specimens. The data of the 17-15 micro-inch roughness specimens lie above that of the majority of the points in the 100 to 1000 psi range, but the slope is about the same. At pressures below 100 psi, there was considerable scatter in the data. Neglecting Fried's 2024-T3 aluminum data, his earliest flat plate results (Reference 11), an average straight line could be drawn through the majority of the data in Figure 6-1. This line, called the "Best Line Through Most of the Aluminum (I) Data Points," is shown in Figure 6-3 as having a slope, m , of 0.88.

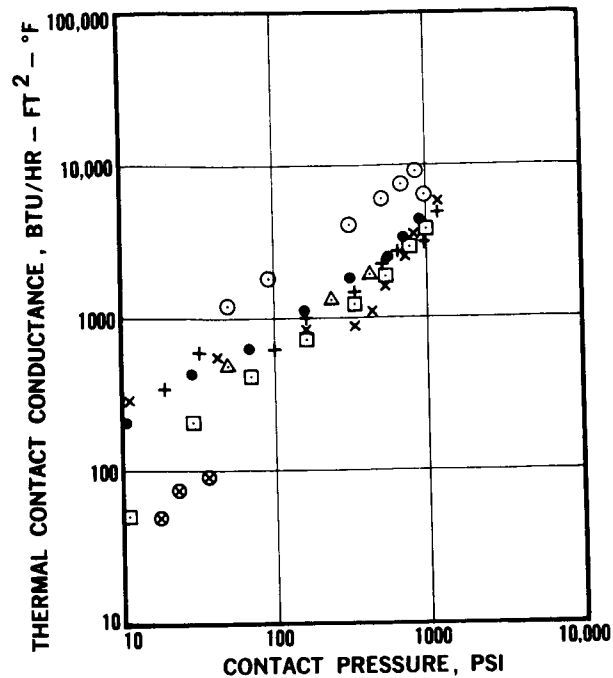
The line drawn through the present 17-15 micro-inch roughness data points has a slope of $m = 0.73$, slightly less than the majority of data in Figure 6-1.

The phenomenon observed by Fried (Reference 6), in which the slope of h versus p_c is low for contact pressures below 150 psi, but suddenly increases for contact pressures above 150 psi, was plotted using Fried's data to 160 psi, neglecting, of course, his earlier 2024-T3 flat plate data. The slope was found to be $m = 0.40$ (Figure 6-3).

The most unusual aspect of plotting these various data on a log-log graphs was the proximity of the data in the 300 to 1000 psi range, al-

THE DEPENDENCY OF CONTACT CONDUCTANCE ON CONTACT PRESSURE -

COMPARISON OF RESULTS AT HIGHER TEMPERATURES FOR ALUMINUM



SYMBOL	INVESTIGATOR (REFERENCE)	LABORATORY	MATERIAL	ROUGHNESS (RMS) (MICRO-INCHES)	FLATNESS DEVIATION (MICRO-INCHES)	T _{mean} (°F)	COOLANT	AMBIENT PRESSURE (TORR)	REMARKS (HARDNESS)
●	Clausing [5]	University of Illinois	Aluminum 2024-T4	40-80	220-220	+235	Water	3x10 ⁻⁶	Spherical Contact Surfaces - 7A (DPH - 145)
□	Clausing [5]	University of Illinois	Aluminum 2024-T4	3-3	220-220	+235	Water	3x10 ⁻⁶	Spherical Contact Surfaces - 6A (DPH - 145)
⊙	Bloom	DACO	Aluminum 7075-T6	17-15	200-200	+75 to +90	Water	4x10 ⁻⁶	Directionally ground surfaces mated perpendicular. (Rockwell B-91)
△	Bloom	DACO	Aluminum 7075-T6	125-135	200-500	+270	Steam	3x10 ⁻⁶	Directionally ground surfaces mated parallel. (Rockwell B-91)
⊗	Fried [11]	G.E.	Aluminum 2024-T3	48-65	1700 Total	+110	Water	10 ⁻⁴ to 10 ⁻⁶	Wide, flat thin plates. (Rockwell B-76)
x	Fried [8]	G.E.	Aluminum 6061-T6	8-16	50 Total	+85	Water	10 ⁻⁴	Lathe cut finish. Samples 13 and 14 (Rockwell F-88 & F-87)
+	Fried [8]	G.E.	Aluminum 6061-T6	50-60	250-100	+110	Water	10 ⁻⁴	Lathe cut finish. Samples 15 and 16 (Rockwell F-93 & F-93)

FIGURE 6-1

though the surface roughness of the specimens varied from 3 to 130 micro-inches in some cases. The results may have been fortuitous since there existed a wide variation of the test parameters, such as hardness, thermal conductivity, mean interfacial temperature, and macroscopic surface configuration, i.e., waviness.

6.1.2 Aluminum (II)

Figure 6-2 differs from Figure 6-1 in one respect only. The data in Figure 6-1 used Clausing's specimens 6A and 7A. The data in Figure 6-2 used Clausing's specimens 1A and 2A. Note that Clausing's data points are closer together in Figure 6-2 than in 6-1. In Figure 6-2 the microscopic surface roughness was the same in both data sets, 12 micro-inches, and the test blocks were rotated 90° with respect to each other. For Clausing's previous data, two different sets of specimens were used, 6A and 7A, as described in Table 6-1, which had widely varying roughnesses.

The present DACO 125-135 micro-inch data and Fried's 6061-T6 data fall slightly below Clausing's data in the 100 to 1000 psi range, but the 17-15 micro-inch data are now closer to Clausing's micro-inch data.

A straight line drawn through all of the data in Figure 6-2 is shown in Figure 6-3; it is called the "Best Line Through Most of the Aluminum (II) Data." The slope is $m = 0.84$, very nearly equal to $m = 0.88$ of the "Best Line Through Most of the Aluminum (I) Data."

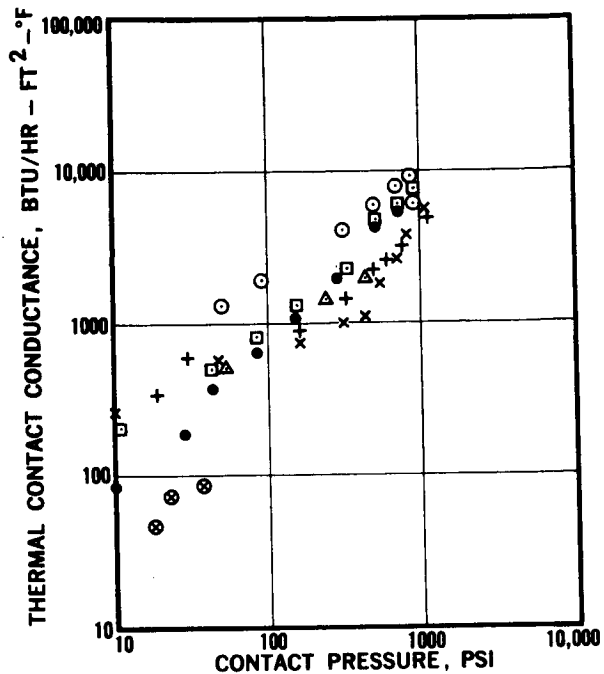
The scatter, below contact pressures of 100 psi, for Aluminum (II) data is too wide to draw a low pressure line as was done for Aluminum (I). Fried's hypothesis of a change in slope at low pressures (below 150 psi) requires further experimental evidence before being firmly established.

6.2 Stainless Steel

Figure 6-4 shows the data reported in the literature for stainless steel specimens in a vacuum environment. Data are also shown for high contact

THE DEPENDENCE OF CONTACT CONDUCTANCE ON CONTACT PRESSURE -

COMPARISON OF RESULTS AT HIGHER TEMPERATURES FOR ALUMINUM (II)



SYMBOL	INVESTIGATOR (REFERENCE)	LABORATORY	MATERIAL	ROUGHNESS (RMS) (MICRO-INCHES)	FLATNESS DEVIATION (MICRO-INCHES)	T _{mean} (°F)	COOLANT	AMBIENT PRESSURE (TORR)	REMARKS (HARDNESS)
●	Clausing [5]	University of Illinois	Aluminum 2024-T4	12-12	Unknown - 230	+220	Water	3x10 ⁻⁶	Spherical Contact Surfaces - 1A (DPH - 145)
□	Clausing [5]	University of Illinois	Aluminum 2024-T4	12-12	Unknown - 230	+238	Water	3x10 ⁻⁶	Spherical Contact Surfaces - 1A Rotated 90° from above orientation.
○	Bloom	DACO	Aluminum 7075-T6	17-15	200-200	+75 to +90	Water	4x10 ⁻⁶	Directionally ground surfaces mated perpendicular. (Rockwell B-91)
△	Bloom	DACO	Aluminum 7075-T6	125-135	200-500	+270	Steam	3x10 ⁻⁶	Directionally ground surfaces mated parallel. (Rockwell B-91)
⊙	Fried [11]	G.E.	Aluminum 2024-T4	48-65	1700 Total	+110	Water	10 ⁻⁴ to 10 ⁻⁶	Wide, flat, thin plates. (Rockwell B-76)
×	Fried [8]	G.E.	Aluminum 6061-T6	8-16	50 Total	+85	Water	10 ⁻⁴	Lathe cut finish. Samples 13 & 14 (Rock well F-88 & F-87)
+	Fried [8]	G.E.	Aluminum 6061-T6	50-60	250-100	+110	Water	10 ⁻⁴	Lathe cut finish. Samples 15 & 16 (Rock well F-93 & F-93)

FIGURE 6-2

M-19316

**THERMAL
CONDUCTANCES OF
ALUMINUM -
LOG-LOG PLOT
SHOWING POWER
DEPENDENCY ON
CONTACT
PRESSURE**

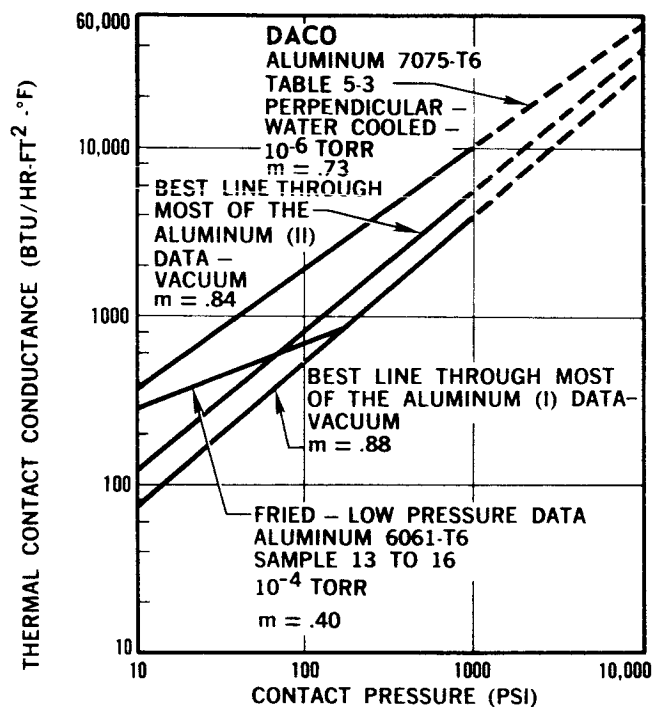


FIGURE 6-3

pressures in a 1 atmosphere environment obtained by Henry of MIT (Reference 10).

The data points fall along three main lines (Figure 6-5). Fried's 50-45 micro-inch data follow a slope of $m = 0.11$ from 10 to 110 psi and $m = 0.81$ thereafter, once again affirming his hypothesis. The majority of data, however, follow a slope of approximately $m = 1.05$ called the "Best Line Through Most of the Stainless Steel Data." For the data taken in air by Henry, the slope is $m = 0.57$, considerably below the majority of data for stainless steel at high pressures. Fried's high pressure slope of $m = 0.81$ was fairly close to the Aluminum (I) and (II) values of $m = 0.88$ and 0.84 , respectively, but less than that of the majority of stainless steel, $m = 1.05$.

6.3 Comments on the Dependence of Contact Conductance Versus Contact Pressure

Figures 6-3 and 6-5 show that at pressures above 100 psi, that h is proportional to $p_c^{0.8}$ to $p_c^{0.9}$ for the case of aluminum, and to $p_c^{1.05}$ for stainless steel. These results would tend to agree with the hypothesis of Fried that above 150 psi, the deformation of surfaces pressed together may not be purely elastic, but a combination of elastic and plastic.

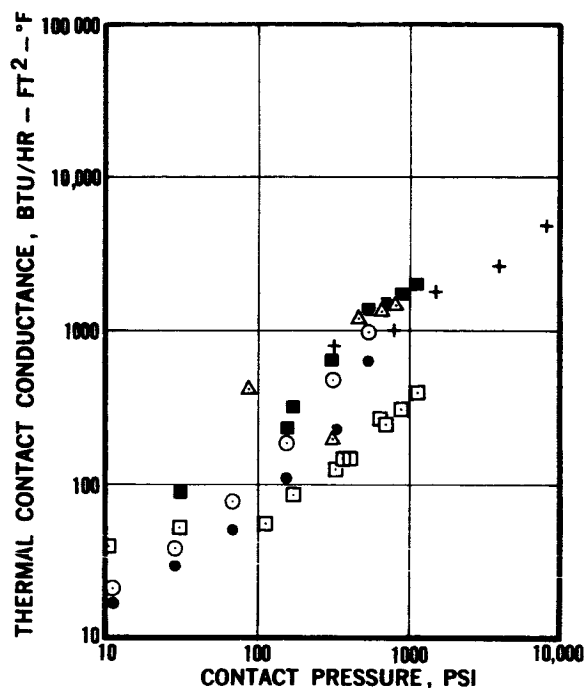
Fried cites Archard's work (Reference 12) to justify that the real area under a spherical indenter pressing against a flat plate would depend on contact pressure to the power of 1 for elastic-plastic deformation and $2/3$ for purely elastic deformation. It would thus seem, assuming conductance is proportional in some way to contact pressure, that for contacts under pressures greater than 150 psi, some plastic as well as elastic deformation is involved.

7. COMPARISON OF LOW AND HIGH TEMPERATURE DATA

In this section, specially selected results for low temperature aluminum 7075-T6 and stainless steel 17-4 PH are presented on log-log graphs. For each metal, three different sets of data, each with a differing roughness,

THE DEPENDENCE OF CONTACT CONDUCTANCE ON CONTACT PRESSURE -

COMPARISON OF RESULTS AT HIGHER TEMPERATURES FOR STAINLESS STEEL



SYMBOLS	INVESTIGATOR (REFERENCE)	LABORATORY	MATERIAL	ROUGHNESS (RMS) (MICRO-INCHES)	FLATNESS DEVIATION (MICRO-INCHES)	T _{mean} (°F)	COOLANT	AMBIENT PRESSURE (TORR)	REMARKS (HARDNESS)
●	Clausing [5]	University of Illinois	S.S. - 303	3-3	25-25	+230	Water	3x10 ⁻⁶	Spherical Contact Surfaces - 1S Increasing P _c . (DPH-250)
⊙	Clausing [5]	University of Illinois	S.S. - 303	3-3	25-25	+230	Water	3x10 ⁻⁶	Spherical Contact Surface - 1S Decreasing P _c . (DPH-250)
+	Henry [30]	MIT	S.S. - 416	150-62	Optically Flat	+200	Water	760	Flat surface rough- ness by blasting with glass beads Data interpolated. (Vickers-3.5 to 6.0 x 10 ⁵ psi)
△	Bloom	DACO	S.S. - 17-14PH	17-17	100-200	+130	Water	2x10 ⁻⁶	Directionally ground surfaces mated perpendicular. (Rockwell C-35.1)
□	Fried [8]	G.E.	S.S. - 304	50-45	-50 to +100	+73	Water	10 ⁻⁴	Ground finish. Samples 3 and 4. (Rockwell B-80 & B-81)
■	Fried [8]	G.E.	S.S. - 304	15-10	12-50	+86	Water	10 ⁻⁴	Ground finish. Samples 1 and 2 (Rockwell B-80 & B-80)

FIGURE 6-4

M-19305

**THERMAL
CONDUCTANCES OF
STAINLESS STEEL -
LOG-LOG PLOT
SHOWING POWER
DEPENDENCY
ON CONTACT
PRESSURE**

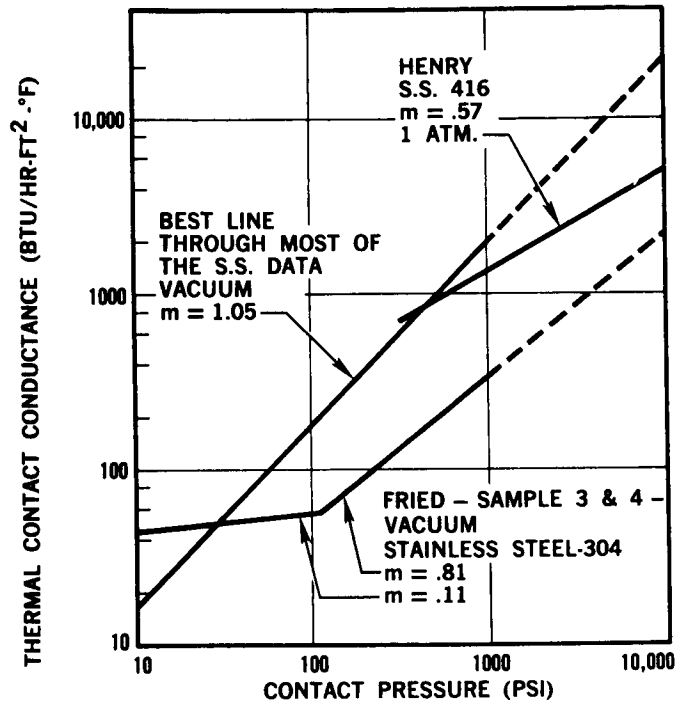


FIGURE 6-5

CONVERSION TABLE FOR HARDNESS OF SPECIMENS USED BY INVESTIGATORS
OF CONTACT CONDUCTANCE

TABLE 6-1

Material	Investigation (Reference)	Hardness Listed for Experimental Data	Hardness (psi)
Aluminum 7075-T6	Bloom	Rockwell B-91	2.7×10^5
Aluminum 6061-T6	Fried (6)	Rockwell F87, 88 F93	1.4×10^5 1.6×10^5
Aluminum 2024-T3	Fried (9)	Rockwell B-76	2.0×10^5
Aluminum 2024-T4	Clausing (2)	DPH - 145	2.1×10^5
Stainless Steel 17-4 PH	Bloom	Rockwell C-35.1	5×10^5
Stainless Steel - 304	Fried (6)	Rockwell B80, 81	2.6×10^5
Stainless Steel - 303	Clausing (2)	DPH - 250	3.5×10^5
Stainless Steel - 416	Henry (8)	(3.5 to 6.0) x 10^5 psi	(3.5 to 6.0) x 10^5

were plotted as a function of contact pressure. Data points for the same roughness were designated by the same symbols and the best straight lines were drawn through those points.

The roughnesses of the mating surfaces, the tables from which the data were obtained, and the slopes, m , of the h versus p_c lines are listed in Figures 7-1 and 7-2. The orientations of the mated surface lays were perpendicular in all cases; the coolant used was liquid nitrogen.

7.1 Aluminum 7075-T6

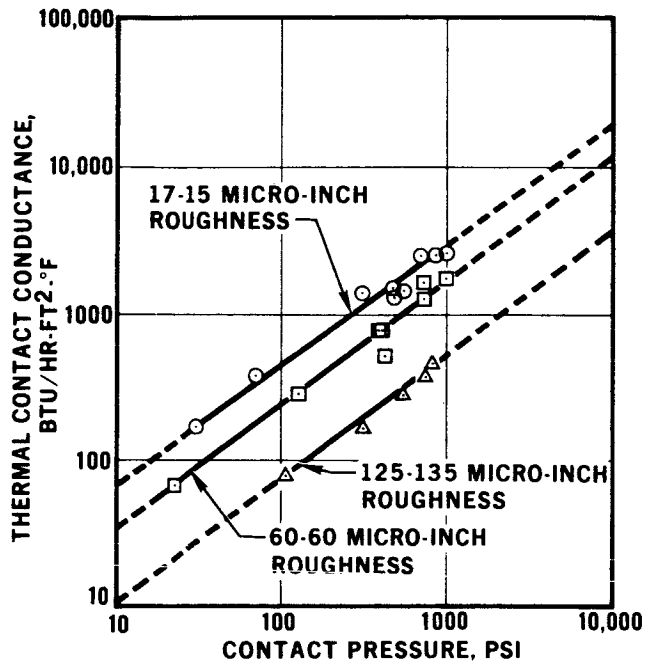
Figure 7-1 shows the results of plotting data from smooth, medium, and rough surfaces in contact on a log-log plot. The slopes of all three sets of data in Figure 7-1 are approximately equal, $m = 0.87, 0.86$ and 0.84 . These slopes compare quite well with the average high temperature slopes of Figure 6-3 of $m = 0.84$ and 0.88 , obtained from data of Clausen (5) and Fried (8). It is interesting to note that the magnitude of the data in Figure 7-1 lies considerably below that of Figure 6-3. For example, at 1000 psi, Aluminum (I) and Aluminum (II) best lines yield conductances of 4000 and 5600 BTU/hr-ft²-°F, while that of the three straight lines in Figure 7-1 yield 2800, 1600 and 460 BTU/hr-ft²-°F. If the middle figure is taken as an average value, then it may be concluded that h increases by a factor of 3 as T_{mean} of aluminum increases from -240°F to +240°F at 1000 psi. If, however, the comparison is made with the DACO data in Figure 6-3 at 1000 psi, then h increases to 10,000 BTU/hr-ft²-°F, by a factor of 6, as T_{mean} increases from -240°F to +240°F.

7.2 Stainless Steel 17-4 PH

Figure 7-2 shows the results of plotting smooth, medium and rough surface data on a log-log plot. As in the case of previous high temperature stainless steel data, the points appear to be scattered more than the aluminum data. It was particularly difficult to draw a best straight line through the 35-35 micro-inch and 100-125 micro-inch roughness data as a result of this scatter. Approximate average straight lines were,

M-19311A

**LOG-LOG PLOT
OF THERMAL
CONDUCTANCE
AT LOW
TEMPERATURES
ALUMINUM
707 5-T6**



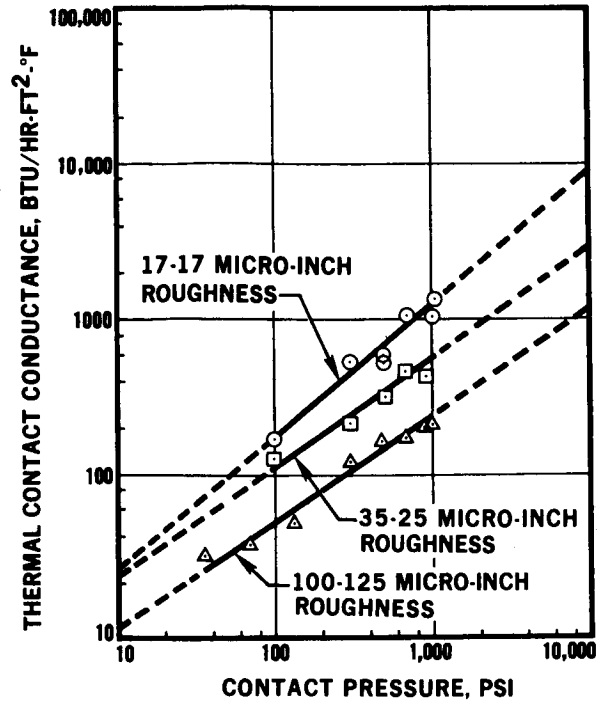
M-21064A

- = PERPENDICULAR MATING 17-15 MICRO-INCH ROUGHNESS
m = .87
- = PERPENDICULAR MATING 60-60 MICRO-INCH ROUGHNESS
m = .87
- △ = PERPENDICULAR MATING 125-135 MICRO-INCH ROUGHNESS
m = .84

FIGURE 7-1

M-19313 A

**LOG-LOG PLOT
OF THERMAL
CONDUCTANCE
AT LOW
TEMPERATURES
STAINLESS STEEL
17-4 PH**



M-21065A

- = PERPENDICULAR MATING 17-17 MICRO-INCHES ROUGHNESS
m = .84
- = PERPENDICULAR MATING 35-35 MICRO-INCHES ROUGHNESS
m = .71
- △ = PERPENDICULAR MATING 100-125 MICRO-INCHES ROUGHNESS
m = .83

FIGURE 7-2

nevertheless, drawn and their slopes computed. The results, smooth to rough respectively, were $m = 0.84$, 0.71 and 0.83 . These slopes were less than the slope of the "Best Line Through Most of the Stainless Steel Data" (Figure 6-5) of $m = 1.05$, but approximately the same for Fried's samples 3 and 4, $m = 0.81$.

It is interesting to note the effect on h of increasing T_{mean} of stainless steel specimens from -100°F to $+200^{\circ}\text{F}$ at 1000 psi contact pressure. The value of h from the "Best Line" at 1000 psi in Figure 6-5 is $2000 \text{ BTU/hr-ft}^2\text{-}^{\circ}\text{F}$. The value of h for 35-35 micro-inch roughness specimens at -100°F in Figure 7-2 is $600 \text{ BTU/hr-ft}^2\text{-}^{\circ}\text{F}$. The value of h , therefore, increases by a factor of 3.3 as T_{mean} increases from -100°F to $+200^{\circ}\text{F}$ at a contact pressure of 1000 psi.

8. APPLICATION OF THERMAL CONTACT CONDUCTANCE DATA TO A TYPICAL BOLTED JOINT

8.1 High Temperature Bolted Joint

Using the pressure profile of Aron and Columbo (Figure 6 of Reference 13) shown in Figures 8-1 and 8-2, it is possible to calculate an average value of h between aluminum 6061-T6 plates fastened together by a steel bolt and aluminum nut. The bolt has been subjected to a torque of 22 inch-pounds or 800 pounds tension. The pressure was plotted as a function of distance from the center line of the bolt. Knowing the pressure, a smooth curve of conductance versus radius was plotted using values of high temperature conductance obtained from the graph in Figure 6-3, "Best Line Through Most of the Aluminum (I) Data," extrapolated to 5000 psi. This line has a lesser slope than a line connecting Fried's 6061-T6, 12 micro-inch aluminum data. Thus, the computed average h , called \bar{h} , at high temperatures will be conservative on the low side. The average value of h is defined as

$$\bar{h} = \frac{\int h dA}{\int dA} = \frac{\sum h_i A_i}{\sum A_i} \quad (8-1)$$

where h_i is the average value of h for the annulus of area A_i , in turn defined as

CROSS-SECTION OF A BOLTED JOINT

RIGID RESTRAINT
APPROXIMATE
UNIFORM
LOADING

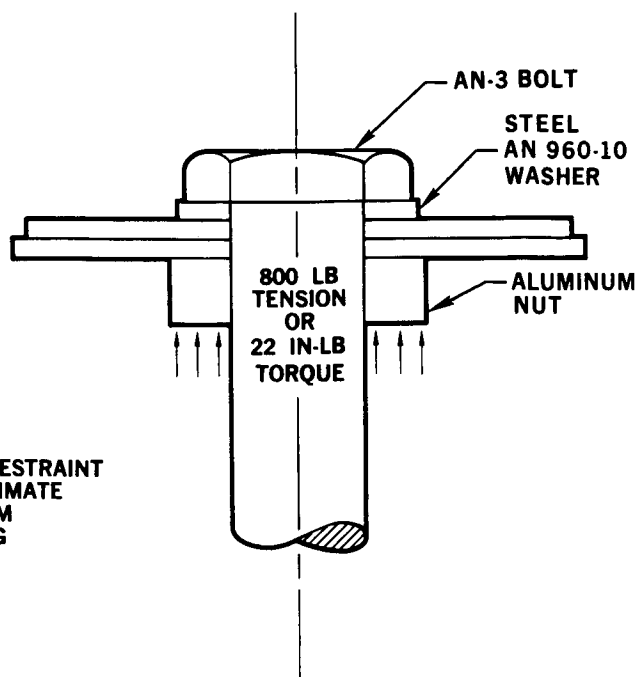


FIGURE 8-1

THERMAL CONDUCTANCE ACROSS A BOLTED JOINT

- CONTACT CONDUCTANCE
BTU/HR-FT²·°F
+200°F = T_{mean}
FROM "BEST
LINE AL. (I)
DATA." - FIGURE
6-3.
- CONTACT CONDUCTANCE
BTU/HR-FT²·°F
-240°F = T_{mean}
FROM
17-15 MICRO-INCH
ROUGHNESS -
FIGURE 7-1
- CONTACT PRESSURE,
PSI UNDER
BOLTED
JOINT

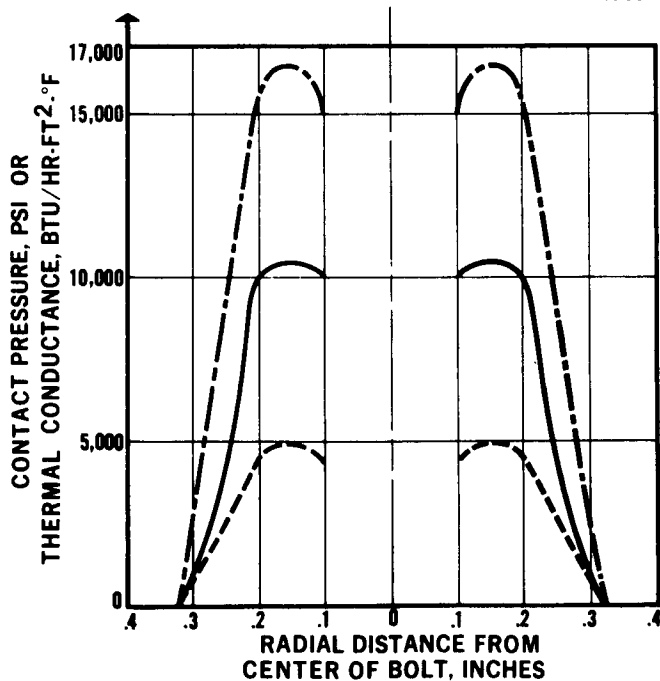


FIGURE 8-2

$$A_i = \pi(r_i^2 - r_{i-1}^2) \quad (8-2)$$

where r_i = radius from center of bolt head. The radii of the circular area under pressure ranged from 0.10-inches to 0.34 inches (the radius at which the pressure dropped to zero), yielding a total contact area of 0.33 in.². The increments in r were 0.10-inches. The average conductance, \bar{h} , was computed to be 10,000 BTU/hr-ft²-°F. This value is 8.6 times greater than the value computed by Aron and Columbo of $\bar{h} = 1170$ BTU/hr-ft²-°F, based on a thermal resistance of 0.7°F/watt and area of 0.33 in.².

8.2 Low Temperature Bolted Joint

The effect of decreasing the temperature of the bolted joint interface to -250°F, holding all other parameters constant, was calculated using the extrapolated values of low temperature data produced in this paper. The data used were from Figure 7-1 for the 17-15 micro-inch roughness line. The calculation resulted in $\bar{h} = 6800$ BTU/hr-ft²-°F, a decrease of 32 percent from the conservative high temperature \bar{h} calculation. The low temperature value of \bar{h} is higher, therefore, by a factor of 5.8 compared to Aron and Columbo's value of 1170 BTU/hr-ft²-°F.

8.3 Summary

An example has been given of a method used to compute the average value of contact conductance across a bolted joint providing that the pressure as a function of the radius from the bolt is known. The method was applied to bolts at high (250°F) and low (-250°F) interface temperatures, which should aid the designer of spacecraft in determining effects of temperature cycling across bolted joints. It was assumed in the calculations that all heat flow was perpendicular to the aluminum plates held together by the bolt-nut combination. The average conductance, \bar{h} , across a bolted joint (22 inch-pounds) was calculated to be 10,000 BTU/hr-ft²-°F at +250°F and 6800 BTU/hr-ft²-°F at -250°F.

9. THE ELECTRICAL ANALOGY OF THERMAL CONSTRICTION RESISTANCE

9.1 A Survey of Two Thermal Contact Conductance Theories

Fenech and Rohsenow Theory - Two theories exist on thermal contact conductance, both of which are currently being compared to conductance data. The first theory, by Fenech and Rohsenow of M.I.T. (Reference 6), was based on a button contact model. The annulus surrounding the button could contain a conducting fluid. Their original model assumed that the contact surfaces were optically flat or perfectly conforming (no macroscopic gaps at the interface). They produced an equation for thermal contact conductance which depends upon thermal conductivities, actual areas in contact, shoulder heights of the buttons, and numbers of contact points. This equation is their first order equation, which means that it takes into account only first order surface irregularities such as roughness.

For a second order surface irregularity (i.e., waviness), Fenech and Rohsenow (Reference 6) produced a second order equation. For cases of conducting interstitial fluids, their two equations are quite complicated. In the case of a vacuum environment, the equations are greatly simplified. Using the first and second order equations as definitions of the microscopic conductance, h_g , and the macroscopic conductance, h_L , calculations were performed on a model like the one Clausing (Reference 5) used, i.e., two spherical surfaces of known radius of curvature pressed together. The calculations used surface roughness data obtained by the analogue method for stainless steel by J. J. Henry of M.I.T. (Reference 10). The calculated conductance values using both the first and second order equations resulted in the theoretical predictions falling far below actual data values. These calculations were made for both stainless steel and aluminum of the same types as used by Clausing and Chao (Reference 5). The differences between Fenech and Rohsenow's theory and the actual data are greatest at low contact pressures, but tend to diminish as contact pressures exceed 1000 psi. The slopes of the conductance versus pressure lines are much greater for the Fenech and Rohsenow theory than for the actual data.

The predominant contribution to the total theoretical conductance, below contact pressures of 1000 psi was from the second order equation. The second order equation depended mainly upon the surface flatness deviation and depended only in a minor way upon the surface roughness.

Clausing and Chao Theory - The second theory of thermal contact conductance, by Clausing and Chao (Reference 5) of the University of Illinois, was derived from the constriction resistance theory of Ragner Holm (Reference 14). Clausing and Chao's model also used the Hertz (Reference 15) theory of elastic deformation of two spheres in contact. Their actual physical model consisted of pressing two cylinders together, the contact surfaces of which had been machined to a convex spherical radius of curvature. The macroscopic contact area would be circular as shown in Figure 9-1 for one cylinder.

Like Fenech and Rohsenow, Clausing and Chao were aware that surfaces have both large and small scale surface irregularities. But Clausing and Chao discovered that the large scale irregularities influenced conductance much more than the small scale irregularities. Large scale deviations from flatness (waviness) resulted in surfaces contacting each other over large scale areas, called macroscopic areas. Small scale deviations from flatness (roughness) are called asperities or protuberances. Within a macroscopic contact area, asperities are in contact over large numbers of small areas. Each of these small areas is called a microscopic contact area. From their theory and test data, Clausing and Chao concluded that the macroscopic resistance was predominant over the microscopic resistance. Recent calculations by this writer, using Clausing's complete theory as applied to his spherical model, verify this conclusion. Only the macroscopic resistance (or conductance) needs to be considered for contact pressures less than those which produce a relatively high conformity of surfaces, i.e., surfaces for which the macroscopic contact area is less than 40 percent of the apparent contact area.

M-20454

CONstriction OF
HEAT FLOW FROM
CYLINDER INTO
MACROSCOPIC
CONTACT AREA

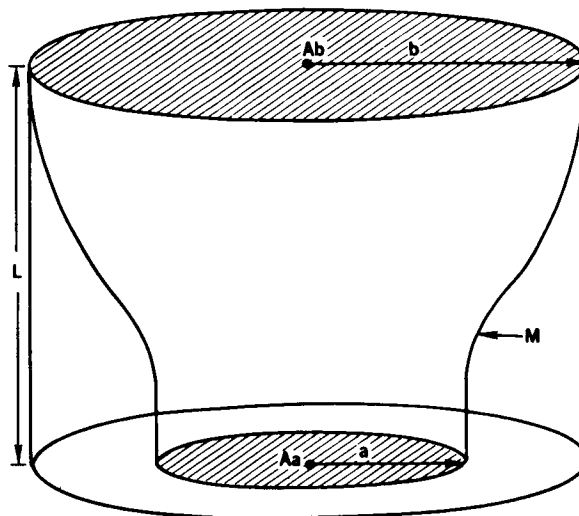


FIGURE 9-1

In Section 9, the thermal constriction resistance theory is clearly related to the electrical constriction resistance theory of Holm. In Section 10, Clausing's conductance equations are briefly developed to serve as basis for calculations performed later.

Section 11 presents Clausing's macroscopic theory predictions. These predictions are made for contacts at both high and low temperatures for aluminum and stainless steel. Both Clausing's and the present DACO data are compared to the theoretical predictions.

9.2 Thermal Constriction Problem

The thermal contact resistance problem is in reality a problem in the constriction of the heat flow from a larger area, A_b , to a smaller area, A_a , (Figure 9-1). In the thermal problem, let ϕ be the temperature potential function in the tubular region bounded by A_a , A_b and the tube M. Inside the tubular region there are no sources or sinks. Therefore,

$$\nabla^2 \phi = 0 \quad (9-1)$$

All of the heat flows along streamlines from the surface A_b , which is at a constant potential ϕ_b , to the surface A_a , at a constant potential ϕ_a . No heat enters or leaves the heat flow tube through the surface, M. Therefore, the normal gradient along the tube

$$\left(\frac{\partial \phi}{\partial n}\right)_M = 0 \quad (9-2)$$

The problem becomes one of determining the thermal constriction resistance of the heat flow tube as a function of the geometry of the flow tube. Once this is accomplished, two flow tubes are placed with their areas A_a in contact. The total thermal constriction resistance is then twice that of the constriction resistance of the previously calculated heat flow tube.

It should be emphasized that at the contact between the flow tubes, there is no contact resistance. This is essentially the case for metal to metal contact in a vacuum environment assuming negligible thermal resistance due to the usual oxide coating on the contact surfaces, A_a . Thus, thermal contact resistance is the result mainly of thermal constriction resistance.

The reasons for the electrical analogy, derived by Holm, and applied to a finite cylinder by Clausing, have never been fully explained in thermal contact resistance literature. The analogy is based on the similar mathematics describing the flow of heat and the flow of electricity between two equipotential surfaces. In the electrical case, a relation is found between the electrical resistance and the capacitance between the two equipotential surfaces, A_b and A_a . The capacitances between two plates of varying geometrical arrangements have been thoroughly investigated and the electrostatic solutions for certain cases are well known. Therefore, the electrical resistance can easily be found as a function of the geometry of the tube. If the electrical analogy is correct, then the thermal resistance, and thus the thermal conductance, can be determined as a function of the geometry of the tube.

9.3 Electrical Constriction Problem

In the electrical problem, the surfaces A_b and A_a are at constant electric potentials ϕ_b and ϕ_a respectively. Current flows between these two surfaces inside of the conducting tube bounded by the surface M.

Equation 9-2 applies to the side boundaries of the electrical tube. Inside the tube, current is flowing and charge must, therefore, be present. There are assumed to be no sources or sinks inside the tube. Surface charge densities are present on the ends of the tube, A_a and A_b , which originate and terminate the electric field lines. It is desired to show that $\nabla^2 \phi = 0$ inside the tube.

Inside the tube, Ohm's law states that

$$\bar{J} = \sigma \bar{E} \quad (9-3)$$

where \bar{J} is the current density, σ conductivity and \bar{E} the electric field.

The conservation of charge equation applies inside the tube at every point, since there are no sources or sinks. Therefore,

$$\frac{\partial \rho}{\partial t} + \nabla \cdot \bar{J} = 0 \quad (9-4)$$

In our case, the current flow is steady state. Therefore

$$\frac{\partial \rho}{\partial t} = 0 \quad (9-5)$$

From equations 9-3, 9-4 and 9-5 we have inside the tube

$$\nabla \cdot \bar{J} = \nabla \cdot (\sigma \bar{E}) = 0 \quad (9-6)$$

The electrical field \bar{E} is defined as

$$\bar{E} = -\nabla \phi \quad (9-7)$$

Therefore, inside the tube,

$$\nabla \cdot (\sigma \nabla \phi) = 0 \quad (9-8)$$

which is the equation governing the potential in the more general case of a non-constant electrical conductivity.

Equation 9-8 is identical to the steady state heat flow equation with no sources or sinks, if the thermal conductivity k replaces the electrical conductivity σ . In the electrical case, σ changes slowly with temperature for a conductor. In the thermal case, k always depends on temperature. The dependency however, is weak over a moderate (50°F) temperature range at temperatures higher than liquid nitrogen for most industrial aluminum and stainless steel metals (Reference 7).

Applying equation 9-8 we have, for constant σ ,

$$\nabla^2 \phi = 0 \quad (9-1)$$

for the electrical case of steady state current between two equipotential surfaces bounding the ends of a conducting current tube.

9.4 Relation Between Electrical Resistance and Capacitance According to Holm (Reference 14)

The charge on A_a is, in cgs - esu units,

$$Q = \frac{1}{4\pi} \int_{A_a} \left(\frac{\partial \phi}{\partial n} \right) dA \quad (9-9)$$

On A_b sits an equal and opposite charge.

The capacitance between A_a and A_b is defined as

$$C = \frac{Q}{\phi_b - \phi_a} \quad (9-10)$$

The current density between A_a and A_b is

$$\vec{J} = \sigma \vec{E} = \sigma \left(\frac{\partial \phi}{\partial n} \right)_{A_a} \quad (9-11)$$

The total current between A_a and A_b is

$$I = \sigma \int_{A_a} \left(\frac{\partial \phi}{\partial n} \right) dA \quad (9-12)$$

Now electrical resistance is defined as

$$R = \frac{\phi_b - \phi_a}{I} \quad (9-13)$$

Substituting 9-9, 9-10, 9-12 into 9-13

$$R = \frac{Q/C}{I} = \frac{\frac{1}{4\pi}}{C \sigma} \frac{A_a \int_{A_a} \left(\frac{\partial \phi}{\partial n}\right) dA}{\int_{A_a} \left(\frac{\partial \phi}{\partial n}\right) dA} \quad (9-14)$$

Thus $R = \frac{1}{4\pi\sigma C}$ (9-15)

Equation 9-15 will form the basis of all future constriction resistance work for it relates the total electrical resistance to the usually known capacitance in terms of the geometry of the physical situation.

9.5 An Application of the Electrical Analogy

The case of interest in the problem of thermal contact conductance is the constriction of heat flow from a large area A_b to a small area A_a . Usually the geometry is one of the heat flowing from a heat source through a metallic cylinder, across an interface in contact with another metallic cylinder, and then to a heat sink.

The heat is assumed to be flowing at first uniformly through the cross section of the first cylinder. The heat is then assumed to be constricted to flow through the macroscopic contact areas (those areas in which there are a large number of asperities or protuberances in contact), and then to constrict even further to flow through the individual asperities of the first cylinder to those of the second. No contact resistance in the form of an oxide layer or film is assumed to exist between the asperities in contact.

The heat then flows from the asperities of the second cylinder to the macroscopic contact area and finally redistributes itself uniformly as it passes into that part of the second cylinder farthest removed from the contact.

Holm (Reference 14) sketches the method and cites the resultant equations used to calculate the capacitance between an infinitely large ellipsoidal shaped shell surrounding a circular spot of radius, a . The rigorous derivation of the capacitance in the more general case of an equipotential, rotational semi-ellipsoid surrounding a smaller, equipotential, semi-ellipsoid is given in Smythe (Reference 16). If the smaller ellipsoid is allowed to shrink to an ellipse on the surface of a semi-infinite body, and further the ellipse is allowed to assume the shape of a circle; and, if the larger ellipsoid is allowed to expand its dimensions to infinity, the capacitance between the circle of radius, a , and the semi-infinite, rotational ellipsoid is

$$C = \frac{a}{\pi} \quad (9-16)$$

Figure 9-2 is a sketch of a rotational semi-ellipsoid surrounding a circular spot of radius a . Equation 9-15, for the expression of constriction resistance as a function of capacitance, (and using the thermal conductivity, k , for electrical conductivity, σ) becomes

$$R = \frac{1}{4ka} \quad (9-17)$$

for one contact member. For two semi-infinite contact members placed together the constriction across a circular spot of radius a would be

$$R = \frac{1}{2ka} \quad (9-18)$$

A modified form of equation 9-18 forms the basis of Clausing's theory (Reference 2).

9.6 Extensions of Holm's Theory to Elliptical Contact Areas

It should also be mentioned that Holm performed calculations for constriction resistances between ellipsoids which were finite in their dimensions, and for contact areas which were elliptical in shape. His resultant equations predict that as the dimensions of the surrounding equipotential ellipse increase, the thermal constriction resistance also increases.

M-20809

ROTATIONAL
SEMI-ELLIPSOID
SURROUNDING A
CIRCULAR SPOT
OF RADIUS a

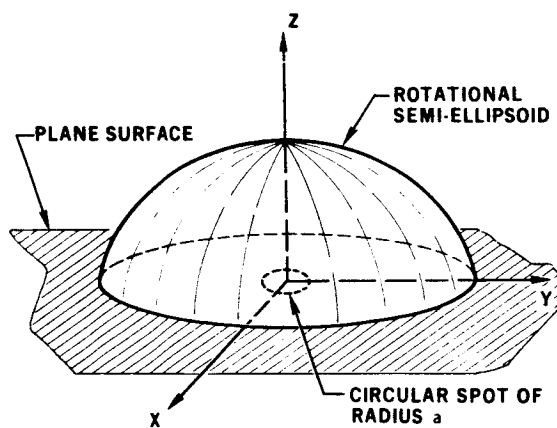


FIGURE 9-2

Furthermore, as the contact area changes from a circle to an ellipse of the same area, all other variables remaining constant, the contact resistance should decrease. At first this prediction apparently contradicts the newly obtained results (Figures 5-10 to 5-13). Perpendicular mated lays produced higher conductance than parallel mated lays for four different roughnesses for stainless steel specimens. The microscopic contact areas would be expected to be more elliptical in shape for the parallel mated lays than for the perpendicular. But the numbers of microscopic contact areas may have been less.

It should be further noted that because the rougher surfaces had also a larger waviness due to the grinding process, it seems unjustified to state that Holm's predictions have been contradicted by the stainless steel data. The actual case may very well have been that better surface conformity, and hence more macroscopic areas of contact, were obtained for perpendicular than for parallel mating.

10. CONSTRICION RESISTANCE THEORY OF CLAUSING AND CHAO

10.1 Roess' Solution of a Concentric Cylinder Applied to Thermal Contact Resistance

The principal contribution of Clausing and Chao to the constriction resistance theory of Holm was to consider theoretically the predominance of the macroscopic constriction resistance over the microscopic constriction resistance.

Clausing used the model of heat flow down a coaxial cylinder of finite radius and then constricted to flow into a smaller circular contact area, A_a (Figure 9-1).

The original solution to the problem of the thermal resistance of a coaxial right circular cylinder of radius b_L , feeding into a constant potential circular spot of radius a_L was solved by Roess (Reference 17). The solution remains the same whether the length of the cylinder is of infinite or of finite length, providing the height L of cylinder is greater than $0.6 b_L$.

Roess assumed a heat flux distribution across the contact area proportional to $(1 - \frac{r^2}{a^2})^{1/2}$ where r is the radial coordinate. This heat flux distribution resulted in an isothermal contact area, unless a_L/b_L was near unity.

Using Roess' numerical calculations for various heat fluxes and temperature distributions, Clausing found that the constriction resistance for the cases of constant temperature and constant heat flux at the contact surface area were almost identical. This result is important because it demonstrates that the constant temperature boundary condition, the unreal case, yields the same answer as the constant heat flux boundary condition, the more real case for conforming contact surfaces.

The macroscopic constriction resistance of a large cylinder of radius b_L feeding into a constant potential circle of radius a_L is

$$R_L = \frac{g(X_L)}{4 a_L k_m} \quad (10-1)$$

where k_m is the harmonic mean thermal conductivity of the mating specimens. The factor $g(X_L)$ was the contribution of Roess who calculated that

$$\begin{aligned} g(X) = & 1 - 1.40925 x + 0.29591 x^3 \\ & + 0.05254 x^5 + 0.02105 x^7 \\ & + 0.01107 x^9 + \dots \end{aligned} \quad (10-2)$$

and X_L , the constriction ratio, is equal to a_L/b_L .

For two cylinders placed end to end, the total macroscopic constriction resistance is

$$R_L = \frac{g(X_L)}{2 a_L k_m} \quad (10-3)$$

10.2 Relationship Between Thermal Resistance and Thermal Conductance

The definitions of thermal resistance and thermal conductance are different as defined by various workers in the field. In this report, the definition of thermal conductance is

$$h = \frac{Q}{\Delta T} \quad (10-4)$$

where h is in units of BTU/hr-ft²-°F, Q is the heat flux across the interface, and ΔT is the temperature difference across the interface. It should be emphasized that thermal resistance is not the reciprocal of thermal conductance. Thermal resistance is defined in a fashion similar to the electrical resistance,

$$R = \frac{\Delta T}{Q \cdot A_b} \quad (10-5)$$

where Q and ΔT are defined as in equation 10-4 and A_b is the area of the cylinder of radius b_L . R is expressed in units of °F/BTU/hr.

The relation between thermal resistance and thermal conductance is therefore

$$R = \frac{1}{h A_b} \quad (10-6)$$

The area A_b is used whether the R in equation 10-6 is microscopic, macroscopic or total thermal resistance.

10.3 Clausings' Model of One Macroscopic Contact Area

The theoretical and experimental model which Clausings used was that of placing two cylinders in contact, the ends of which had been machined to a convex spherical radius of curvature. The contact area of two cylinders in contact could be determined using the Hertz equation which defines the radius of the circular contact area to be

$$a_L = \frac{3P}{4} \left[\left(\frac{1 - \nu_1^2}{E_1} + \frac{1 - \nu_2^2}{E_2} \right) \left(\frac{1}{r_1} + \frac{1}{r_2} \right)^{-1} \right]^{1/3} \quad (10-7)$$

where ν is Poisson's ratio, E the modulus of elasticity, P the load, and r the curvature radius of the sphere. Clausing determined that the predicted values of the macroscopic thermal resistance were reasonably close to the experimental values providing a_L/b_L was less than 0.65. The value of b_L was always 1-inch for Clausing's specimens. Beyond $a_L/b_L = 0.65$, the theoretical predictions of Clausing were found to diverge increasingly from the data. The simple macroscopic constriction resistance formula for two cylinders was not an accurate prediction of actual total resistance. The microscopic asperities (surface roughness) should, therefore, be considered in order to predict the correct total thermal resistance.

10.4 Definition of Total Thermal Conductance

The total thermal resistance at the interface between the specimens is equal to (no oxide coating is assumed)

$$R = R_L + R_s \quad (10-8)$$

The total thermal conductance, substituting equation 10-6 and cancelling A_b , is

$$\frac{1}{h} = \frac{1}{h_L} + \frac{1}{h_s} \quad (10-9)$$

where h_L is the macroscopic thermal conductance, and h_s is the microscopic thermal conductance. Substitution from equation 10-3 yields for h_L ,

$$h_L = \frac{2 a_L k_m}{A_b g(X_L)} = \frac{2 X_L k_m}{\pi b_L g(X_L)} \quad (10-10)$$

10.5 Microscopic Thermal Conductance

The microscopic constriction resistance theory of the asperities was developed by Clausing in an identical manner as that of the macroscopic constriction resistance. If there are n_s microscopic circular contact areas, each of radius a_s , into which the heat is feeding from a bundle

of parallel cylinders of radius b_s , the resistances of each of the contact spots are added in parallel. Therefore, the microscopic resistance of one member is

$$R_s = \frac{g(X_s)}{4 k_m a_s n_s} \quad (10-11)$$

For the case of two bundles of cylinders placed end to end, the microscopic constriction resistance is doubled and

$$R_s = \frac{g(X_s)}{2 k_m a_s n_s} \quad (10-12)$$

From equation 10-6, the microscopic conductance is

$$h_s = \frac{2 k_m a_s n_s}{A_b g(X_s)} \quad (10-13)$$

Clausing made three assumptions concerning microscopic conductance. First, he assumed that the radius of the cylinders b_s was much larger than a_s , which results in $g(X_s) = 1$ from equation (10-2). Clausing secondly assumed that the radius of the microscopic contact area a_s was equal approximately to the rms roughness δ .

The third assumption of Clausing was that the asperities were deformed elastically, not plastically as Fenech assumed (Reference 6), and the load bearing area was defined as

$$A_s = n_s \pi a_s^2 = \frac{P}{\xi H} \quad (10-14)$$

where P is the load, H the hardness, and $\xi = 0.3$, a factor used to take into account the increase of conductance due to non-circular contact areas and the greater contact area due to microscopic elastic deformation. Clausing (Reference 5) states that "This value may be low for rough surfaces and is undoubtedly too high for well-polished surfaces." (Fenech used $\xi = 1$ for his button contact model.)

Using the relation between microscopic contact pressure ξH and apparent pressure p_c ,

$$\frac{A_s}{A_b} = \frac{n_s \pi a_s^2}{\pi b_L^2} = \frac{p_c}{\xi H} \quad (10-15)$$

Substituting for A_b in equations 10-12 and 10-6, the microscopic constriction conductance was found to be, assuming $g(X_s) = 1$, (calculations bear out this assumption),

$$h_s = \frac{2}{\pi} \frac{p_c}{\xi H} \frac{k_m}{a_s} \quad (10-16)$$

where k_m is the harmonic mean thermal conductivity defined as

$$k_m = \frac{2 k_1 k_2}{k_1 + k_2}$$

10.6 Ratio of Macroscopic to Microscopic Constriction Resistance

Using the assumptions in Section 10.5, the expression R_L/R_s , the ratio of macroscopic to microscopic constriction resistance, was computed by Clausing to be

$$\frac{R_L}{R_s} = \frac{h_s}{h_L} = \left(\frac{p_c}{\xi H} \right) \left(\frac{b_L}{a_s} \right) \frac{g(X_L)}{X_L} \quad (10-17)$$

where

$$X_L = 1.285 \left[\left(\frac{p_c}{E_m} \right) \left(\frac{b_L}{d_t} \right) \right]^{1/3} \quad (10-18)$$

derived by the Hertz equation 10-7, where d_t is total surface flatness deviation.

Calculations were made by Clausing for R_L/R_g based on equation 10-17 for two roughnesses (20 and 40 micro-inches), for three contact pressures (100, 200 and 400 psi), and three total flatness deviations (200, 400 and 800 micro-inches) for stainless steel and aluminum. The ratio for stainless steel 303 ranged from 38 to 130; for aluminum 2024-T4, 29 to 116. Clausing concluded that it was difficult to see how these ratios were in error by even as much as an order of magnitude, despite the assumptions involved in the calculation of R_g . He concluded that "in many cases the resistance due to small scale constrictions is negligible; and the macroscopic constriction resistance is the dominating resistance."

Clausing's theory, however, was based on the Hertz equation and assumed elastic deformation of the macroscopic contact areas. In actual practice, Clausing verified that his theory agreed with experimental results for values of X_L less than 0.65. Beyond $X_L = 0.65$, the macroscopic areas in contact may be plastically deformed and the Hertz equation would have to be modified or a new expression for macroscopic contact area used. Furthermore, as the macroscopic area in contact increases, the ratio of macroscopic to microscopic constriction resistance decreases until the microscopic resistance comprises a significant fraction of the total resistance. This would be the case for optically flat surfaces, or for wavy surfaces under high contact pressures where good surface conformity was obtained. Under these conditions, the best theoretical prediction of total conductance would be a combination of macroscopic conductance due to waviness and microscopic conductance due to roughness.

The microscopic constriction conductance becomes significant at a contact pressure depending upon the surface flatness deviation as well as the modulus of elasticity of the mating materials (equations 10-17 and 10-18). The following section contains graphical predictions of macroscopic conductance as a function of contact pressure. It should be noted that the condition $X_L = 0.65$ is obtained for various contact pressures depending on the surface flatness deviation and on the Young's modulus of the mating materials.

11. COMPARISON OF CLAUSING'S MACROSCOPIC CONSTRICTION RESISTANCE THEORY TO DATA

11.1 Clausing's Macroscopic Theory Compared to Clausing's Data

Figures 11-1 and 11-2 present theoretical predictions of Clausing and Chao's macroscopic theory from equations 10-10 and 10-18.

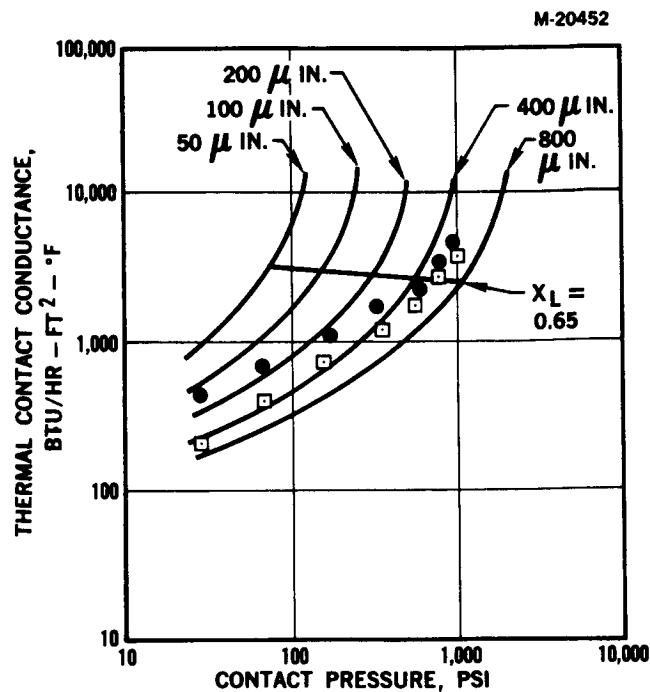
The total surface flatness deviations are indicated for each theoretical curve on the figures. The necessary information upon which the curves were computed are listed at the bottom of Figures 11-1 and 11-2. The value of $b_L = 1.0$ inches for theoretical curves and experimental data.

In Figure 11-1, the data for aluminum 2024-T4 specimens, 3-3 micro-inch roughness, falls almost exactly along the 400 micro-inch flatness deviation line up to pressures of 300 psi at which pressure the theoretical curve begins to diverge increasingly from the data points. At 1000 psi, the data points produce values of h of about $4000 \text{ Btu/hr-ft}^2\text{-}^\circ\text{F}$ and the theory predicts values of $12,000 \text{ Btu/hr-ft}^2\text{-}^\circ\text{F}$, a difference of a factor of 3.

For the aluminum specimens of 40-80 micro-inches, values of h lie above the 400 micro-inch flatness deviation indicating that the actual flatness deviation of the specimens may have been less than 400 micro-inch due to the sandblasting process of roughening the contact surfaces, after the measured 440 micro-inch flatness deviation had been obtained. Observe that these data points also fall below the 400 micro-inch surface flatness deviation as the contact pressure is increased, by about the same amount as the 3-3 micro-inch surface flatness roughness specimens.

The results for stainless steel 303 and the necessary information to compute the curves are presented in Figure 11-2. For the cases of both increasing and decreasing pressure, the values of h lie below the theoretical 50 micro-inch total surface flatness deviation curve. The frequently reported hysteresis effect (References 4, 5, 8 and 11) of conductance versus pressure is a probable explanation of the values

**CLAUSING'S
MACROSCOPIC
CONSTRICTION
THEORY
COMPARED TO
CLAUSING'S DATA
FOR ALUMINUM
2024-T4**



M-21066

- = CLAUSING'S MACROSCOPIC CONDUCTANCE THEORY PREDICTION.
TOTAL FLATNESS DEVIATION IS INDICATED FOR EACH CURVE.
- = CLAUSING'S DATA FOR 440 MICRO-INCH TOTAL FLATNESS
DEVIATION; 40-80 MICRO-INCH RMS ROUGHNESS.
- = CLAUSING'S DATA FOR 440 MICRO-INCH TOTAL FLATNESS
DEVIATION; 3-3 MICRO-INCH RMS ROUGHNESS.

ALUMINUM 2024-T4 DATA

$$T_{\text{mean}} = +235^{\circ}\text{F}$$

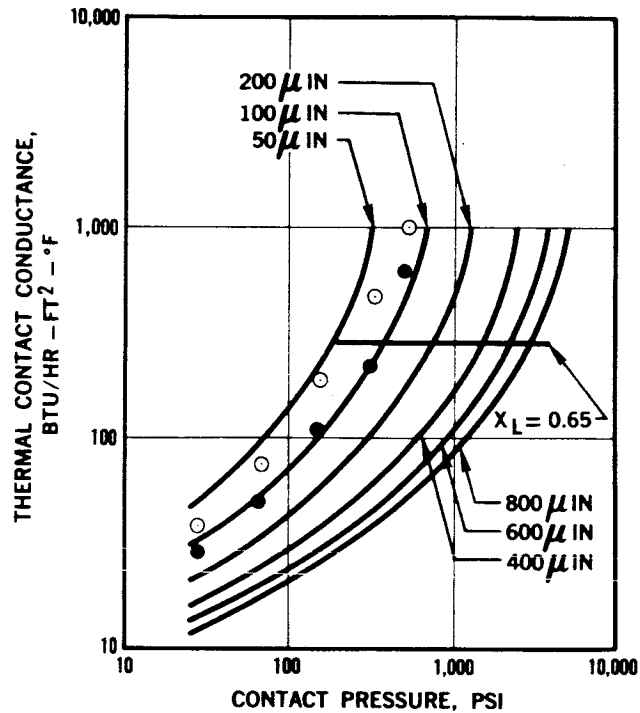
$$E_m = 1.0 \times 10^7 \text{ PSI}$$

$$K_m = 80 \text{ BTU/HR-FT-}^{\circ}\text{F}$$

FIGURE 11-1

M-20455

CLAUSING'S MACROSCOPIC CONSTRICTION THEORY COMPARED TO CLAUSING'S DATA FOR STAINLESS STEEL 303



M-21067

- = CLAUSING'S MACROSCOPIC CONDUCTANCE THEORY PREDICTION. TOTAL FLATNESS DEVIATION INDICATED FOR EACH CURVE.
- = CLAUSING'S DATA FOR 50 MICRO-INCH TOTAL FLATNESS DEVIATION; 3-3 MICRO-INCHES RMS ROUGHNESS; INCREASING CONTACT PRESSURE.
- = CLAUSING'S DATA FOR 50 MICRO-INCH TOTAL FLATNESS DEVIATION; 3-3 MICRO-INCHES RMS ROUGHNESS; DECREASING CONTACT PRESSURE.

STAINLESS STEEL 303 DATA

$T_{\text{mean}} = +230^{\circ}\text{F}$
 $E_m = 2.8 \times 10^7 \text{ PSI}$
 $K_m = 9.3 \text{ BTU/HR-FT}^2\text{-}^{\circ}\text{F}$

FIGURE 11-2

of h being greater for the decreasing pressure data. It is interesting to observe that at 300 psi, the value of h theoretical is 800 Btu/hr-ft²-°F while that of h experimental (increasing p_c) is about 200 Btu/hr-ft²-°F, a difference of a factor of four. Beyond 300 psi, the theoretical curve diverges to infinity, but the data points appear to increase steadily along a curve whose slope is increasing with pressure.

Considering the relationship between h , h_L , and h_s ,

$$\frac{1}{h} = \frac{1}{h_L} + \frac{1}{h_s} \quad (10-9)$$

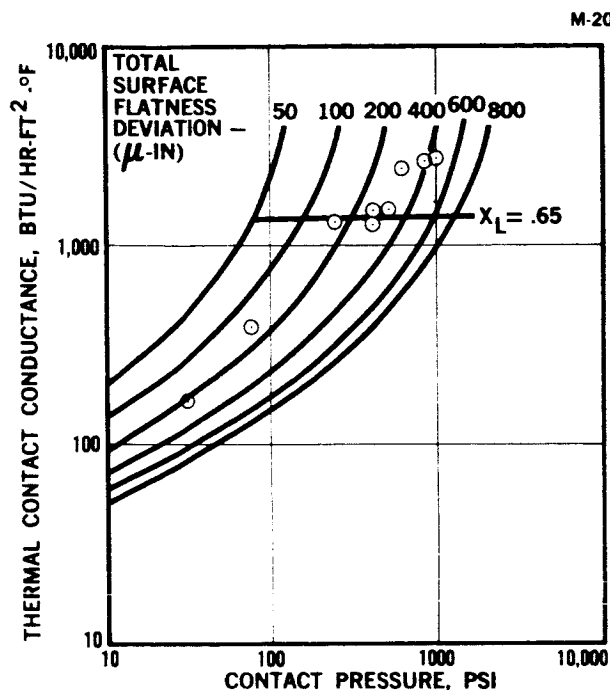
it is seen that as p_c increases, h_L may approach the same order of magnitude as h_s , because the macroscopic area in contact comprises a significant fraction of the contact area, A_b . This is the condition which probably occurs when X_L is greater than 0.65. For these cases of large macroscopic contact areas, both h_L and h_s must be considered in determining the total value of h . Furthermore, the Hertz equation, which assumes elastic deformation between spheres may have to be modified at higher loads to take account elastic-plastic deformation.

11.2 Clausing's Macroscopic Theory Compared to DACO's Low Temperature Data

Figures 11-3 and 11-4 present Clausing's macroscopic constriction theory curves for various total flatness deviations based on the Clausing spherical contact surface model. The curves were plotted using the physical property data of aluminum 7075-T6 and stainless steel 17-4 PH at those temperatures at which the thermal conductance data was obtained (Reference 18).

The Merz Electronic Gauge was used to measure the surface flatness deviations of the aluminum specimen after the test was completed. The maximum total flatness deviation was found to be 500 micro-inches (Figure 2-8) for the aluminum 7075-T6 test specimens. Before testing, the height gauge, accurate to 50 micro-inches, recorded surface flat-

CLAUSING'S
MACROSCOPIC
CONSTRICTION
THEORY
COMPARED TO
DACO LOW
TEMPERATURE
DATA FOR
ALUMINUM
7075-T6



M-21068 A

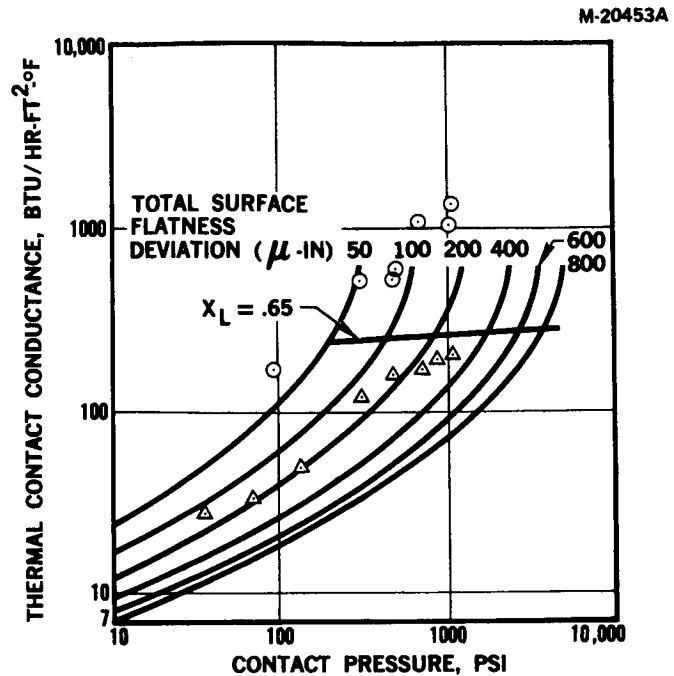
- = CLAUSING'S MACROSCOPIC CONDUCTANCE THEORY PREDICTION FOR ALUMINUM 7075-T6. TOTAL FLATNESS DEVIATION IS INDICATED FOR EACH CURVE.
- = DACO DATA FOR 600 MICRO-INCH TOTAL FLATNESS DEVIATION; 17-15 MICRO-INCHES RMS ROUGHNESS.

ALUMINUM 7075-T6 DATA

$T_{\text{mean}} = -250^{\circ}\text{F}$
 $E_m = 1.15 \times 10^7 \text{ PSI}$
 $K_m = 46.2 \text{ BTU/HR-FT}^2 \cdot ^{\circ}\text{F}$

FIGURE 11-3

**CLAUSING'S
MACROSCOPIC
CONSTRICTION
THEORY COMPARED
TO DACO LOW
TEMPERATURE
DATA FOR
STAINLESS STEEL
17-4 PH**



M-21069A

- = CLAUSING'S MACROSCOPIC CONDUCTANCE THEORY PREDICTION FOR STAINLESS STEEL 17-4 PH. TOTAL FLATNESS DEVIATION IS INDICATED FOR EACH CURVE.
- = DACO DATA FOR 400 MICRO-INCH TOTAL FLATNESS DEVIATION; 17-17 MICRO-INCHES RMS ROUGHNESS.
- Δ = DACO DATA FOR 400 MICRO-INCH TOTAL FLATNESS DEVIATION; 100-125 MICRO-INCH RMS ROUGHNESS.

STAINLESS STEEL 17-4 PH DATA

$T_{\text{mean}} = -150^{\circ}\text{F}$
 $E_m = 3.0 \times 10^7 \text{ PSI}$
 $K_m = 8.5 \text{ BTU/HR-FT}^2\text{-}^{\circ}\text{F}$

FIGURE 11-4

ness deviations of 200 micro-inches for each test block, or a total of 400 micro-inches.

The actual data for aluminum 7075-T6 17-15 micro-inch roughness, falls considerably above the 400 and 600 micro-inch curves up to contact pressures of 500 psi. The data then begin to approach the 400 micro-inch flatness deviation curve. One explanation for the greater values of h than those predicted by theory would, of course, rest on the fact that the present contact surfaces were ground on a stone grinder and were not spherical in shape. Surface flatness deviations would assume the form of macroscopic hills and valleys, or high areas and low areas, (Figure 2-8). Depending upon how the specimens were placed together, various numbers of macroscopic contact areas might be obtained, and therefore, the model of a multi-macroscopic contact area would be more applicable than a single macroscopic contact area.

A similar situation prevails for the stainless steel 17-4 PH data compared to Clausing's macroscopic theoretical predictions (Figure 11-4). It is interesting to observe that the smoother specimens produced data considerably above the 400 micro-inch curve and closely approximating the 200 micro-inch curve up to nearly 1000 psi. The measured total flatness deviation was, however, 400 micro-inches for both smooth and rough test specimens. The most plausible explanation for the difference would again be based on a multi-macroscopic contact area rather than a single macroscopic contact area as assumed by the theoretical curves.

The decreased total conductance of the rougher specimens compared to the smoother specimens could be attributed also to the decreased conductance of the microscopic asperities within the macroscopic contact areas for the rougher specimens.

11.3 Summary of Comparisons of Clausing's Macroscopic Theory to Data

Clausing's macroscopic theoretical curves were compared to Clausing's experimental data for both aluminum 2024-T4 and stainless steel 303. In both cases, the experimental values of h lay below the theoretical values of h for values of X_L greater than 0.65.

Clausing's macroscopic theoretical curves were next compared to DACO low temperature experimental data for aluminum 7075-T6 and Stainless Steel 17-4 PH. For both metals the experimental values of h lay above the theoretical values of h . A plausible explanation for the greater conductance than predicted could lay in a multi-macroscopic contact interface between the specimens rather than a single contact assumed by Clausing's theory.

12. CONCLUSIONS - THERMAL CONTACT CONDUCTANCE IN A VACUUM ENVIRONMENT

12.1 Low Temperature Aluminum 7075-T6 Data

The effect of increasing T_{mean} from -240°F to $+80^{\circ}\text{F}$ was to increase h by a factor of 3.5. See Figure 5-3. The effect of increasing T_{mean} from -230°F to $+300^{\circ}\text{F}$ was to increase h by a factor of 6. See Figure 5-6.

Low temperature values of h equalled high temperature values if a thin layer of vacuum grease was applied to the contact surfaces. See Figure 5-3. Using oil at the interface resulted in h values 3 times those of grease.

Values of h increased steadily with contact pressure for bare joints. For cases where grease and oil were used, values of h appeared to be independent of contact pressure over the pressure range from 40 to 700 psi. See Figure 5-3.

Values of h were obtained for cases in which air at 1 atmosphere was trapped in the interface and then the atmospheric pressure decreased. These values resulted in increases in h up to 40 percent over the h values obtained for cases where the contact surfaces were exposed to a vacuum. See Figure 5-6.

Specimens were mated with their lays perpendicular and then parallel. From the conductance data, it was not possible to determine which mating orientation produced higher values of h . Inconsistent values of h probably resulted from different conformity of surfaces for perpendicular and parallel cases, and not necessarily from different numbers of microscopic asperities in contact.

Values of h increased as surface roughness decreased. The rate of increase of h increased as surface roughness decreased. See Figure 5-16. The grinding process usually resulted in a greater waviness occurring with a greater surface roughness. Therefore, the effects of roughness on h would include an effect of waviness also.

12.2 Low Temperature Stainless Steel 17-4 PH Data

Values of h increased steadily with contact pressure up to 1000 psi. Exceptions to this is the wide data spread of very smooth, lapped surfaces. See Figure 5-8.

As T_{mean} increased from -100°F to $+130^{\circ}\text{F}$, values of h increased by a factor of 2. See Figure 5-10.

For very smooth, flat surfaces, the data spread was quite large, but it decreased with contact pressure. See Figure 5-8. Vacuum grease increased the value of h of the smoothest specimen by a variable factor, depending on T_{mean} and contact pressure. See Figure 5-9.

Entrapping air molecules at 1 atmosphere pressure resulted in increasing h up to 50 percent compared to exposing the contact surfaces to a vacuum before mating. See Figures 5-10 and 5-11.

As the roughness of the mating surfaces increased, regardless of the measured flatness of the surfaces, the values of h decreased. See Figure 5-16.

Perpendicular mated surfaces resulted always in a higher value of h than parallel mated surfaces. See Figures 5-10 to 5-13.

12.3 Mating of Dissimilar Metals at Low Temperatures

Changes in the h with direction of heat flow were studied. Heat was passed from aluminum to stainless steel and then the specimens were reversed. The spread in data was too great for any definite conclusions to be made. See Figures 5-14 and 5-15. The values of h were inexplicably lower than both the stainless steel and the aluminum results obtained previously.

12.4 Dependence of h Upon Contact Pressure

12.4.1 High Temperature Results - Aluminum

Plotting all the available data in the literature on log-log graph paper resulted in

$$h \sim p_c^m$$

where $m = 0.8$ to 0.9

for contact pressures between 300 and 1000 psi. See Figure 6-3.

Fried's hypothesis of a change in slope at pressures below 150 psi (or thereabouts) requires further experimental evidence before being established. For Fried's specimens $m = 0.4$ for p_c less than 150 psi. The high temperature data for all investigators lay close together despite the wide variation in aluminum alloys used for $300 < p_c < 1000$ psi. See Figures 6-1 and 6-2.

12.4.2 High Temperature Results - Stainless Steel

A plot on a log-log graph of all the available data in the literature resulted in the relationship

$$h \sim p_c^m$$

where $m = 1.05$

for most of the data in the literature. See Figure 6-5.

Below contact pressures of 110 psi, Fried's data for 50 micro-inch roughness has a sudden change in slope to $m = 0.11$. This sudden change in slope was not observed for Clausing's data.

12.4.3 Low Temperature Results - Aluminum 7075-T6

For three different roughnesses, DACO low temperature experimental h values were plotted against contact pressure. The best straight lines were drawn through each set of points. See Figure 7-1.

The log-log plots yielded straight lines relating h to p_c such that

$$h \sim p_c^m$$

where for all three roughnesses the slopes were approximately equal to

$$m = 0.85.$$

The value of m was approximately equal to that at high temperatures. The low temperature values of h differed from the high temperature values by a factor of from 2 to 10 as the rms roughness of the low temperature specimens increased from 15 to 130 micro-inches. No sudden change of slope of h versus p_c at low values of p_c was observed.

12.4.4 Low Temperature Results - Stainless Steel 17-4 PH

For three different roughnesses, DACO low temperature experimental h values were plotted against contact pressure. The best straight lines were drawn through each set of points. See Figure 7-2.

The log-log plots yielded three straight lines relating h to p_c such that

$$h \sim p_c^m$$

where $m = 0.84$ for $\delta = 17-17 \mu\text{-in.}$

$m = 0.71$ for $\delta = 35-25 \mu\text{-in.}$

$m = 0.83$ for $\delta = 100-125 \mu\text{-in.}$

The magnitudes of h for high compared to low temperature stainless steel are greater by a factor of 1.5 to 6.5 as the rms roughness δ increased from 17 to 125 micro-inches at 500 psi.

12.5 Application of Contact Conductance Results to a Typical Bolted Joint

The average value of h across a typical bolted joint was calculated. The contact pressure was known as a function of the radius from the

literature. Values of h at both high and low temperatures are known as a function of pressure from the literature and from data presented in this report.

The average value of h at $+250^{\circ}\text{F}$ was found to be $10,000 \text{ Btu/hr-ft}^2\text{-}^{\circ}\text{F}$ or 8.6 times higher than Aron and Columbo's calculation.

The average value of h at -250°F was found to be $6800 \text{ Btu/hr-ft}^2\text{-}^{\circ}\text{F}$, a decrease of 32 percent from high temperature data.

It was assumed that all heat flow was perpendicular to the aluminum plates held together by the bolt-nut combination. See Figures 8-1 and 8-2.

12.6 Comparison of Theory to Data

12.6.1 Clausing's Macroscopic Constriction Theory Compared to Clausing's Data at High Temperatures

Clausing's experimental values of h were compared to his macroscopic theory using his spherical contact model. See Figures 11-1 and 11-2. The theory predicts that

$$h_L = \frac{2a_L k_m}{A_b g(X_L)} . \quad (10-10)$$

For the case of aluminum, the theory and data for smooth specimens were in good agreement up to $p_c = 500 \text{ psi}$. Then theory predicted far higher values of h than data produced as p_c increased.

For the case of stainless steel, both theory and data are in good agreement up to 200 psi ; then theory begins to exceed data.

For both cases, theory predicts infinite values of h at contact pressures for which experimental values of h were finite. This occurred near 1000 psi for aluminum and 400 psi for stainless steel data.

The tendency for theory to predict much larger values of h than data usually occurred when more than 42 percent of the total apparent area was in macroscopic contact. This would correspond to the $X_L = 0.65$ line in the figures.

The reason for the discrepancy between theory and data is attributed to three possible sources. Firstly, the conductance due to the asperities was not considered. If considered, it would decrease the total conductance at high contact pressures. Secondly, the macroscopic contact area predicted by the Hertz equation is only valid for elastic spherical indentations. Thus, for the case of contact pressures high enough to cause elastic-plastic indentations, the predicted macroscopic areas would differ from the actual contact area. Thirdly, and most important, the theoretical value of h_L will tend to infinity from the very nature of the macroscopic constriction resistance solution (equation 10-10). As X_L approaches 1, $g(X_L)$ approaches zero.

12.6.2 Clausen's Macroscopic Constriction Theory Compared to DACO Data at Low Temperatures

Theoretical curves were plotted for h versus p_c using Clausen's spherical contact model and macroscopic theory only. The experimental values of h at low temperatures were compared to the theoretical curves. See Figures 11-3 and 11-4. The experimental contact surfaces were not spherically ground, but had a large scale waviness.

For contact pressures up to 1000 psi, both the aluminum 7075-T6 and stainless steel 17-4 PH conductance data exceeded macroscopic theory predictions. A probable reason for this result would be a multi-macroscopic contact interface between the specimens. The Clausen theory was based on a single macroscopic contact area.

13. RECOMMENDATIONS FOR FUTURE VACUUM CONDUCTANCE WORK

13.1 Experimental Work

The pressures under a typical bolt and nut joint were as high as 5000

psi for a torque of 22 inch-pounds. Therefore, data should be obtained for common structural materials, aluminum and stainless steel, for contact pressures up to 5000 psi, at least.

Conductance values should be obtained for the mating of dissimilar materials. Tests should also be made on mating metals with non-metals, and non-metals with non-metals. New titanium alloys used in advanced aircraft should also be tested.

The effect on contact conductance of interstitial materials such as grease, oils, foils, and other materials should be further investigated over a range in interface temperatures and contact pressures.

Effort should be undertaken to obtain a flatness deviation relief map for each of a pair of mating surfaces. When the surfaces are mated, in the perpendicular or parallel orientation, data could be obtained leading to a theory of multi-macroscopic contact areas. The purpose of the tests would be to predict the size and numbers of the multi-macroscopic contact areas as a function of apparent contact pressure.

13.2 Analytical Work

First consider Clausing's spherical contact model. Comparison of the Clausing and Chao macroscopic constriction theory to Clausing's data shows that the theory diverges to infinity, whereas the data were finite, at moderate contact pressures. Combining Clausing's microscopic theory with his macroscopic theory resulted in only a small decrease compared to the case of the macroscopic predictions alone. Recent calculations in which Fenech and Rohsenow's microscopic theory was combined with Clausing's macroscopic theory also resulted in only a small decrease in the macroscopic prediction. These calculations employed analogue data for stainless steel (Reference 10). The microscopic conductances produced were larger than the macroscopic by two or three orders of magnitude. If the microscopic conductance was less than the macroscopic at moderate pressures, then the Fenech and Rohsenow microscopic model would have been combined with the Clausing and Chao

macroscopic theory in order to reduce the magnitude of theoretical conductance predictions.

Therefore, a microscopic theory should be developed, such that the conductance values which it predicts can prevent the total conductance from diverging to infinity at contact pressures less than 5000 psi, or a better macroscopic theory should be constructed which does not diverge so rapidly.

Consider the more usual type of surface which has a waviness in addition to the roughness. Mate two of these surfaces together. There will definitely be more than one macroscopic area. What is needed, therefore, is a model of a surface which approximates the waviness of a ground specimen. If the macroscopic conductance is predominant over the microscopic, as Clausing and Chao assert, then this model may be sufficient up to moderate pressures. If, however, the theory once more predicts divergence to infinity of conductance at moderate pressures, then the microscopic conductance would have to be considered in addition to the multi-macroscopic.

The DACO low temperature data indicated that conductance varied inversely with roughness. But it should be noted that for surfaces ground on a Thompson stone grinder, waviness tended to increase as rms roughness increased. It may be difficult to separate the effect of one order of surface irregularity (waviness) from another order (roughness).

If the simple concept of macroscopic and microscopic conductance fails, a spectrum of surface irregularities may ultimately have to be considered. The contacts between two ground surfaces would then be made up of a spectrum of contact areas. This spectrum would range between the macroscopic, the semi-macroscopic and the microscopic. All would be combined to predict the total contact conductance for a vacuum environment.

14. REFERENCES

1. Bloom, M.F., "A Review of the Parameters Influencing Thermal Contact Conductance Between Metal Interfaces," Douglas Aircraft Company, SM Report 42082, August, 1962.
2. Bloom, M.F., "Preliminary Results From a New Thermal Contact Conductance Apparatus," Douglas Aircraft Company Engineering Paper 1672, August, 1963.
3. Shenker, Lauritzen, Corruccini and Lunberger, "Reference Tables for Thermocouples," NBS Circular 561, April 27, 1955, page 27.
4. Barzelay, M.E., K. N. Tong, and G. F. Holloway, "Effects of Pressure on Thermal Conductance of Contact Joints," NACA TN 3295, (1955).
5. Clausing, A.M., and B. T. Chao, "Thermal Contact Resistance in a Vacuum Environment," University of Illinois, Report ME-TN-242-1, August, 1963.
6. Fenech, H., and W. M. Rohsenow, "Thermal Conductance of Metallic Surfaces in Contact," U.S. Atomic Energy Commission Report NYO-2136, May, 1959.
7. Powell, R.L., and W. A. Blanpied, "Thermal Conductivity of Metals and Alloys at Low Temperatures," NBS Circular 556 National Bureau of Standards, September, 1954.
8. Fried, Erwin, "Study of Interface Thermal Contact Conductance Summary Report," General Electric Document No. 64SD652, May, 1964.
9. Fenech, H., and W. M. Rohsenow, "Prediction of Thermal Conductance of Metallic Surfaces in Contact," Journal of Heat Transfer, Volume 85, pages 15-24, February, 1963.
10. Henry, J.J., "Thermal Contact Conductance of Metallic Surfaces in Contact," M.I.T., Heat Transfer Laboratory, AEC Report NYO-9459, February, 1963.
11. Fried, E., "Thermal Joint Conductance in a Vacuum," ASME Paper 63-AHGT-18, April, 1963.
12. Archard, J.F., "Elastic Deformation and the Laws of Friction," Royal Society of London Proceedings A Vol. 243 page 190, 1957.
13. Aron, W., and Columbo, G., "Controlling Factors of Thermal Conductance Across Bolted Joints in a Vacuum," ASME Paper 63-W-196, November, 1963.
14. Holm, Ragnar, "Electric Contacts Handbook," Springer Verlag, 1958.
15. Hertz, Heinrich, "Study on the Contact of Elastic Solid Bodies," Journal Für die Reine und Angewandte Mathematik, Vol. 29, pages 156-171, 1882. SLA translations SLA-57-1164.

16. Smythe, W.R., "Static and Dynamic Electricity," McGraw-Hill, 1939.
17. Roess, L.C., "Theory of Spreading Conductance," Appendix A of an Unpublished Report of the Beacon Laboratories of Texas Company, Beacon, New York.
18. "Cryogenic Materials Data Handbook," PB 171809, Department of Commerce, Office of Technical Services, N.B.S. Boulder, Colorado.

15. NOMENCLATURE

A	cross-sectional area through which heat or electrical charges pass (ft ²)
a	radius of a contact area
b	radius of a cylindrical specimen
C	electrical capacitance between two conductors
d	small change in
d _t	total flatness deviation (micro-inches)
E	modulus of elasticity (psi) or electric field
g(x)	Roess series defined by equation 10-2
H	hardness of mating materials (psi)
h	thermal contact conductance (BTU/hr-ft ² -°F)
I	electrical current
J	electrical current density
k	thermal conductivity (BTU/hr-ft-°F)
L	length of cylindrical specimen
M	sides of heat or electrical flow tube
m	power dependency of h on contact pressure
n	number of points in contact or outward normal to a surface
P	load (lb)
p _c	contact pressure (psi)
Q	heat rate (BTU/hr) or total charge on a capacitor surface
q	heat flow rate or heat flux (BTU/hr-ft ²)
R	electrical or thermal resistance (°F/BTU/hr)
r	radius of curvature of spherical contact surface or radial coordinate

T	temperature ($^{\circ}\text{F}$)
ΔT	interfacial temperature difference ($^{\circ}\text{F}$)
T_{mean}	arithmetic mean interfacial temperature ($^{\circ}\text{F}$)
t	time
X	constriction ratio = a/b
δ	rms, surface roughness (micro-inches)
μ	micro
ν	Poisson's ratio
ξ	proportionality constant between p_c and H
ρ	net, free charge density
σ	electrical conductivity
ϕ	electrical or temperature potential

SUBSCRIPTS

a	circle of radius a
b	circle of radius b
i	i th element
L	macroscopic or large scale
m	harmonic mean
s	microscopic or small scale
t	total
1	surface or specimen 1
2	surface or specimen 2